

VERTICAL TRANSPORT IN SUPERLATTICES

Thesis submitted for a degree of
Doctor of Philosophy
by
Daniel L. Miller

Submitted to the Senate of The Hebrew University of Jerusalem in 1996.

This work was done under the supervision of Professor Boris Laikhtman.

To my family.

*Sicut aquae tremulum labris ubi lumen ahenis
Sole repressum, aut radiantis imagine Lunae
Omnia pervolat late loca jamque sub auras
Erigitur, summique ferit laquearia tecti.*

[As when ruffled water in a bronze pot reflects the light of the sun and the shining face of the moon, sending shimmers flying high into the air and striking against the paneled ceilings. Virgil, *Aeneid*, VIII, 22.]¹

Preface

We are not busy with some particular physical problem. We are “ranging to and fro over the wastelands of” the modern physics similar to Virgil’s sunlight reflections. This thesis consists from a number of parts. They are completed separate works motivated by recent experiments. The words “superlattice” and “current” are common in these works and widely used. Two chapters, 1 and 3, were written *especially* for this thesis. They are actually unpublished results and discussions. The kind atmosphere of the Racah Institute of Physics helps us a lot. I’m grateful to this place. I would like to acknowledge my and Boris Laikhtman’s discussions with Holger Grahn, S. Luryi, Y. Lyanda-Geller, Yehuda Naveh, M. Raikh, Leonid Shvartzman, and V. Zevin. I thank F. Bass for permission to use Part II, “Quantum superlattices”, of his book, prior to publication.

All the principal results of this work concern the vertical transport in generic three dimensional superlattices. In the 1st chapter we make an historical introduction, then we discuss the geometry of the problem, and the physical parameters associated with structure of electron minibands and strength of external fields. We found the effect of collisionless transverse magnetoresistance, and we discuss it in the 2nd chapter. This effect is similar to collisionless Landau damping in a plasma and we utilize the same name. In the 3rd chapter we provide quantum mechanical reasons for the above effect; we show how a magnetic field bends narrow superlattice minibands, and we classify the states into Landau-type and Stark-type. In the 4th chapter we compute longitudinal magnetoresistance of superlattices due to the imperfections of the interfaces. Correlation length of the interface roughness can be measured independently by this method. In the 5th chapter we discuss the current-voltage characteristic of superlattice when an electric field destroys the one-miniband transport. We found that the structure of the high-field domains in the superlattices is complicated, but can be described analytically with great accuracy. This structure reveals itself in the details of the current-voltage characteristics. All our results are consistent with existing experiments, and we make careful comparison of theoretical predictions and experimental results in all chapters.

Contents

1	Introduction	5
1.1	Generalities	5
1.2	Motivations and the program	7
1.3	Four conditions of miniband transport	9
1.4	Effective Hamiltonian	12
1.5	Appendix: matrix elements of Y in the tight and weak binding approximations.	13
2	Transverse magnetoresistance. I	15
2.1	Introduction	15
2.2	Electron dynamics	16
2.3	Solution of the Boltzmann equation	18
2.4	Calculation of the electric current	19
2.4.1	Weak magnetic field, $(\Omega_B\tau)^2 \ll \Lambda/T$	19
2.4.2	Intermediate field, $\Lambda/T \ll (\Omega_B\tau)^2 \ll 1$	20
2.4.3	Strong magnetic field, $\Omega_B\tau \gg 1$	20
2.5	Estimation of the role of the Hall effect.	21
2.6	Discussion	22
2.7	Comparison with experiment	23
2.8	Conclusions	25
2.9	Appendix A	25
2.10	Appendix B	25
3	Transverse magnetoresistance. II	26
3.1	Quantum kinetic equation.	26
3.1.1	Quantization of the effective Hamiltonian.	26
3.1.2	Orthogonality conditions for Stark type wave functions.	28
3.1.3	Matrix elements in the Stark representation.	29
3.1.4	Equation for density matrix	29
3.2	Calculation of the current	30
3.3	Appendix: Collision integral of the quantum kinetic equation.	32
3.4	Appendix: Gauge and translationally invariant equations.	33
4	Longitudinal magnetoresistance	35
4.1	Introduction	35
4.2	Perturbation theory for potential fluctuations	35
4.3	Averaged current and longitudinal magnetoresistance	37
4.4	Discussion and summary	38
4.5	Derivation of the Green function	40
4.6	Wave-vector-dependent in-plane magnetoconductivity	41
5	Theory of high-field-domain structures in superlattices.	42
5.1	Introduction	42
5.2	Physical picture	43
5.3	Electric current between adjacent wells.	44
5.4	Low-field region upstream of the domain.	45
5.5	Description of the high-field region.	47

5.6	Low-field region downstream of the domain.	48
5.7	Discussion	50

Chapter 1

Introduction

1.1. GENERALITIES

We consider theoretically semiconductor superlattices. A superlattice is a one-dimensional periodic potential in monocrystalline semiconductor. The superlattice potential would be obtained by a periodic variation of alloy composition introduced during epitaxial growth. It would consist of alternating ultrathin layers of two semiconductors that closely match in lattice constant.

We put forth a more specific definition: A superlattice is a stack of coupled quantum wells. Each quantum well limits electron motion in one direction and leads to quantization of energy; that is the elementary example in quantum mechanics textbooks. Coupling of quantum wells means that the electron can tunnel through the barrier separating adjacent quantum wells.

Our definition is more accurate because variation of alloy composition leads to variation of all band structure parameters. They cannot be described by a simple periodic potential. They modify electron wave functions in potential wells and tunneling amplitude through potential barriers. Our definition is particularly useful when variation of superlattice periodic potential is much larger than mean kinetic energy of electrons. In this case electrons are really sitting in the wells of the superlattice potential.

The evolution of molecular beam epitaxy has allowed access to superlattices. High-quality devices started to be available to experimentalists in the early seventies. For example, effects of energy quantization and tunneling were observed in 1974, see review of Weisbuch.²

Original motivations of superlattice research were to obtain devices with negative differential conductance³, and amplification of radiation^{4,5}. These effects were predicted for a superlattice placed in strong electric field perpendicular to the layers (vertical transport). Unfortunately, instability of electric potential profile in vertical (growth) direction and formation of high- and low-field domains made realization of these ideas impossible.⁶

Structure and dynamics of the high-field domains in superlattices is a separate branch of research. Attempts to build a microwave laser⁷ and a microwave radiation detector⁸ motivated the investigation of electric field domains. The first project was not realized for many years

due to the relatively small life time of excited carriers⁹. Progress in making a quantum cascade laser was reported only recently.¹⁰ Structure of the high-field domains, i.e. potential profile in a vertical direction, remains to be a subject of intensive research. This potential profile, for example, carries a lot of information concerning the quality of the device.¹¹

There are some similarities between instabilities of the potential profile in superlattices and in Gunn diodes.¹² Therefore, one hopes to see high-field domains running through the superlattice. This was one of the possible explanations of the time dependent oscillations of the potential profile which had been reported.^{13,14,15} However, numeric simulations show that the strengths of the high- and low- field domains change periodically in time with the domain boundary being pinned within a few quantum wells.^{16,17}

Modern technology uses superlattices for construction of optical devices. The physics of such devices is tightly related to properties of excitons in quantum wells. We will not touch the world of optics in the present work. Besides the device application, growth of superlattices is still a challenge for laboratories employing molecular beam epitaxy.

Typical superlattice geometry is shown in Fig. 1.1(a). The horizontal sheets schematically show a superlattice sandwiched between materials providing electrical contacts. The superlattice itself is formed by alternating layers of wide and narrow band gap materials. The real potential profile of such a device is complicated, and depends on the materials and doping level. The part of the potential profile related to the superlattice is shown schematically in Fig. 1.1(b). The potential energy of electrons changes periodically in the y direction and remains constant in the x and z directions.

This potential defines the sequence of the quantum wells separated by the barriers. Potential wells limit electron motion in the y direction and lead to energy quantization. We have chosen the energy of lowest electron state to be the zero of energy. We show the case of two electron states in a well, they are marked by black rectangles in Fig. 1.1(b). The energy gap between these two states is E_g , and it is one of three main parameters characterizing the superlattice potential.

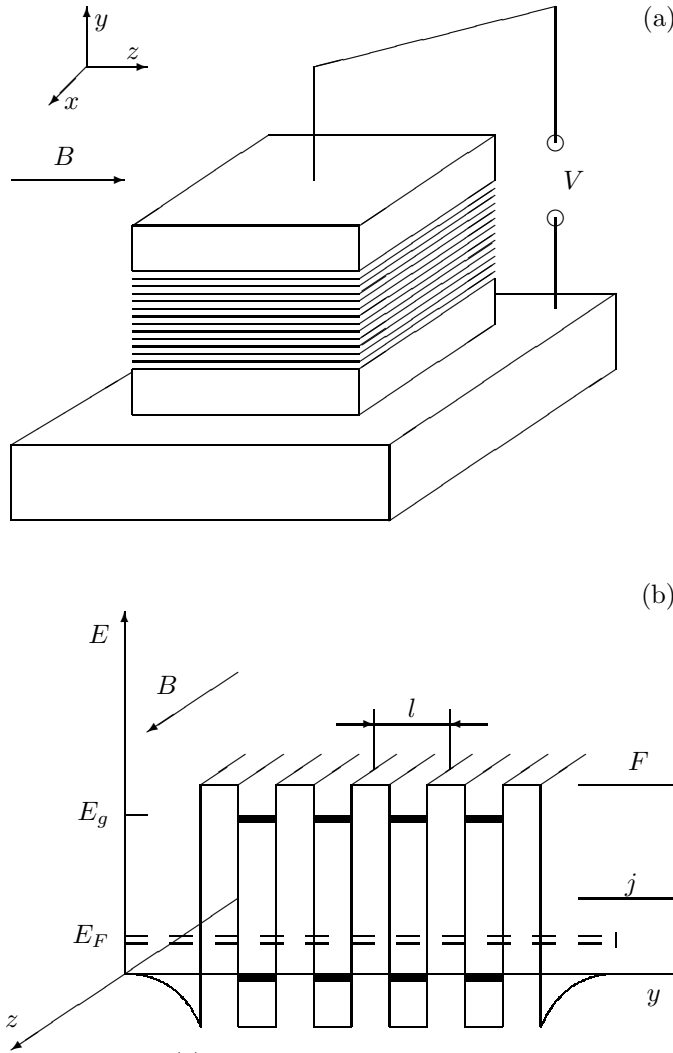


FIG. 1.1. (a) – Measurement of the vertical current in a superlattice. Current goes in the y -direction, transverse magnetic field is applied in the z -direction. (b) – One miniband transport through a superlattice. The Fermi energy (dashed lines), E_F , lies slightly above the lowest level in the quantum well. Energy of the lowest level is zero. Energy of the second level is $E_g \gg E_F$.

The superlattice structure brings to semiconductor physics a new length scale, which is the period of the superlattice, l , and a new energy scale, which is tunneling energy, Λ . These are two other parameters mentioned above, and their typical values in 1974 were 500\AA and 1meV correspondingly. Modern technology allows growth of superlattices having very fine structure. For example, the barriers of only three monatomic layers width were reported in Ref. 18. The typical superlattice potential period in 1996 is about 50\AA and tunneling energy may reach 40meV .

The resonance between energy levels in adjacent quantum wells leads to formation of minibands, and one can associate the tunneling energy with a quarter miniband width. This energy can be measured by photocurrent spectroscopy¹⁹ and results are in agreement with prediction of Kronig-Penney model.²⁰ However, calculation of minibands of holes is a much more complicated problem, because wave functions of holes are four component spinors.^{21,22} We will not consider holes in this work.

The energy gap E_g is assumed to be very large in the theory of the one-miniband transport, much larger than the Fermi energy, temperature, potential drop of electric field per period, energy uncertainty due to scattering and miniband width. In Fig. 1.1(b) we showed the Fermi energy between two minibands, i.e., the second miniband is empty. A high electric field destroys these minibands and leads to formation of low- and high-field domains. Inside the high-field domain E_g is of the order of the electric potential drop per period. For this reason, the physics of high-field domains stands separately from the physics of one-miniband transport.

The tunneling energy is usually so small, that the coherence of tunneling through subsequent barriers can be easily destroyed by external fields, sample imperfections or impurities. If it is known that sequential tunneling is incoherent, one can introduce the conductivity of the barrier or the transition time of an electron through the barrier.²³ We will use this approach in Chapters 4 and 5. If it is known that the tunneling is coherent, one can write down the usual kinetic equation for an electron gas with anisotropic dispersion. This dispersion contains all information about quantum mechanical effects (tunneling), and the kinetic equation is already a classical object. We will use it in Chapter 2. Very often, it is not known whether tunneling is coherent or not, and it is possible to scan all intermediate situations by changing external fields. For this reason we will consider the quantum kinetic equation derived by Keldysh's technique. It is the only tool which can describe the destruction of a miniband by a high electric field. We will derive it in Chapter 3.

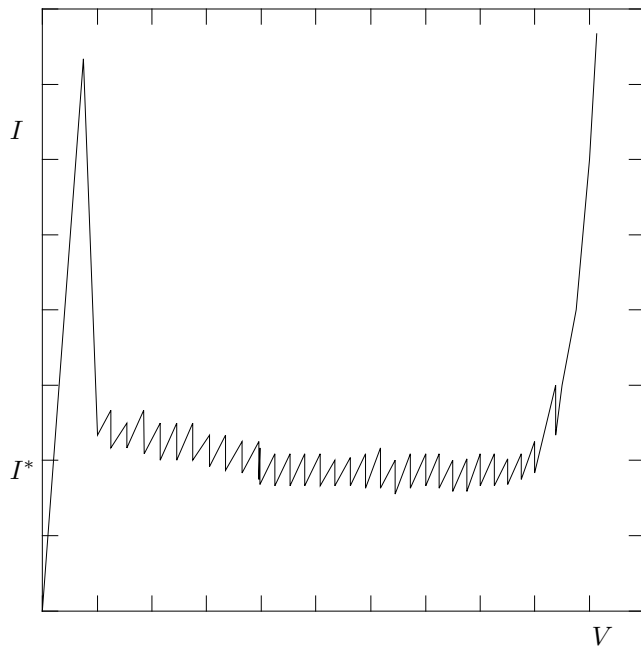


FIG. 1.2. Measured²⁴ I - V characteristics of the superlattice. The first discontinuity is the instability point of the one-miniband transport and corresponds to the formation of the high-field domain. Further increasing of the bias leads to the expansion of domains and small current oscillations near the value I^* . This is the first plato, see details in Chap. 5.

1.2. MOTIVATIONS AND THE PROGRAM

This project is actually a collection of a few works concerning vertical transport in superlattices which were motivated by recent experiments. Motivation for each of these individual works and related experiments are considered in their introductions, but we need to put all of them in the proper context here.

A lot of experiments and theoretical problems concerning one-miniband transport were discussed in the literature in the years 1970-1985, however interpretation of the recent experiments with high-quality devices is not always possible in the framework of the old theories. Most of the recent experimental results are collected in the book of Grahn²⁵. The modern theories of superlattice physics are considered in this book only briefly.

The simplest transport measurement is detection of the I - V curve. The typically observed I - V curve is very non-linear, and it exhibits a sequence of discontinuities, see Fig. 1.2. The first discontinuity corresponds to the destruction of single miniband. The nature of this instability point was considered for the first time by Laikhtman²³ and Laikhtman and Miller²⁶. The latter work contains the derivation of the quantum kinetic equation which is valid near the first instability point. The instability development leads to high-field domain formation. At least two states in each quantum well become involved in transport, see Fig. 1.3.

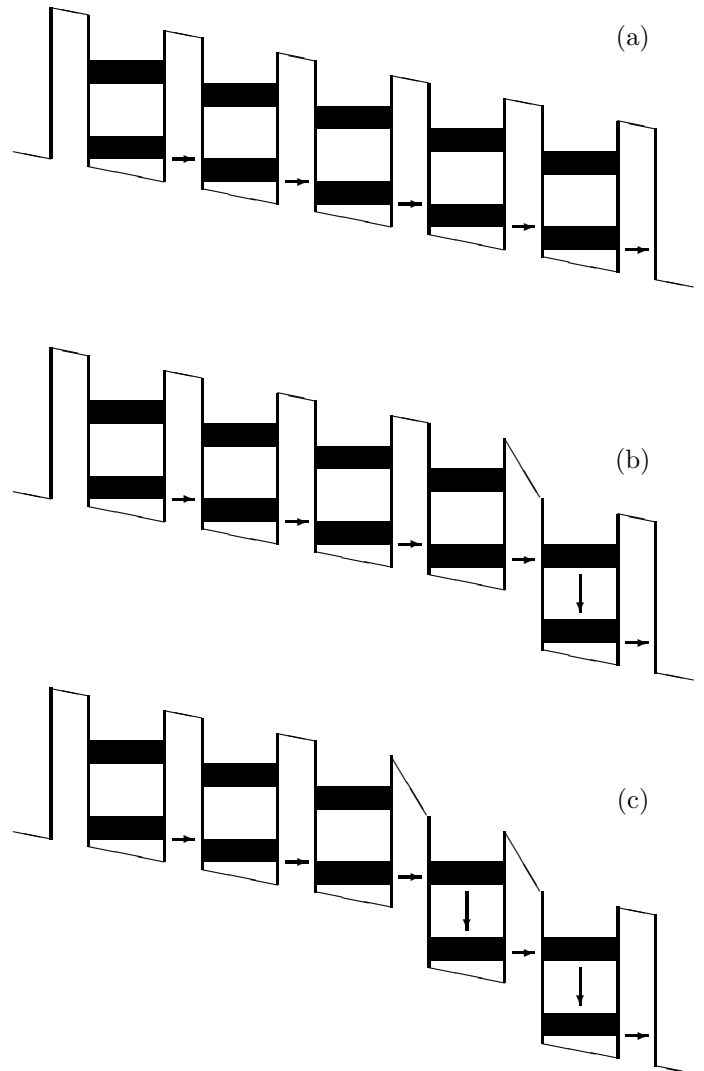


FIG. 1.3. Superlattice potential is shown schematically for several values of applied bias: before the first instability point (a), at the formation of the high-field domain (b), corresponding to expansion of the domain (c).

The structure of the high-field domain was calculated for the first time by Miller and Laikhtman²⁷. We reproduce this work in Chap. 5. Since this publication, the structure of the domains has been intensively considered in the literature. For example, additional effects, like imperfections and fluctuation of barrier size, were considered recently by Schwarz et al¹¹. Chapter 5 considers the parameters of the typical I - V curve, Fig. 1.2, in great detail. Recent measurements^{28,29,25} are also in agreement with this theory. The physical problems considered in Chapter 5 are

- limiting of the current by diffusion,
- minimal domain size,
- nonresonant tunneling of electrons inside the domain,
- time resolved process of the domain formation near the instability threshold,
- mechanism of the domain expansion,
- possibility of domain formation near the cathode and therefore injection of electrons into the second miniband and two-miniband transport.

It is very well known that transverse magnetic field shifts discontinuities of the superlattice I - V curve to higher bias. Concerning the first instability point we can mention the recent experiment of Aristone et al³⁰ and much more data can be found in the book of Grahn²⁵. It is believed that this discontinuity corresponds to the maximum of the I - V curve of the uniform superlattice. The position of the current peak is usually calculated by numeric solution of the kinetic equation in one miniband.²⁵ Analytical results were obtained first by Epshtein^{31,32}. They show a quadratic shift with magnetic field of the I - V curve peak. However, when magnetic field becomes stronger, the peak shifts linearly with magnetic field. The explanation was given by Miller and Laikhtman³³ in terms of resonant group of electrons. We reproduce this work in Chapter 2. The new results of Chapter 2 are

- resonant group of electrons which give the main contribution to the current,
- “collisionless” current – analog of collisionless Landau damping of plasma waves.
- difference between transverse magnetoresistance and magnetoconductance.

The use of the Boltzmann kinetic equation in Chapter 2 has to be justified. In certain cases one has to use the more general quantum kinetic equation as it was done by Levinson and Yasevichute³⁴, Suris and Shchamkhalova³⁵ and Laikhtman and Miller²⁶. We will follow the last work in order to show that

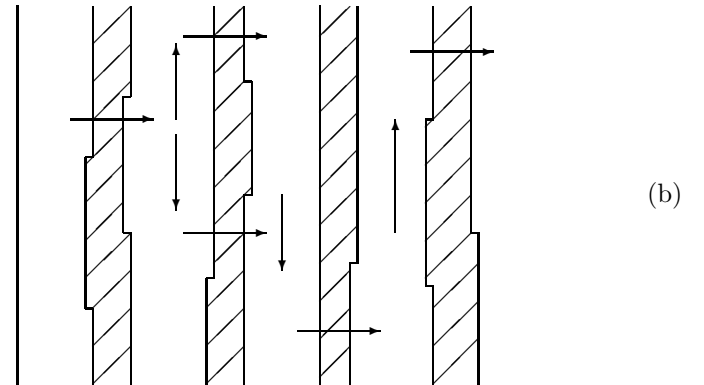
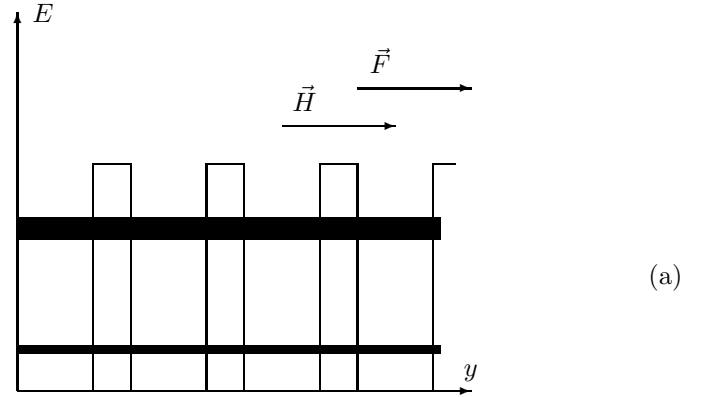


FIG. 1.4. Vertical current through superlattice in presence of longitudinal magnetic field.(a) Current goes around thick areas of the barriers and becomes sensitive to the magnetic field.(b)

- electron states in the narrow miniband in the presence of the parabolic potential created by a magnetic field are of two types Landau-like and Stark-like,
- the quantum kinetic equation supports qualitatively results of the semiclassical approach of Chapter 2,
- heating of the electron gas near the current peak can be important for wide interval of magnetic fields.

The solution to the kinetic equation in the miniband is possible only if we are in the regime of the miniband transport. Four conditions of the miniband transport are given in the next section. It may happen, that some of these conditions are violated and we have to solve the quantum kinetic equation. In this case we have to justify also the effective Hamiltonian method and that is done in Sec. 1.4.

The quality of the superlattices is determined basically by the quality of the interfaces. Surface roughness destroys the coherence of electron tunneling, and

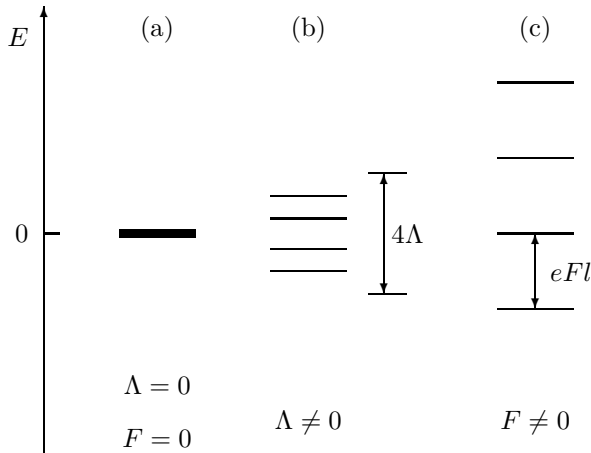


FIG. 1.5. Structure of energy levels in superlattice. (a) - Zero coupling and zero electric field; (b) - Coupling of quantum wells lifts degeneracy; (c) - strong electric field breaks miniband to Stark ladder.

measurement of roughness parameters is very important technologically. It was suggested recently, that surface roughness can be responsible for longitudinal magnetoresistance of superlattice.³⁶ If the superlattice layers are isotropic, there should not be classical longitudinal magnetoresistance, (see the geometry of the experiment in Fig. 1.4(a)). Magnetoresistance was explained by the roughness induced in-plane currents, see Fig. 1.4(b), which are sensitive to the magnetic field perpendicular to the layers. Theory of this effect was developed by Miller and Laikhtman³⁷. We reproduce this work in Chapter 4. The main result is that longitudinal magnetoresistance of superlattices is very sensitive to the correlation length of the roughness and allows calculation of this length.

1.3. FOUR CONDITIONS OF MINIBAND TRANSPORT

In this section we introduce the main parameters characterizing electron states and electron transport in a superlattice. An example of a superlattice having $N = 4$ periods is shown in Fig. 1.1. Bold horizontal lines mark the positions of the electron levels in the quantum wells as if these wells are isolated. Then, the lowest states in all four wells have the same energy $E = 0$, and we mark it by single bold line in Fig. 1.5(a).

Coupling of quantum wells lifts this degeneracy. The tunneling energy, Λ , depends strongly on the height of the potential barrier separating adjacent wells and on the effective mass of an electron under the barrier. Coupling of quantum wells spreads energies of electron states in the interval of width 4Λ , see Fig. 1.5(b). In the limit of the infinitely long superlattice $N \rightarrow \infty$, this interval is covered densely by the levels. The energy interval $[-2\Lambda, 2\Lambda]$ is called a *miniband*. Therefore, by definition, a miniband exists in an infinitely long idealized super-

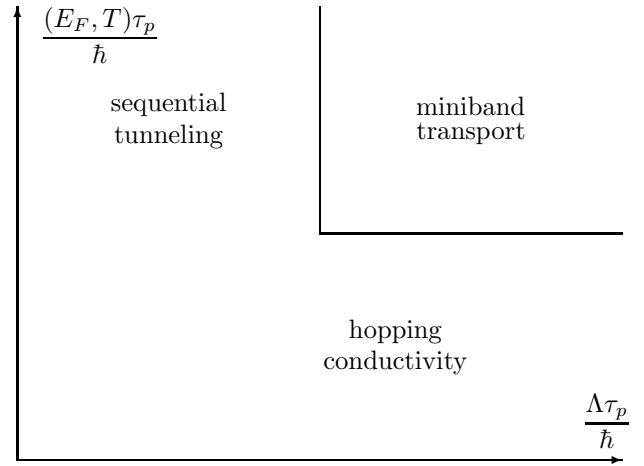


FIG. 1.6. Mechanisms, which govern vertical transport, are shown in the diagram.

lattice, without impurities, interface roughness, phonons and external fields.

An electric field, F , applied in the vertical direction, see Fig. 1.1, causes a relative potential shift of quantum wells. The drop of the electron potential energy per period is $eFl = eV/N$, where e is the electron charge, l is the superlattice period, N is the number of periods, and V is the applied voltage. If the coupling energy is zero, then this potential drop destroys the degeneracy of electron states and makes them equally spaced with the interval eFl , see Fig. 1.5(c). This structure of the electron levels is called a *Stark ladder*.

However, if both energies eFl and Λ are not zero, one can observe the transition from the level structure of Fig. 1.5(b) to the level structure of Fig. 1.5(c). This transition is called the Stark effect. It has been intensively studied during the whole superlattice history.^{38,39,40} Stark states have a finite size in the vertical direction $\Delta y \sim \Lambda/(eF)$.

A Stark ladder appears when the electric field satisfies the condition

$$eFl \gtrsim \frac{\Lambda}{N}, \quad (1.1)$$

i.e. when the mean spacing of the Stark ladder exceeds the mean spacing of the miniband. We see, therefore, that in the infinitely long superlattice the infinitesimal field destroys the miniband. Nevertheless, the picture of miniband transport is justified under the conditions which will be discussed in the rest of this section.

The scattering of the electrons by charged impurities and by phonons can be characterized by the elastic τ_p and the inelastic τ_ε relaxation times. The scattering destroys plane waves of the free electrons and also Bloch waves of the electrons in the superlattice. However, the plane waves approximate the electron wave function well if the mean kinetic energy of the electron gas is large enough

$$E_F, T \gg \hbar/\tau_p, \hbar/\tau_\varepsilon. \quad (1.2)$$

This is the first condition of miniband transport. If it is violated one can talk only about hopping between spatially localized states, which leads to *hopping conductivity*.

The condition Eq. (1.2) compares the kinetic energy of the electrons with the energy uncertainty due to scattering. However, it may happen that the miniband width is smaller than this energy uncertainty. In this case the subsequent tunneling events lose their coherence and there are no more plane waves propagating in the vertical direction. Therefore, we obtain the second condition of miniband transport

$$\Lambda \gg \hbar/\tau_p, \hbar/\tau_\varepsilon. \quad (1.3)$$

If this condition is violated then electron propagation in the vertical direction is called *sequential tunneling*.

The two inequalities Eqs. (1.2) and (1.3) define the phase diagram Fig. 1.6. In this diagram we show the three main regimes of superlattice transport. In the regime of miniband transport one can safely make use of the classical kinetic equation. In the regime of sequential tunneling there are no plane waves propagating in the vertical direction and therefore one should compute transport coefficients from the quantum kinetic equation. Various percolation type models can be used for investigation of transport in the hopping regime.

The strength of the electric field is also limited in the regime of miniband transport. It is clear that the Stark effect can be observed if eFl is much larger than $\hbar/\tau_p, \hbar/\tau_\varepsilon$, and that is very well known from the optical measurements³⁸. In the opposite case we can consider the electric field as a force driving electrons and that is precisely what we want. Therefore, we obtain the third condition of miniband transport

$$\lambda \lesssim \frac{\hbar}{\tau_p}, \frac{\hbar}{\tau_\varepsilon}. \quad (1.4)$$

Violation of this condition leads to the so-called *field-induced localization* of the electrons in the Stark states and to the transport of the *sequential hopping* type. This means the hopping between the subsequent Stark states.⁴¹ This regime cannot be observed experimentally because of the potential profile instability.

The field induced localization is an interesting physical phenomenon. It has, of course, something to do with a Stark transition, but we would like to discuss it also in different terms. The main purpose of the following discussion is to obtain the condition of miniband transport in the presence of a transverse magnetic field.

Let us assume that all conditions of the miniband transport Eqs. (1.2), (1.3), and (1.4) are fulfilled. In this case one can introduce the semiclassical picture of the miniband inclined by an electric field. The energy of the electron having zero in-plane momenta $p_x = p_z = 0$ lies in the interval

$$eFy - 2\Lambda \leq E \leq eFy + 2\Lambda. \quad (1.5)$$

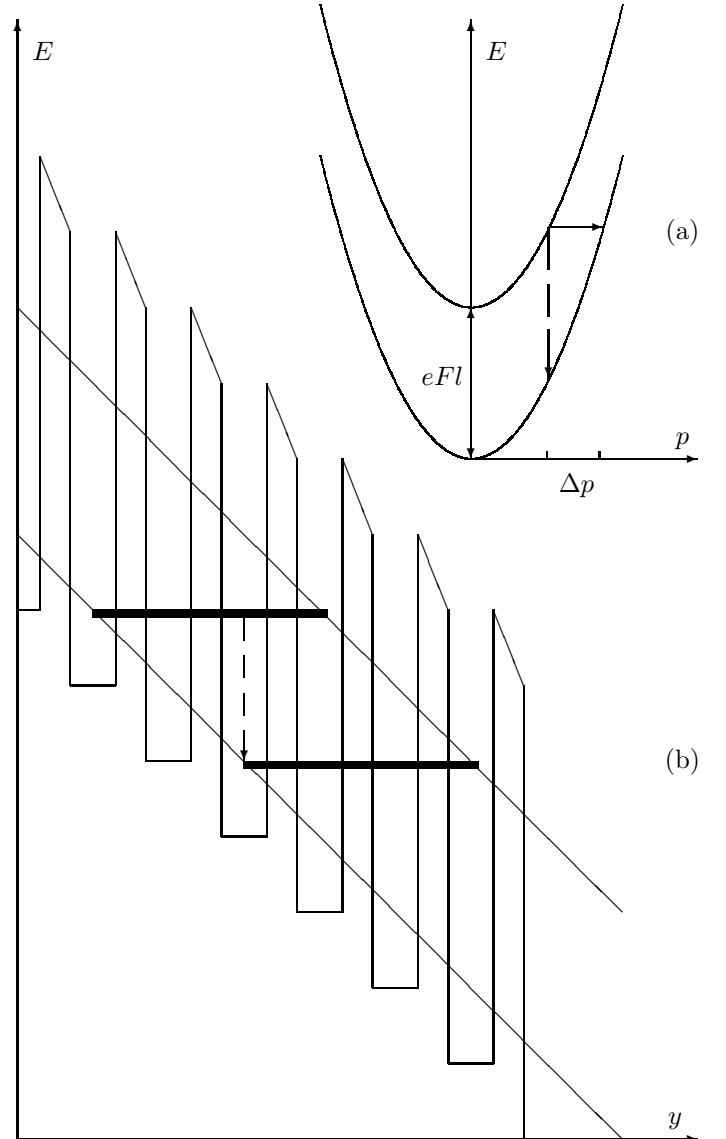


FIG. 1.7. Electrons reflects many times from the miniband boundaries before being scattered. The electron orbits are shown by thick lines (b). The Elastic scattering is accompanied by the large momentum transfer Δp (a), and therefore the inelastic process may be important. The inelastic transition is shown by the dashed lines, see (a) and (b).

This equation is semiclassically correct, because it contains both the coordinate y of the electron and the kinetic energy of the vertical motion of the electron.

We show an inclined miniband in Fig. 1.7 on the background of the superlattice potential. The relative shift of the subsequent quantum wells is eFl . In semiclassical language, the electron sitting at the bottom of the miniband is accelerated by the electric field. It crosses the miniband having passed the distance $\Delta y \approx 4\Lambda/(eF)$ and hits the upper boundary of the miniband. After reflection it goes back to the bottom of the miniband.

The period of such a trip can be estimated by dividing Δy by the mean electron velocity in the miniband $\Lambda l/\hbar$, which gives $\sim \hbar/(eFl)$. The periodic motion of the electron between the bottom and the top of the miniband is called a Bloch oscillator. It has been observed in optical four-wave mixing experiments.^{42,43} The semiclassical language gives another physical meaning to Eq. (1.4), namely that the electron does not swing a long time between the miniband boundaries because of the scattering.

The swinging of the electron means that there is field induced localization, because the electric field is applied but cannot drive the electric current. This picture is very clear and there is no reason not to use the semiclassical theory of the miniband transport at least near the transition point

$$eFl\tau_p \sim \hbar. \quad (1.6)$$

Far from the transition point, where $eFl\tau_p \gg \hbar$ the main contribution to the current is given by the hopping between subsequent Stark levels, and the contribution of the next neighbor hopping contains the small parameter $\hbar/(eFl\tau)$. This is not true at the instability point given by Eq. (1.6), where hopping between all Stark levels contributes to the current. A number of works, which ignore summation over all Stark levels near the instability point, have been published and show a wrong condition for instability and current peak⁴¹.

It is known that elastic relaxation processes are usually faster than inelastic ones. For this reason we put τ_p in Eq. (1.6) and not τ_e . However, inelastic scattering processes can be important near the field induced localization transition. In Fig. 1.7(a) we showed the in-plane dispersion of the electron energy for two subsequent Stark states. The electron may need to transfer a large in-plane momentum to the impurity in order to jump between these states elastically. At the same time the inelastic process may be very effective.

The acceleration of the electron by the electric field is equivalent to the presence of a linear potential, and to the motion of the electron in the tilted miniband, as it is shown in Fig. 1.7. The transverse magnetic field creates a parabolic potential, see Fig. 1.8. In this case, the size of the electron orbit depends very much on the in-plane electron characteristic velocity \bar{v}_x (let the magnetic field be z -directed see Fig. 1.1(a)). In order to see how it happens, we introduce the so-called effective Hamil-

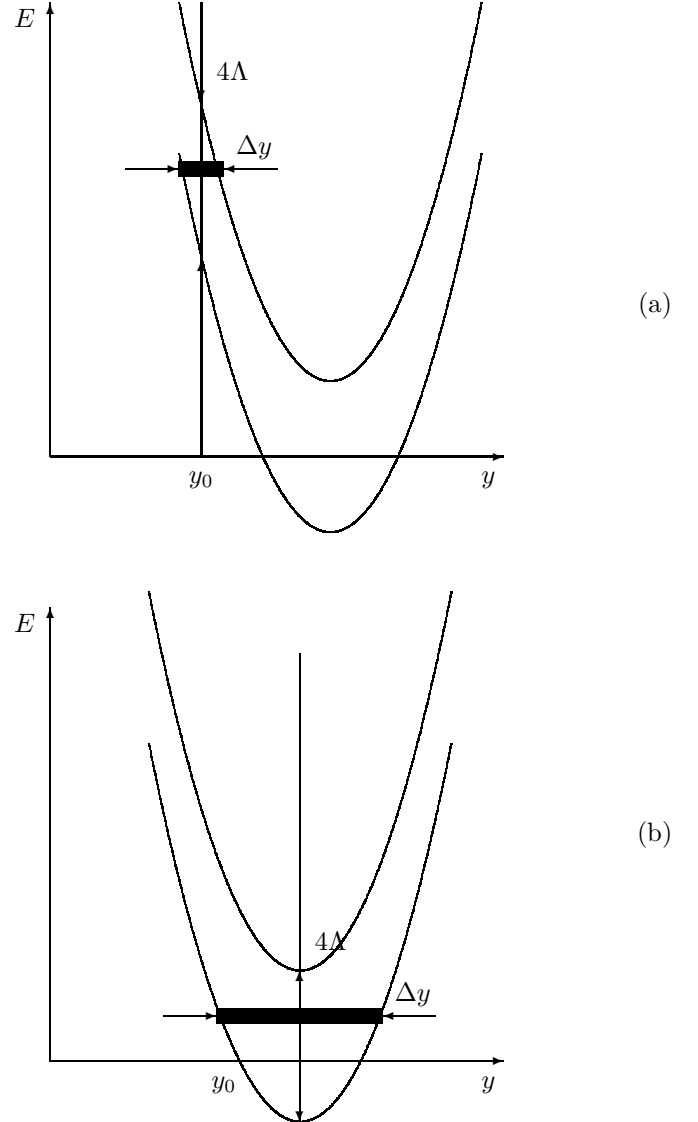


FIG. 1.8. The semiclassical picture of the superlattice miniband bended by the transverse magnetic field. (a) – Bloch oscillator like orbits. (b) – Usual cyclotron orbits.

tonian; see the next section for the justification of this approach.

$$\begin{aligned} \mathcal{H} &= \frac{p_z^2}{2m} + \frac{p_x^2}{2m} + 2\Lambda \left[1 - \cos\left(\frac{p_y l}{\hbar}\right) \right] - eFy \\ p_x &= P_x + eBy, \end{aligned} \quad (1.7)$$

where we used the MKS units and the tight-binding approximation for the dispersion law of the superlattice miniband. The coordinates here correspond to the Fig. 1.1.

Two integrals of motion P_x and guiding center of the orbit y_0 allow us to introduce another conserving quantity, the in-plane characteristic velocity $\bar{v}_x \equiv (P_x + eBy_0)/m$. We can obtain the one-dimensional Hamiltonian for the particle with defined values of \bar{v}_x and y_0 :

$$\begin{aligned} \mathcal{H}' &= 2\Lambda \left[1 - \cos\left(\frac{p_y l}{\hbar}\right) \right] \\ &+ (e\bar{v}_x B - eF)(y - y_0) + \frac{[eB(y - y_0)]^2}{2m}. \end{aligned} \quad (1.8)$$

This equation shows that the kinetic energy of the vertical motion is limited by two inequalities

$$E \leq 2\Lambda + (e\bar{v}_x B - eF)(y - y_0) + \frac{[eB(y - y_0)]^2}{2m}, \quad (1.9)$$

$$E \geq -2\Lambda + (e\bar{v}_x B - eF)(y - y_0) + \frac{[eB(y - y_0)]^2}{2m}, \quad (1.10)$$

which are quite analogous to the case of Eq. (1.5). This energy lies between two parabolas, see Fig. 1.8.

There is a basic difference between two parallel lines and two ‘‘parallel parabolas’’. Whereas the energy distance between them is constant 4Λ , the size of the orbit, Δy , in the real space depends very much on \bar{v}_x . The expression for the size of the orbit at the origin of the parabolas Fig. 1.8(b) is different from the expression for the orbit in the branches Fig. 1.8(a). Therefore, we have two cases:

$$\Delta y = \begin{cases} \frac{2\Lambda}{|eF - e\bar{v}_x B|} & |F/B - \bar{v}_x| > \sqrt{\frac{\Lambda}{2m}} \\ \frac{\sqrt{2\Lambda m}}{|eB|} & |F/B - \bar{v}_x| < \sqrt{\frac{\Lambda}{2m}} \end{cases}. \quad (1.11)$$

The first case corresponds to a slightly modified Bloch oscillator and the second case corresponds to the usual anisotropic cyclotron orbits.

The periods of these orbits can be obtained by the division of Δy by the mean electron velocity in the miniband $\sim \Lambda l/\hbar$. The magnetic and electric fields induce localization of the electrons when these periods for most of electrons are of the order of the relaxation time. This happens either when

$$\Omega_B \tau_p \sim 1, \quad \hbar\Omega_B > |eFl - ev_F Bl|, \quad (1.12)$$

or when

$$|eFl - ev_F Bl| \tau_p \sim \hbar, \quad \hbar\Omega_B < |eFl - ev_F Bl|. \quad (1.13)$$

Here we replaced \bar{v}_x by Fermi velocity v_F . In the non-degenerate case one has to substitute here the thermal velocity \sqrt{mT} . The cyclotron frequency introduced here is defined by

$$\Omega_B \equiv \frac{eB}{\sqrt{mm_\perp}} = \frac{eBl}{\hbar} \sqrt{\frac{\Lambda}{2m}}. \quad (1.14)$$

Note that the condition of the magnetic field induced localization Eq. (1.12) is valid for bulk semiconductors, while the condition Eq. (1.13) is specific for superlattices.

The analogy between Eqs. (1.12) and (1.13) from one side and Eq. (1.6) from other side leads to the *fourth* condition of the miniband transport:

$$\max \hbar\Omega_B, |eFl - eBv_F l| \lesssim \max \frac{\hbar}{\tau_p}, \frac{\hbar}{\tau_\varepsilon}. \quad (1.15)$$

In order to provide the quantum mechanical arguments, as we did for Eq. (1.4), we have to quantize the effective Hamiltonian and compare the level spacings with relaxation rates. The structure of the eigenenergies of the effective Hamiltonian is discussed in Sec. 3.13.1.1 and one can check that conditions Eq. (1.15) are correct.

1.4. EFFECTIVE HAMILTONIAN

In the previous section we derived conditions of the miniband transport Eqs. (1.2), (1.3), (1.4), and (1.15). The last one was obtained by making use of the effective Hamiltonian method. In this section we derive conditions justifying this method.

The dynamics of a Bloch electron in the presence of a magnetic field can be described approximately by an effective Hamiltonian, introduced first by Peierls⁴⁴. The effective Hamiltonian is obtained from the spectrum of the Bloch electron $E(\mathbf{p})$ by the replacement of the momentum \mathbf{p} by $\mathbf{p} - e\mathbf{A}$, where \mathbf{A} is the vector potential of the magnetic field. Luttinger⁴⁵ justified this approach for a weak magnetic field. Blount⁴⁶ calculated corrections to the effective Hamiltonian for a general three dimensional lattice. Berezhkovskii and Suris⁴⁷ made the accurate calculation of the electron spectrum in a superlattice and the external magnetic field applied perpendicular to the growth direction. They assumed that the effective Hamiltonian can be applied if the magnetic field does not affect much the electron wave functions in separate wells of the superlattice. This results in the condition

$$\hbar\Omega_c E_F \ll E_g^2, \quad (1.16)$$

where $\Omega_c = eB/m$, E_F is Fermi energy, and E_g is the energy gap between minibands, see Fig. 1.1(b). The condition of the applicability of the effective Hamiltonian

Eq. (1.16) can be considered as generally accepted, for the case of metals, see Ref. 48.

Lifshitz and Pitaevsky⁴⁹ have assumed that the effective Hamiltonian method can be used if the space between energy levels in the presence of magnetic field is much smaller than the minimal energy scale of the band structure. We find a different condition.

In this section we show that the condition Eq. (1.16) is not enough. We carry out the derivation of the effective Hamiltonian and find another necessary condition which can be more severe. We obtain our condition by the calculation of corrections to the effective Hamiltonian.

In the absence of magnetic field, the eigenfunctions of the Hamiltonian $\mathcal{H}_0 = (\hbar^2 \nabla^2 / 2m) + U(y)$, where $U(y)$ is a periodic potential, are

$$\psi_{s\mathbf{k}} = \frac{1}{\sqrt{\mathcal{V}}} e^{i\mathbf{k}\mathbf{r}} u_s(k_y, y), \quad (1.17)$$

where s is the miniband number and the Bloch amplitude u_s is periodic in y . So, with the help of the unitary matrix

$$S_s(r', r) = \sum_{\mathbf{k}} \frac{1}{\sqrt{\mathcal{V}}} e^{-i\mathbf{k}\mathbf{r}} \psi_{s\mathbf{k}}(\mathbf{r}') \quad (1.18)$$

the Hamiltonian can be transformed to the form where its wave functions are plane waves and the spectrum is the electron spectrum in the periodic potential, $E_s(\mathbf{k})$,

$$S_s^\dagger \left[\frac{\hbar^2 \hat{\mathbf{k}}^2}{2m} + U(y) \right] S_s = E_s(-i\nabla). \quad (1.19)$$

In the presence of a constant vector potential this equation becomes

$$S_{s,\mathbf{A}}^\dagger \left[\frac{(\hbar \hat{\mathbf{k}} - e\mathbf{A})^2}{2m} + U(y) \right] S_{s,\mathbf{A}} = E_s \left(-i\nabla - \frac{e}{\hbar} \mathbf{A} \right). \quad (1.20)$$

The matrix $S_{s,\mathbf{A}}$ is obtained from Eqs. (1.17,1.18) by the replacement of $u_s(k_y, y)$ by $u_s(k_y - eA_y/\hbar, y)$.⁴⁹

If the vector potential is not a constant then equation Eq. (1.20) is not exact. First of all, the matrix $S_{s,\mathbf{A}}$ introduced above, in general, is not unitary and has to be corrected. However, in a one dimensional superlattice and a uniform magnetic field it is possible to choose a gauge where $A_y = 0$, and the transformation matrix S_s is independent of the vector potential. Even with such a transformation matrix there are corrections to the right-hand side of Eq. (1.20) because S_s does not commute with the coordinate dependent vector potential.

It's well known from the theory of Bloch wave functions that

$$\langle s'k'_y | y | sk_y \rangle = \left(i \frac{\partial}{\partial k_y} + \langle s' | Y | s \rangle \right) \delta(k_y - k'_y), \quad (1.21)$$

where $\langle s | Y | s' \rangle = \langle u_s | i(\partial/\partial k_y) | u_{s'} \rangle$ is a function of k_y . Here states $\langle u_s |$ are chosen in such a way that $\langle s | Y | s \rangle =$

0. Thus, the diagonal matrix element of the Hamiltonian is

$$\mathcal{H}_{ss} = E_s \left(-i\nabla - \frac{e}{\hbar} \mathbf{A} \right) + \frac{e^2 B^2}{2m} (Y^2)_{ss}, \quad (1.22)$$

where B is the component of the magnetic field perpendicular to the superlattice axis. The first term on the right-hand side of this equation is called the effective Hamiltonian. In order to estimate the second term we make use of an equation for the operator Y . This equation can be obtained by calculating the commutator $[[\mathcal{H}_0, y], y]$ directly and with the help of Eq.(1.21),

$$\sum_{s''} (E_s + E_{s'} - 2E_{s''}) Y_{ss''} Y_{s''s'} + i(E_s - E_{s'}) \frac{d}{dk} Y_{ss'} + 2iY_{ss'} \frac{d}{dk} (E_s - E_{s'}) + \left(\frac{\hbar^2}{m} - \frac{d^2 E_s}{dk^2} \right) \delta_{ss'} = 0 \quad (1.23)$$

If there are no band crossings, that is $E_1 < E_2 < E_3 < \dots$ for any k , the diagonal part of this equation gives the following inequality

$$(Y^2)_{11} \leq \frac{\hbar^2}{2} \frac{1/m - 1/m_\perp}{E_2 - E_1}, \quad (1.24)$$

where $1/m_\perp(k) = d^2 E_1 / (dk^2)$. In the case of the smooth potential $U(y)$ the right-hand side of this inequality can be considered as estimation for the matrix element $(Y^2)_{11}$ in the left-hand side, see Appendix Sec 1.5. The variance of this matrix element in the Brillouin zone is, therefore, of the order of $(\hbar^2/m)(\Lambda/E_g^2)$, i. e. it's proportional to the miniband width divided by the square of the energy gap between the first and second minibands, $E_g = \min(E_2 - E_1)$.

The last term in Eq. (1.22) in the case $s = 1$ can be neglected if it is much smaller than the miniband width, which gives the condition for the magnetic field

$$\hbar \Omega_c \ll E_g, \quad (1.25)$$

Note that this condition is stronger than Eq. (1.16) unless the Fermi energy is comparable or larger than the E_g .

The offdiagonal with respect to the miniband matrix element of the effective Hamiltonian can be neglected under the condition that is similar to Eq. (1.16).

1.5. APPENDIX: MATRIX ELEMENTS OF Y IN THE TIGHT AND WEAK BINDING APPROXIMATIONS.

In the tight binding approximation, $\Lambda \ll E_g$, both sides of Eq. (1.24) can be represented as a power series of the parameter $1/\Theta \sim \Lambda/E_g$. For example for a superlattice with rectangular wells, narrow barriers, and period π

$$(Y^2)_{11} = \frac{\pi^2}{12} - \frac{1}{2} + \frac{1}{\Theta} \left[-\frac{\pi}{6} - \frac{2}{\pi} + \left(\frac{2\pi}{3} + \frac{2}{\pi} \right) \sin^2(k\pi/2) \right] + O\left(\frac{1}{\Theta^2}\right) \quad (1.26)$$

For the same case the right-hand side of Eq. (1.24) is

$$\frac{1}{3} + \frac{1}{\Theta} \left[-\frac{\pi}{3} - \frac{4}{9\pi} + \left(\frac{2\pi}{3} + \frac{20}{9\pi} \right) \sin^2(k\pi/2) \right] + O\left(\frac{1}{\Theta^2}\right). \quad (1.27)$$

So, in this particular case the calculated coefficients are different by about 3%.

In the weak binding approximation, when band width is much larger than the gap, let

$$U_n = \frac{1}{\pi} \int_0^\pi \cos(2ny) U(y) dy, \quad (1.28)$$

where the superlattice potential $U(y)$ is an even function with period π , and $U_0 = 0$. We assume that this potential is smooth; in other words we assume that the amplitude of the first harmonic U_1 is larger than all other harmonics. In the gap region $|k| \sim 1$ Eq. (1.24) becomes equality in the zero order perturbation theory:

$$(Y^2)_{11} = \left[\frac{1}{2} \frac{U_1}{(1 - |k|)^2 + U_1^2} \right]^2. \quad (1.29)$$

where we put $\hbar = m = 1$. For small and intermediate k the second order perturbation theory gives

$$(Y^2)_{11} = \sum_{s=2}^{\infty} U_{[\frac{s}{2}]}^2 \frac{1}{E_1(k) - E_s(k)} \frac{d^2}{dk^2} \left(\frac{1}{E_1(k) - E_s(k)} \right) \quad (1.30)$$

For the same case the right-hand side of Eq. (1.24) is

$$\frac{1}{E_1(k) - E_2(k)} \sum_{s=2}^{\infty} U_{[\frac{s}{2}]}^2 \frac{d^2}{dk^2} \left(\frac{1}{E_1(k) - E_s(k)} \right). \quad (1.31)$$

Under the assumption that $U_1 \geq |U_n|$ for any n , the difference between the left hand side and right hand side of Eq. (1.24) is less than 15%.

Chapter 2

Transverse magnetoresistance. I

The motion of the Bloch electron in the crossed electric, F , and magnetic, B , fields is studied for the case of the anisotropic band structure that usually exists in superlattices. The electron trajectories are calculated from the so-called effective Hamiltonian with an electric field applied in the growth direction of a superlattice and a magnetic field parallel to layers. We solve the kinetic equation and calculate the electric current for the case when the miniband width is much smaller than the characteristic kinetic energy of electrons. If the magnetic field is strong enough, only electrons that have a velocity component perpendicular to both electric and magnetic fields equal to the drift velocity, $v_A = F/B$, contribute into the current. The current reaches its maximum value when v_A is close to the Fermi velocity, v_F , or to the thermal velocity, v_T , whatever is larger. However, as the magnetic field goes to zero the current peak position goes to its limit F_{th} like B^2 . The magnetoresistance at low magnetic field changes its sign at the field $F_{th}/\sqrt{3}$. The quantitative agreement with experiment is obtained for these results without fitting parameters. We also find that electric current is independent on the relaxation time in some interval of the applied field. This can be called the effect of collisionless conductivity.

2.1. INTRODUCTION

The nonlinear transport phenomena in superlattices have attracted much interest in recent years. These phenomena come from the narrow width of electronic minibands in superlattices³. Experiments show that with the increase of the applied bias the electric current first grows linearly, then reaches a maximum⁵⁰. At this point the uniform potential distribution across the superlattice becomes unstable, and the superlattice breaks into low- and high-field domains⁶. Further increase of the applied voltage leads to the expansion of the high-field domain, which appears as a series of peaks on the I - V characteristic.

Measurements of the vertical current in the presence of a magnetic field parallel to the layers^{51,52,53,54,55,56,57,58} reveal a new interesting effect. It was found that all peaks on the I - V characteristic of a superlattice are shifted by magnetic field toward the higher bias. A linear theory of

the magneto-conductivity of superlattices (i.e. a theory for the Ohm's law region) developed by Shik⁵⁹, Ando⁶⁰ and a theory of electron transport in the Harper band developed by Suris and Shchamkhalova⁶¹ cannot explain the behavior of current peaks. A qualitative explanation of this phenomenon was suggested by Movaghar⁶². Numeric calculations performed by Sibille et al.⁵⁴, Palmier et al.⁶³, and Hutchinson et al.⁵⁸ also lead to the same qualitative behavior and some of them can be fitted to experiment⁶³. An analytical solution of the kinetic equation and results for magneto-conductivity of superlattice have been published³². The final results were expanded in powers of magnetic field and they are reproduced by Eq. (2.25) here. In the present paper we calculate analytically the I - V characteristic of a superlattice in strong electric and magnetic fields. The theory agrees quantitatively with the behavior of the current peaks measured in different experiments.

The qualitative arguments suggested by Movaghar⁶² are based on the quantum mechanical explanation of negative differential conductivity (NDC) in superlattices. NDC in an electric field applied parallel to the superlattice axis (y axis) comes about because this field localizes electrons at Stark levels. A magnetic field applied parallel to the layers (in the z direction) causes the localization of electrons in the (x, y) plane. In a weak electric field the spatial size of electron states is limited by the magnetic field and it is smaller than the length of possible Stark states, $\Lambda/(eF)$. Therefore the electric field does not affect the electron states, and usual positive magnetoresistance is observed. In other words the I - V characteristic in a magnetic field goes below that without a magnetic field. With the increase of the electric field the size of Stark states eventually becomes smaller than the length of the possible magnetic states. At this electric field the effect of the magnetic field can be neglected and the I - V characteristic passes to the falling branch of the I - V curve without magnetic field. Because of the positive magnetoresistance, the peak of the I - V characteristic is shifted to a higher electric field.

Sibille et al.⁵⁴ calculated the I - V characteristic making use of the hydrodynamical model similar to that used by Esaki and Tsu³. The classical equation of motion for electrons in a superlattice in electric and magnetic fields

has been solved numerically. The electron drift velocity was calculated by averaging of the electron velocity along the trajectory with some relaxation time. Although the hydrodynamic model gives a qualitatively correct I - V characteristic it does not describe the experimental results quantitatively. In a more recent work of Palmier et al.⁶³ the I - V characteristic was obtained from the numeric solution of the Boltzmann kinetic equation in good agreement with the experiment.

In this work we make an analytic calculation of the current in a superlattice in the presence of electric and magnetic fields with the help of the classical Boltzmann equation. The equations of electron motion in the crossed electric and magnetic fields in the superlattice are obtained in Sec. 2.2 from the effective Hamiltonian. These equations are similar to the equations of motion of a nonlinear pendulum⁶⁴, but in our case two degrees of freedom are mixed and this complicates the solution. Electron trajectories are expressed in terms of Jacobian elliptic functions. In the v_x - v_y plane trajectories are closed orbits confined in a strip $|v_y| \leq 2\Lambda l/\hbar$ due to reflection from miniband boundaries. Here Λ is the tunneling matrix element between electron wave functions in adjacent quantum wells and l is the superlattice period. The centers of the trajectories are located at the v_x axis. The size of each trajectory in the v_x direction is also limited from above, $\text{Var}(v_x) \leq 4\sqrt{2\Lambda/m}$, where m is the in-plane effective mass. The frequency of electron motion along an orbit has a minimum, when the center of the orbit is located at $v_x = v_A \equiv F/B$. The frequency increases with the distance of the center from this point.

In Sec. 2.3 we solve the Boltzmann equation in a superlattice miniband to calculate the electron distribution function, f . We assume that the characteristic electron energy (temperature or the Fermi energy) is much larger than the miniband width and the main scattering mechanism is elastic scattering by impurities or surface roughness. We do not make any assumption concerning the relative importance of external fields and collisions for the shape of the distribution function. This means that, in general, electrons may travel rather a long distance in physical space as well as in momentum space before being scattered. To solve the Boltzmann equation in this case we introduce as coordinates two integrals of motion characterizing a trajectory in the momentum space and a coordinate characterizing electron position along the trajectory. The electron distribution is asymmetric along the trajectory with respect to the direction of the electric field. The asymmetric part is proportional to the relaxation time τ when it is smaller than the period of motion along the trajectory and is proportional to $1/\tau$ in the opposite case.

The electric current is calculated in Sec. 2.4. The contribution of an electron to the current is proportional to its velocity. The velocity in the growth direction, v_y , is an oscillating function of the electron momentum in the same direction, p_y . This momentum is changing in time under the electric field and the Lorentz force. For

that reason v_y , oscillates and the average contribution to the current is zero. However, the Lorentz force in y direction is proportional to the velocity in the direction perpendicular to the electric and magnetic fields, v_x , and for some value of this velocity the force due to the electric field and the Lorentz force cancel each other. This means that there is a resonant group of electrons with a time independent p_y that contributes to the current. Scattering complicates this picture because for a nonzero contribution to the current it is enough that an electron does not change v_y between two scattering events. The width of the resonant region in the momentum space is determined by competition between the electron motion in the external fields and scattering. For some values of the fields a resonance region appears at the exponential tail of the electron distribution function. In this case a nonresonant contribution to the current, which is proportional to the probability for an electron to be scattered during one period of the orbital motion has to be taken into account.

Application of a magnetic field perpendicular to the electric current generates an electric field parallel to the layers (in the x -direction). This field is introduced into the kinetic equation in Sec. 2.5. We show that the correction to the current in the superlattice direction due to this field (Hall effect) can be neglected.

In a certain range of the magnetic field we found that the electric current is independent of the scattering rate. This result suggests that the kinetic equation can be solved without considering the collision term, as is done for plasma, see Ref. 65. That is the regime of the collisionless conductivity considered specifically in Sec. 2.6. In Sec. 2.7 we compare the theoretical predictions with available experimental data. The summary of the results is given in Sec. 2.8.

2.2. ELECTRON DYNAMICS

We consider a superlattice in the tight binding approximation when, without external fields, the electron spectrum in the first miniband is

$$E_{\mathbf{p}} = \frac{p_x^2 + p_z^2}{2m} + 2\Lambda \left[1 - \cos\left(\frac{p_y l}{\hbar}\right) \right], \quad (2.1)$$

where m is the electron effective mass, Λ is the overlap integral between adjacent wells, and l is the superlattice period. In an electric field in the y direction and a magnetic field in z direction it is convenient to choose a gauge where the vector potential depends only on y , $\mathbf{A} = (-By, 0, 0)$.

The external fields can be approximately taken in to account by the effective Hamiltonian method introduced first by Peierls⁴⁴. The effective Hamiltonian is obtained from the spectrum of the Bloch electron $E_{\mathbf{p}}$ by the replacement of the momentum \mathbf{p} by $\mathbf{p} - e\mathbf{A}$, (see justification of this approach in Sec. 1.4). The Hamiltonian has the form

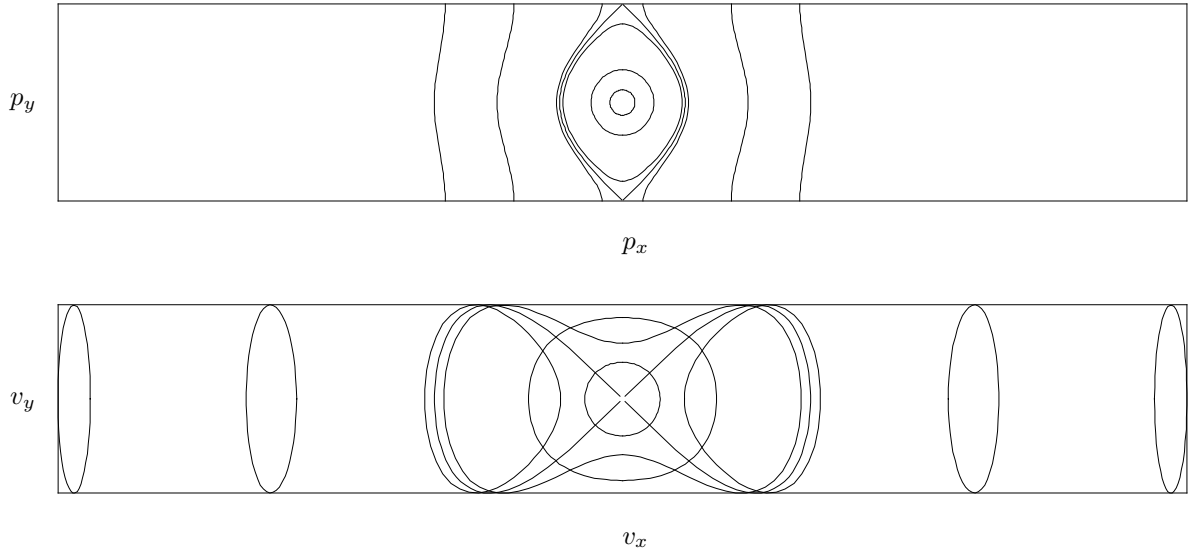


FIG. 2.1. The trajectories in p - and in v -space. The quantity p_y ranges from $-\pi\hbar/d$ to $\pi\hbar/d$, p_x ranges from $mF/B - 18p_\Lambda$ to $mF/B + 18p_\Lambda$, v_y ranges from $-2v_\perp$ to $2v_\perp$, and v_x ranges from $F/B - 6p_\Lambda/m$ to $F/B + 6p_\Lambda/m$. Trajectories in the p space are closed for $\Omega < \Omega_B$ and open in the opposite case. The values of the ratio Ω/Ω_B for the trajectories shown at the figure are 0.2, 0.5, 0.95, 1.0, 1.05, 2, and 3.

$$\mathcal{H} = \frac{p_z^2}{2m} + \frac{1}{2m} (P_x + eBy)^2 + 2\Lambda \left[1 - \cos\left(\frac{p_y l}{\hbar}\right) \right] - eFy, \quad (2.2)$$

and gives the following expressions for the velocity components,

$$v_x = \frac{p_x}{m}, \quad v_y = 2v_\perp \sin\left(\frac{p_y l}{\hbar}\right), \quad v_z = \frac{p_z}{m}, \quad (2.3)$$

where $p_x = P_x + eBy$, and $v_\perp = \Lambda l/\hbar$. The equations of motion resulting from the Hamiltonian Eq. (2.2) are

$$\dot{p}_x = ev_y B = \Omega_B p_\Lambda \sin\left(\frac{p_y l}{\hbar}\right), \quad (2.4a)$$

$$\dot{p}_y = eF - ev_x B = eF - \frac{eB}{m} p_x, \quad (2.4b)$$

where

$$\Omega_B = \frac{eB}{\sqrt{mm_\perp}}, \quad (2.5)$$

$p_\Lambda = \sqrt{2m\Lambda}$, and $m_\perp = \hbar^2/(2\Lambda l^2)$ is the electron effective mass at the bottom of the miniband. Equations (2.4) have the following integral

$$\sin^2\left(\frac{p_y l}{2\hbar}\right) + \frac{(mF/B - p_x)^2}{4p_\Lambda^2} = \left(\frac{\Omega}{\Omega_B}\right)^2, \quad (2.6)$$

where $\Omega > 0$ is a constant of the integration. Equations (2.4) are pendulum equations and their solution is expressed in terms of elliptic functions, see Fig. 2.1. In

the case $\Omega > \Omega_B$ there are two solutions for each value of Ω . We have for first solution $p_x < mF/B$ and

$$p_y(t) = \frac{2\hbar}{l} \text{am}(\Omega t) \quad (2.7a)$$

$$p_x(t) = \frac{mF}{B} - 2p_\Lambda \frac{\Omega}{\Omega_B} \text{dn}(\Omega t), \quad (2.7b)$$

where the modulus of the elliptic functions is $k = \Omega_B/\Omega$. These equations describe open trajectories in momentum space. Since the values of the electron quasimomentum p_y are limited by the interval $-\pi\hbar/l < p_y < \pi\hbar/l$ only a fractional part $\text{am}(\Omega t)/\pi$ should be kept in Eq. (2.7a). The second solution, which corresponds to $p_x > mF/B$, can be obtained from Eqs. (2.7a,2.7b) by changing Ω to $-\Omega$.

In the case $\Omega < \Omega_B$ electron trajectories are closed and there is only one trajectory for each value of Ω . Electron momenta $p_y(t)$ and $p_x(t)$ are again expressed in terms of elliptic functions, but the modulus is different, $k = \Omega/\Omega_B$,

$$p_y(t) = \frac{2\hbar}{l} \arcsin\left[\frac{\Omega}{\Omega_B} \text{sn}(\Omega_B t)\right] \quad (2.7c)$$

$$p_x(t) = \frac{mF}{B} - 2p_\Lambda \frac{\Omega}{\Omega_B} \text{cn}(\Omega_B t). \quad (2.7d)$$

In the case $\Omega = \Omega_B$ the solution is expressed in the elementary functions

$$p_y(t) = \pm \frac{2\hbar}{l} \arcsin[\tanh(\Omega t)] \quad (2.7e)$$

$$p_x(t) = \frac{mF}{B} \mp 2p_\Lambda \text{sech}(\Omega t). \quad (2.7f)$$

For further calculations we also need expressions for the y -component of the electron velocity,

$$v_y(t) = \begin{cases} 4v_{\perp} \text{sn}(\Omega t) \text{cn}(\Omega t), & k = \Omega_B/\Omega < 1, \\ 4v_{\perp} k \text{sn}(\Omega_B t) \text{dn}(\Omega_B t), & k = \Omega/\Omega_B < 1, \\ 4v_{\perp} \tanh(\Omega t) \text{sech}(\Omega t), & \Omega = \Omega_B. \end{cases} \quad (2.8)$$

The motion of the electron in real space can be obtained by the integration of electron velocities. The integration of Eq. (2.8) shows that the y -coordinate oscillates around some value y_0 , which can be considered as the third integral of the motion after p_z and Ω . The total electron energy is conserved and can be represented as a function of the integrals of the motion

$$E = \frac{p_z^2}{2m} + \frac{1}{2m} \left(\frac{mF}{B} - 2p_{\Lambda} \frac{\Omega}{\Omega_B} \right)^2 - eFy_0. \quad (2.9)$$

2.3. SOLUTION OF THE BOLTZMANN EQUATION

For the calculation of the current we make use of the Boltzmann equation for one electron distribution function $f(\mathbf{p})$

$$eBv_y \frac{\partial f}{\partial p_x} + (eF - eBv_x) \frac{\partial f}{\partial p_y} = \left(\frac{\partial f}{\partial t} \right)_{\text{coll}}. \quad (2.10)$$

The collision integral on the right hand side of this equation includes elastic scattering mechanisms (impurity scattering, surface roughness scattering and, possibly, absorption and immediate emission of an optical phonon) and inelastic ones (acoustic and optical phonons). Elastic relaxation time is typically about 10^{-13} sec. Concerning inelastic relaxation, we assume that both the Fermi energy and temperature are smaller than the optical phonon energy $\hbar\Omega_{LO}$ so that the energy relaxation due to optical phonon emission can be neglected.^{26,43} The inelastic relaxation time due to acoustic phonon scattering typically is about 10^{-10} sec or larger. This means that the main relaxation mechanism in Eq. (2.10) is elastic scattering.

We will consider the elastic scattering of the electrons as point scattering, when the electron position and electron kinetic energy, $E_{\mathbf{p}}$, are conserved. This approximation is justified if the electron wavelength is much larger than the length scale of the scatter. For electron motion in the growth direction the electron wavelength ranges from one superlattice period to the superlattice length. At the same time, scattering in the adjacent wells can be considered as uncorrelated. The electron in-plane wavelength depends on the electron kinetic energy, that is typically about or less than 10meV, and leads to the wavelength $\gtrsim 5000\text{\AA}$. The length scale of the in-plane

elastic scattering is very short because in superlattices the spacer separating impurities from electrons in quantum wells is smaller than the superlattice period and the correlation length of the surface roughness typically is about 500\AA (see e.g. Ref. 66 and Section 4.4).

It is important to note that $E_{\mathbf{p}}$ is not an integral of motion and is not conserved along a trajectory. Elastic collisions lead to relaxation of the electron distribution to its average over the surface of constant kinetic energy,

$$\bar{f}(E) = \frac{\int d\mathbf{p} f(\mathbf{p}) \delta(E - E_{\mathbf{p}})}{\int d\mathbf{p} \delta(E - E_{\mathbf{p}})}. \quad (2.11)$$

The locality of elastic scattering means also that the matrix element of the scattering is a constant, which allows us to describe the elastic collision operator with the help of the constant relaxation time, $[\bar{f}(E_{\mathbf{p}}) - f(\mathbf{p})]/\tau$.

The electron gas can be appreciably heated by a strong electric field $\Omega_E \tau \sim 1$. In this case $f(E)$ can be significantly different from the equilibrium function. In this work we will elaborate two limiting cases when the difference between $\bar{f}(E)$ and the Fermi function with some effective temperature T , $f_0(E)$, is not important for the calculation of the current. In the first case, $T \ll E_F$, the electron gas is degenerate and a detailed structure of the electron distribution near the Fermi surface does not make any difference. In the second case, $E_F \ll T \approx T_s$ where T_s is the lattice temperature, electron heating can be neglected.²⁶ It is worth noting that at strong magnetic fields, quantum corrections to the classical Boltzmann equation (2.10) can be neglected only at high enough electron temperature,⁶⁷

$$\frac{\hbar\Omega_B}{2\pi^2 T} \ll 1. \quad (2.12)$$

It is convenient to transform Eq. (2.10) to other variables connected with electron trajectories⁶⁸. These variables are the integrals of motion Ω and p_z , and time $t_{\mathbf{p}}$ necessary for an electron to move from some fixed point in momentum space to the point \mathbf{p} . In the new variables the kinetic equation becomes

$$\frac{\partial f}{\partial t_{\mathbf{p}}} = \frac{f_0(E_{\mathbf{p}}) - f(\mathbf{p})}{\tau}. \quad (2.13)$$

The formal solution to this equation is $f(\mathbf{p}) = f_0(E_{\mathbf{p}}) + f_1(\mathbf{p})$ where

$$f_1(\mathbf{p}) = - \int_{-\infty}^{t_{\mathbf{p}}} eFv_y(t) f'_0(E_{\mathbf{p}}(t)) e^{-(t_{\mathbf{p}}-t)/\tau} dt. \quad (2.14)$$

Here f'_0 is the derivative of the distribution function. Terms depending on time in $E_{\mathbf{p}}$ are of the order of Λ . If these terms are neglected then f'_0 can be considered time independent and Eq. (2.14) becomes

$$f_1(\mathbf{p}) = -eF\tau Q_{\mathbf{p}} \frac{df_0}{dE_{\mathbf{p}}}, \quad (2.15)$$

where

$$= \int_{-\infty}^{t_{\mathbf{p}}} v_y(t) e^{-(t_{\mathbf{p}}-t)/\tau} dt = (1 + \tau \partial / \partial t_{\mathbf{p}})^{-1} v_y. \quad (2.16)$$

is a periodic function of time. The Fourier series representation of $Q_{\mathbf{p}}$ is given in Appendix 2.9.

Corrections to Eq. (2.15) contain $\Lambda^n f_0^{(n+1)}$ which formally is of the order of $(\Lambda/T)^n$. The electric current, however, contains integrals of this function and after an integration by parts, $f_0^{(n+1)}$ in the integrand is replaced by a quantity of the order of $f_0' / \max(E_F, T)^n$. Therefore, for the calculation of current, Eq. (2.15) is justified when

$$\Lambda \ll \max(E_F, T), \quad (2.17)$$

which is assumed to be satisfied in this work.

The factor $Q_{\mathbf{p}}$ can be separated into two parts, $Q_{\mathbf{p}} = Q_{\mathbf{p}}^x + Q_{\mathbf{p}}^y$ where $Q_{\mathbf{p}}^x$ is even and $Q_{\mathbf{p}}^y$ is odd with respect to v_y . Only the odd part contributes to the current in the y direction. From Eqs. (2.3) and (2.4) it is obvious that v_y is odd in time so that the parity with respect to v_y is the same as the parity with respect to time. For that reason $Q_{\mathbf{p}}^y$ is obtained from the second expression in Eq. (2.16) keeping only even derivatives of v_y . Therefore

$$Q_{\mathbf{p}}^y = \frac{1}{1 - \tau^2 \partial^2 / \partial t_{\mathbf{p}}^2} v_y. \quad (2.18)$$

This function is easily calculated in two limiting cases. Far from the region of closed trajectories given by the condition $\Omega \gg \Omega_B$, we have $v_y = 2v_{\perp} \sin(2\Omega t)$. Then $\partial^2 \sin(2\Omega t) / \partial t^2 = -(2\Omega)^2 \sin(2\Omega t)$ and we obtain

$$Q_{\mathbf{p}}^y = \frac{v_y}{1 + (2\Omega\tau)^2}. \quad (2.19)$$

Under the same condition, $2\Omega \approx \Omega_B |mF/B - p_x| / p_{\Lambda}$, which means that $Q_{\mathbf{p}}^y$ as a function of p_x has a resonance at $p_x = mF/B$. The width of the resonance is $p_{\Lambda} / (\Omega_B \tau)$. If this width is much larger than the width of the region of closed trajectories, p_{Λ} , that is $\Omega_B \tau \ll 1$, the latter can be neglected and Eq. (2.19) can be used for all values of p_x .

The second limiting case is a strong magnetic field when $\Omega_B \tau \gg 1$, i.e., the width of the resonance in Eq. (2.19) is smaller than the width of the region of closed trajectories. Then the unit in Eq. (2.18) can be neglected compared to the second derivative, so that $-\tau^2 (\partial^2 Q_{\mathbf{p}}^y / \partial t^2) = v_y$. The integration is carried out with the help of the equation of motion, Eq. (2.4), and the result is

$$Q_{\mathbf{p}}^y = \frac{2v_{\perp}}{(\Omega_B \tau)^2} \begin{cases} \frac{p_y d}{\hbar} - \frac{\pi t_{\mathbf{p}}}{T_{\mathbf{p}}}, & \Omega > \Omega_B \\ \frac{p_y d}{\hbar}, & \Omega < \Omega_B \end{cases}, \quad (2.20)$$

where half of the period $T_{\mathbf{p}}$ is given by Eq. (2.63). One can verify that Eqs. (2.19) and (2.20) have the same asymptotic behavior when $1/\tau \ll \Omega_B \ll \Omega$.

These two limits show that the perturbation of the distribution function due to an electric field has a resonant behavior. The physical reasons of the resonance have been discussed in Sec. 2.1. If the resonance region is wider than the region of closed trajectories the maximum value of $Q_{\mathbf{p}}^y$ is of the order of v_{\perp} . If the relaxation time is very long, $\Omega_B \tau \gg 1$, the value of $Q_{\mathbf{p}}^y$ is reduced by the factor of $(\Omega_B \tau)^2$ due to oscillations of v_y along the electron trajectory during the time τ .

2.4. CALCULATION OF THE ELECTRIC CURRENT

The part of the distribution function which depends only on $E_{\mathbf{p}}$ does not contribute to the electric current, and the current in the field direction is

$$j = -2e^2 F \tau \int \frac{d\mathbf{p}}{(2\pi\hbar)^3} \frac{df_0}{dE_{\mathbf{p}}} Q_{\mathbf{p}}^y v_y(\mathbf{p}). \quad (2.21)$$

Two factors in the integrand, $df_0/dE_{\mathbf{p}}$ and $Q_{\mathbf{p}}^y$, have maxima and the value of the integral crucially depends on the relation between the widths of these maxima. The width of the $Q_{\mathbf{p}}^y$ maximum depends on the value of $\Omega_B \tau$. If this product is small then the width is $p_{\Lambda} / (\Omega_B \tau)$. In the opposite case it is p_{Λ} . The width of the distribution function derivative is of the order of $p_T \equiv \sqrt{2mT}$. Three cases are possible, $(\Omega_B \tau)^2 \ll (p_{\Lambda} / p_T)^2 = \Lambda/T$ when the region of closed trajectories is not important and the width of $Q_{\mathbf{p}}^y$ is much larger than the width of $df_0/dE_{\mathbf{p}}$, $\Lambda/T \ll (\Omega_B \tau)^2 \ll 1$ when the region of closed trajectories also is not important but the width of $Q_{\mathbf{p}}^y$ is much smaller than the width of $df_0/dE_{\mathbf{p}}$, and $\Omega_B \tau \gg 1$ when only the vicinity of closed trajectories contributes to the resonance. We consider these three cases separately.

2.4.1. Weak magnetic field, $(\Omega_B \tau)^2 \ll \Lambda/T$

In this case Eq. (2.19) can be used for computation of $Q_{\mathbf{p}}^y$ on the right hand side of Eq. (2.21). After the integration with respect to p_y one obtains

$$j_y = -\frac{4e^2 F l \tau \Lambda^2}{\hbar^2} \int \frac{dp_x dp_z}{(2\pi\hbar)^2} \times \frac{df_0}{dE_{\mathbf{p}}} \left[1 + \left(\Omega_F \tau - \Omega_B \tau \frac{p_x}{p_{\Lambda}} \right)^2 \right]^{-1}, \quad (2.22)$$

where we introduced frequency of the Bloch oscillations

$$\Omega_F = \frac{eFl}{\hbar}.$$

Under the condition in the title of this subsection the absolute value of the momentum in the integral is controlled by $df_0/dE_{\mathbf{p}}$ and

$$\begin{aligned} j_y &= \frac{e^2 F l \tau \Lambda^2 m}{\pi^2 \hbar^4} \int_0^{2\pi} \frac{d\phi}{1 + (\Omega_F \tau - \Omega_B \tau p_F \cos \phi / p_\Lambda)^2} \\ &= \frac{\sqrt{2} e^2 F l \tau \Lambda^2 m}{\pi \hbar^4} \frac{\sqrt{r - \eta}}{r}, \end{aligned} \quad (2.23)$$

where

$$\begin{aligned} \eta &= \Omega_F^2 \tau^2 - \Omega_B^2 \tau^2 \frac{p_F^2}{p_\Lambda^2} - 1, \\ r^2 &= (\eta + 2)^2 + 4 \Omega_B^2 \tau^2 \frac{p_F^2}{p_\Lambda^2} \end{aligned} \quad (2.24)$$

In the nondegenerate case the main contribution into the integral Eq. (2.22) is given by $p_x \lesssim p_T$ which is small compared to $p_\Lambda / \Omega_B \tau$. If p_x is neglected in the square brackets in Eq. (2.22) the result is independent of the magnetic field. So in this case the magnetic field introduces just a small correction computed for the first time by Epshtein³¹,

$$j_y = \frac{4e\Lambda^2 n}{\hbar T} \frac{\Omega_F \tau}{1 + (\Omega_F \tau)^2} \left\{ 1 + \Omega_B^2 \tau^2 \frac{T}{2\Lambda} \frac{3(\Omega_F \tau)^2 - 1}{[1 + (\Omega_F \tau)^2]^2} \right\}, \quad (2.25)$$

where n is the sheet concentration. Both of the results, Eqs. (2.23) and (2.25) describe an I - V characteristic that has a peak. At zero magnetic field the peak position is given by the condition $\Omega_F \tau = 1$. With the increase of the magnetic field this peak shifts to a higher bias.

Equation (2.25) shows that magnetoresistance changes its sign at $\Omega_F^2 \tau^2 = 1/3$, or $F = \hbar l / (e\tau\sqrt{3})$. The magnetoresistance is positive for a weaker electric field and negative for a stronger one. For the Fermi statistics the same effect takes place when the magnetic field goes to zero, which can be proved by expansion of Eq. (2.23).

2.4.2. Intermediate field, $\Lambda/T \ll (\Omega_B \tau)^2 \ll 1$

In this case Eq. (2.22) also can be used. However, the value of p_x is controlled now by the Lorentz factor. This factor picks up particles from the phase space, which have values of momentum near $p_x = p_\Lambda \Omega_F / \Omega_B = mF/B$, see Fig. 2.2. Then the integration with respect to p_x gives

$$j = \frac{e^2 F l \Lambda^2 m}{\pi \hbar^4 \Omega_B} \Phi(F, B), \quad (2.26a)$$

$$\Phi(F, B) = \frac{p_\Lambda}{m} \int dp_z \left(\frac{\partial f_0}{\partial E} \right)_{p_x = mF/B}$$

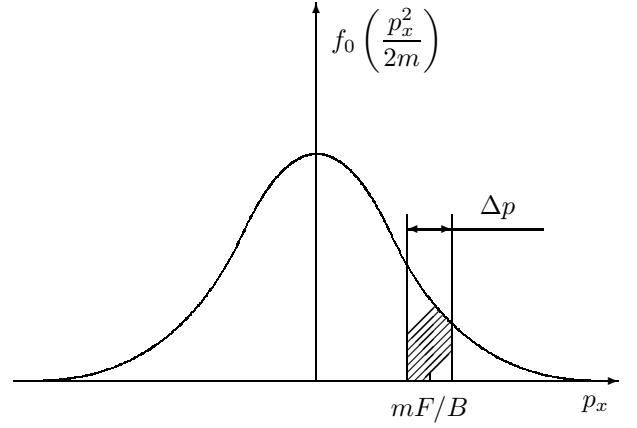


FIG. 2.2. The division of the electron distribution into a nonresonant part and a resonant part (hatching area) in an intermediate and strong magnetic field. The width of the resonance, Δp , is p_Λ or $p_\Lambda / (\Omega_B \tau)$, whichever is larger.

$$= \begin{cases} \frac{\sqrt{2} \hbar^2 n}{(mT/\pi)^{3/2}} p_\Lambda e^{-(mF/B)^2 / p_T^2}, & T \gg E_F \\ \frac{p_\Lambda}{\sqrt{p_F^2 - (mF/B)^2}}, & T \ll E_F \end{cases}, \quad (2.26b)$$

In the case of Fermi statistics, Eq. (2.26b) is valid only if $p_F - mF/B \gg p_T$. This result is also the limiting form of Eq. (2.23) when $p_F - mF/B \gg p_\Lambda / (\Omega_B \tau)$. Therefore the reciprocal square root singularity obtained near the point $mF/B = p_F$ is smeared either due to the temperature or due to the width of the resonance, whichever is larger. When $mF/B > p_F$ the current drops off and the position of the current maximum is given by $mF/B = p_F$, i.e., $F = (p_F/m)B$. In the case of Boltzmann statistics, the position of the current maximum is $mF/B = p_T / \sqrt{2}$, i.e., $F = (p_T / m\sqrt{2})B$, meaning that in the intermediate magnetic field limit the current peak shifts linearly with B .

2.4.3. Strong magnetic field, $\Omega_B \tau \gg 1$

The calculation in this case is similar to that in the previous section. The only difference is that it is necessary to use Eq. (2.20) for $Q_{\mathbf{p}}^y$ and the integration with respect to p_y can be carried out in a different way. After the separation of the integration with respect to p_x

$$j = \frac{8R}{\pi^2} \frac{e^2 m \Lambda^2 l}{\hbar^4 \Omega_B^2 \tau} F \Phi(F, B), \quad (2.27)$$

where the dimensionless constant of the order of unity,

$$R = \left(32\pi \frac{p_\Lambda \hbar}{l} \frac{v_\perp^2}{(\Omega_B \tau)^2} \right)^{-1} \int Q_{\mathbf{p}}^y v_y dp_x dp_y, \quad (2.28)$$

is calculated in Appendix. 2.10.

It is instructive to note that Eq. (2.27) can be written down in the form similar to that in the bulk,

$$j = \frac{\tilde{n}e^2}{m_{\perp}} \frac{F}{\Omega_B^2 \tau}. \quad (2.29)$$

Here \tilde{n} is the effective electron concentration, i.e., the number of the electrons inside the resonance region

$$\tilde{n} = \frac{4R}{\pi^2} \frac{m\Lambda}{\hbar^2 l} \Phi(F, B) \quad (2.30)$$

2.5. ESTIMATION OF THE ROLE OF THE HALL EFFECT.

Typically, in the current-voltage characteristic measurement in superlattices, Hall contacts are not fabricated. Then, in a magnetic field, a Hall voltage comes about which can affect the value of the current. As a result of this effect in a weak electric field the quantity measured in the experiment is not the conductivity σ_{xx} but the resistivity ρ_{xx} . In this section we show that the effect of the Hall voltage on the current-voltage characteristic in a superlattice can be neglected.

The Hall field F_x and the current in the growth direction can be calculated from the equations

$$j_y = j_y^{(0)} + \sigma_{yx} F_x, \quad (2.31)$$

$$j_x = j_H + \sigma_{xx} F_x = 0. \quad (2.32)$$

where $j_y^{(0)}$ is the value of the current for zero Hall field and j_H is the Hall current under the same condition. All the components of the conductivity may depend on the field F_y . Both $j_y^{(0)}$ and j_H nontrivially depend on F_y . The conductivity components σ_{yx} and σ_{xx} also can depend on F_y . This dependence results from a narrow miniband characterizing the electron motion in this direction. There is no such small energy scale for the in-plane electron motion, so that the effect of F_x on $j_y^{(0)}$, j_H , and the conductivity components can be neglected.

In the calculation of the Hall current

$$j_H = 2e \int \frac{d\mathbf{p}}{(2\pi\hbar)^3} v_x f_1(\mathbf{p}), \quad (2.33)$$

it is convenient to make use of the identity

$$\int_{-\pi\hbar/d}^{\pi\hbar/d} f_1(\mathbf{p}) dp_y = -eB\tau \frac{\partial}{\partial p_x} \int_{-\pi\hbar/d}^{\pi\hbar/d} v_y f_1(\mathbf{p}) dp_y, \quad (2.34)$$

which is obtained by the integration of the Boltzmann equation (2.10) with respect to p_y . The substitution of Eq. (2.34) into Eq. (2.33) gives the result

$$j_H = \frac{eB\tau}{m} j_y^{(0)} \quad (2.35)$$

which is very well known for the bulk semiconductors with a constant relaxation time.

In order to calculate σ_{xx} and σ_{yx} it is necessary to introduce into the Boltzmann equation a small x -component of the electric field and calculate the perturbation of the distribution function, f_2 , caused by this field. After the linearization with respect to this field, the Boltzmann equation becomes

$$eF_x \frac{\partial f}{\partial p_x} + \frac{\partial f_2}{\partial t_{\mathbf{p}}} = -\frac{f_2}{\tau}, \quad (2.36)$$

where $f = f_0 + f_1$ is the distribution function obtained in Sec. 2.3 for the case $F_x = 0$.

The integration of Eq. (2.36) with respect to p_y gives the identity

$$\int_{-\pi\hbar/d}^{\pi\hbar/d} f_2(\mathbf{p}) dp_y = -eF_x \tau \frac{\partial f}{\partial p_x} - eB\tau \frac{\partial}{\partial p_x} \int_{-\pi\hbar/d}^{\pi\hbar/d} v_y f_2(\mathbf{p}) dp_y, \quad (2.37)$$

that results in the relation between the conductivities,

$$\sigma_{xx} = \frac{ne^2\tau}{md} + \frac{eB\tau}{m} \sigma_{yx}. \quad (2.38)$$

Therefore only one of them, say σ_{yx} , has to be calculated.

A formal solution to Eq. (2.36) is

$$f_2 = \frac{-eF_x\tau}{1 + \tau\partial/\partial t_{\mathbf{p}}} \frac{\partial}{\partial p_x} \frac{1}{1 + \tau\partial/\partial t_{\mathbf{p}}} f_0(E_{\mathbf{p}}) \quad (2.39)$$

Then

$$\sigma_{yx} = \left\langle v_y \frac{1}{1 + \tau\partial/\partial t_{\mathbf{p}}} \frac{\partial}{\partial p_x} \frac{1}{1 + \tau\partial/\partial t_{\mathbf{p}}} f_0(E_{\mathbf{p}}) \right\rangle, \quad (2.40)$$

where

$$\langle \dots \rangle = -2e^2\tau \int \frac{d\mathbf{p}}{(2\pi\hbar)^3}. \quad (2.41)$$

We will show now that σ_{yx} can be expressed in terms of σ_{yy} which is defined by the relation $j_y^{(0)} = \sigma_{yy} F_y$. With the help of the definition Eq. (2.41)

$$\sigma_{yy} = \left\langle v_y \frac{1}{1 + \tau\partial/\partial t_{\mathbf{p}}} v_y \frac{\partial f_0}{\partial E} \right\rangle. \quad (2.42)$$

With the help of the commutation relation

$$\left[\frac{\partial}{\partial t_{\mathbf{p}}}, \frac{\partial}{\partial p_x} \right] = \frac{eB}{m} \frac{\partial}{\partial p_y} \quad (2.43)$$

it is easy to show that

$$\begin{aligned} & \left(1 + \tau \frac{\partial}{\partial t_{\mathbf{p}}}\right)^{-1} \frac{\partial}{\partial p_x} = \frac{\partial}{\partial p_x} \left(1 + \tau \frac{\partial}{\partial t_{\mathbf{p}}}\right)^{-1} \\ & - \frac{eB\tau}{m} \left(1 + \tau \frac{\partial}{\partial t_{\mathbf{p}}}\right)^{-1} \frac{\partial}{\partial p_y} \left(1 + \tau \frac{\partial}{\partial t_{\mathbf{p}}}\right)^{-1}. \end{aligned} \quad (2.44)$$

The substitution of Eq. (2.44) into Eq. (2.40) gives

$$\begin{aligned} \sigma_{yx} &= -\frac{eB\tau}{m} \\ & \times \left\langle v_y \frac{1}{1 + \tau \partial/\partial t_{\mathbf{p}}} \frac{\partial}{\partial p_y} \left(\frac{1}{1 + \tau \partial/\partial t_{\mathbf{p}}} \right)^2 f_0(E_{\mathbf{p}}) \right\rangle \end{aligned} \quad (2.45)$$

Now we make use of the commutation relation

$$\left[\frac{\partial}{\partial t_{\mathbf{p}}}, \frac{\partial}{\partial p_y} \right] = -\frac{eB}{m} \frac{dv_y}{dp_y} \frac{\partial}{\partial p_y} \quad (2.46)$$

to estimate the commutator of the operator factors in Eq. (2.45). If we take into account that $\partial/\partial t_{\mathbf{p}} \sim \Omega$ then the ratio of the commutator of $\partial/\partial p_y$ and $(1 + \tau \partial/\partial t_{\mathbf{p}})^{-1}$ to the product of these operators is of the order of $[\Omega_B \tau / (1 + \Omega \tau)] (p_{\Lambda} / p_x)$. The last quantity is much smaller than unity due to Eq. (2.17) and $\Omega_B \lesssim \Omega$, which means the commutator of $\partial/\partial p_y$ and $(1 + \tau \partial/\partial t_{\mathbf{p}})^{-1}$ can be neglected in Eq. (2.45). Then Eq. (2.45) becomes

$$\sigma_{yx} = -\frac{eB\tau}{m} \left\langle v_y \left(\frac{1}{1 + \tau \partial/\partial t_{\mathbf{p}}} \right)^3 v_y \frac{\partial f_0}{\partial E} \right\rangle \quad (2.47)$$

The expression above is proportional to the second derivative of the σ_{yy} with respect to the field, which can be proved as follows. First of all Eq. (2.42) gives

$$\begin{aligned} \frac{\partial^2}{\partial F_y^2} \sigma_{yy} &= 2e^2 \tau^2 \left\langle v_y \frac{1}{1 + \tau \partial/\partial t_{\mathbf{p}}} \right. \\ & \times \left. \frac{\partial}{\partial p_y} \frac{1}{1 + \tau \partial/\partial t_{\mathbf{p}}} \frac{\partial}{\partial p_y} \frac{1}{1 + \tau \partial/\partial t_{\mathbf{p}}} v_y \frac{\partial f_0}{\partial E} \right\rangle \\ &= -2 \left(\frac{e\tau d}{\hbar} \right)^2 \left\langle v_y \left(\frac{1}{1 + \tau \partial/\partial t_{\mathbf{p}}} \right)^3 v_y \frac{\partial f_0}{\partial E} \right\rangle. \end{aligned} \quad (2.48)$$

Here we neglect the commutator of $\partial/\partial p_y$ and $(1 + \tau \partial/\partial t_{\mathbf{p}})^{-1}$ once again, and make use of $\partial^2 v_y / \partial p_y^2 = -(d^2/\hbar^2)v_y$. The comparison of Eq. (2.47) with Eq. (2.48) gives

$$\sigma_{yx} = \frac{eB\tau}{2m} \left(\frac{\hbar}{e\tau l} \right)^2 \frac{\partial^2 \sigma_{yy}}{\partial F_y^2}. \quad (2.49)$$

In the limit of a small F_y one can easily verify that $-\sigma_{yx} = \sigma_{xy} \equiv j_H / F_y$.

Now we can estimate the value of the second term in Eq. (2.31). Making use of Sec. 2.4 we have the relation of the second term in Eq. (2.31) to the first one

$$\begin{aligned} \frac{\sigma_{yx} F_x}{j_0} &= \frac{eB\tau}{m} \frac{\sigma_{yx}}{\sigma_{xx}} \\ &\sim \begin{cases} \Omega_B^2 \tau^2 \frac{\Lambda}{E_F, T}, & \Omega_B^2 \tau^2 \ll \frac{\Lambda}{E_F, T} \\ \frac{1}{\Omega_B \tau} \left(\frac{\Lambda}{E_F, T} \right)^{5/2}, & \frac{\Lambda}{E_F, T} \ll \Omega_B^2 \tau^2 \ll 1 \\ \frac{1}{\Omega_B^2 \tau^2} \left(\frac{\Lambda}{E_F, T} \right)^{5/2}, & 1 \ll \Omega_B^2 \tau^2 \end{cases} \end{aligned} \quad (2.50)$$

and one can see that this ratio is small in all considered limits.

2.6. DISCUSSION

One of the most interesting results of Sec. 2.4 is that in some region of magnetic field, $\Lambda/T \ll (\Omega_B \tau)^2 \ll 1$, the current does not depend on the relaxation time, see Eq. (2.26). That means that a finite resistivity of a superlattice exists even without scattering. To understand the physical reason of this result it is instructive to note that the considered problem is quite similar to the propagation of a longitudinal wave in a collisionless plasma. Indeed, if we consider the miniband width as a small parameter ($v_y = [2\Lambda l/\hbar] \sin[p_y l/\hbar]$ and for $\Lambda = 0$ the current in the growth direction is zero) then in the linear approximation in Λ and neglecting collisions, Eq. (2.10) takes the form

$$eB \left(v_x - \frac{F}{B} \right) \frac{\partial f}{\partial p_y} - \frac{2eB\Lambda l}{\hbar} \sin \frac{p_y l}{\hbar} \frac{\partial f_0(E_{\mathbf{p}})}{\partial p_x} = 0. \quad (2.51)$$

On the other hand, the Boltzmann equation for a collisionless plasma with an electric field in the wave $F_0 \sin k(x - v_p t)$ is⁶⁵

$$(v_x - v_p) \frac{\partial f}{\partial x} + eF_0 \sin k(x - v_p t) \frac{\partial f_0(E_{\mathbf{p}})}{\partial p_x} = 0. \quad (2.52)$$

The comparison of these equations shows that there is a one to one correspondence

plasma	superlattice
$x - v_p t$	p_y / eB
k	eBl/\hbar
v_p	F/B
eF_0	$-2eB\Lambda l/\hbar$

In a plasma there exists a resonant group of electrons moving with the velocity close to the wave velocity, v_p . This group of electrons strongly interacts with the wave, resulting in the collisionless Landau damping. A similar resonant group of electrons exists in a superlattice. Those are electrons moving in the x direction with the Hall drift velocity, F/B . For those electrons the Lorentz force

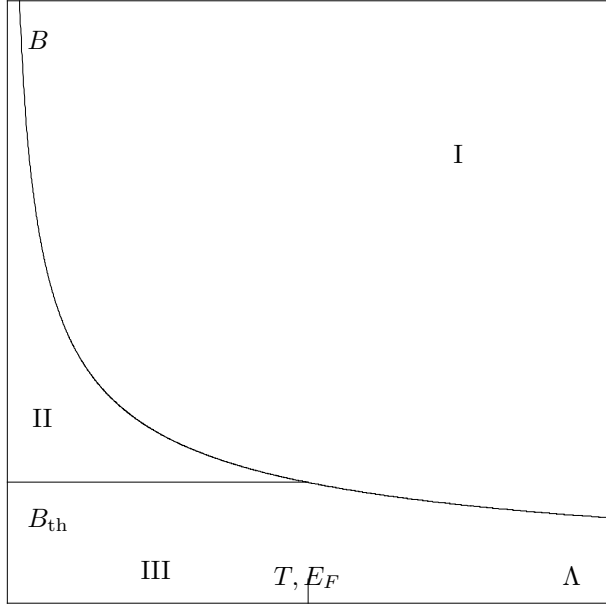


FIG. 2.3. I,-region of the strong magnetic field, II,-region of the collisionless conductivity, and III,-region of the weak magnetic field. The threshold value of the magnetic field, $B_{\text{th}} \sim \hbar m/[el\tau(p_F, p_T)]$, is only a few T for superlattices.

cancels out with the force of the electric field and their velocity in the y direction does not oscillate in time. As a result their contribution to the current is nonzero.

The correspondence between a monochromatic plasma wave and a superlattice in crossed electric and magnetic fields can be extended even beyond the linear Landau damping in plasma and the linear in Λ theory in a superlattice. Because of some specifics of collisions in a gas plasma, a close correspondence in this case exists between the superlattice and the solid state plasma⁶⁹. We show here only the correspondence between the applicability conditions for the linear theory.

In plasma a wave with a finite amplitude traps the resonant electrons and they oscillate in potential wells of the wave. The linear theory is applicable if the period of the oscillation is larger than a scattering time which can be written as $eF_0k\tau^2/m \ll 1$. The above correspondence between the plasma and superlattice quantities immediately gives the condition for the superlattice, $\Omega_B^2\tau^2 \ll 1$. The physical meaning of that condition is quite similar to the plasma one. A finite width of the miniband in the superlattice leads to Bloch oscillations of resonant electrons. Then the theory which is linear in Λ is justified if the period of the oscillation is larger than the relaxation time.

The situation when the collision term can be neglected in the kinetic equation is typical for plasma and given by the condition⁶⁵ $kp_T\tau/m \gg 1$. Regarding the superlattice, this condition becomes the condition of the inter-

mediate magnetic field $\Omega_B\tau(p_T/p_\Lambda) \gg 1$. In the case of the degenerate electron gas important for superlattices, the collisions can be neglected under a more weak condition. Equation. (2.22) takes the form of the Eq. (2.26) for $E_F \gg T$, when $\Omega_B\tau(p_F/p_\Lambda) \gg 1$, i.e. the range of the magnetic field when the collisionless conductivity takes place in superlattices is

$$\frac{\Lambda}{E_F, T} \ll \Omega_B^2\tau^2 \ll 1. \quad (2.53)$$

The existence of this effect depends on the relation between miniband width and characteristic electron energy which is schematically shown in the diagram Fig. 2.3. The plane B - Λ in this diagram is divided into three parts corresponding to the different regimes. The collisionless conductivity (intermediate magnetic field regime) can be observed only if $\Lambda \ll E_F, T$, region II in the diagram Fig. 2.3. The strong magnetic field limit, region I in Fig. 2.3, is the same for small and large Λ ; electric current exhibits $1/\tau$ dependence. The positive or negative magnetoresistance can be observed in the regime of the weak magnetic field, region III in Fig. 2.3, depending on the electric field. Due to the large period of the superlattice the boundary between regions II and III lies in the experimentally available range of the magnetic fields.

2.7. COMPARISON WITH EXPERIMENT

The influence of the electric and magnetic fields on the current in the superlattice was measured in two types of experiments. In the first kind of experiments^{51,57} the I - V curve of the superlattice was measured in the presence of the constant magnetic field. The position of the current peak depends on the magnetic field and this dependence can be plotted in the B - F diagram. In the other kind of experiments^{57,58} the dependence of the electric current on the magnetic field was measured in the presence of a constant electric field. A peak in the I - B curve has been detected, and its position can be plotted as a function of the electric field in the B - F diagram.

We describe now the predictions of the present theory for such experiments. The peak on the I - V curve can be obtained from the equation $dj/(dF) = 0$. In the absence of a magnetic field the position of the peak is given by $\Omega_F\tau = 1$, or $F = F_{\text{th}} \equiv \hbar/(el\tau)$. When a weak magnetic field is applied, $B \ll B_{\text{th}}$, where

$$B_{\text{th}} = \begin{cases} \frac{\hbar m}{ep_F l\tau}, & E_F \gg T, \\ \sqrt{2} \frac{\hbar m}{ep_T l\tau}, & E_F \ll T, \end{cases} \quad (2.54)$$

the peak position is shifted by small amount $F - F_{\text{th}} \ll F_{\text{th}}$. In the lowest order of the magnetic field the shift obtained from Eqs. (2.23) and (2.25) is

$$F - F_{\text{th}} \approx \frac{eB^2 d \max(E_F, T)}{2m \hbar/\tau}. \quad (2.55)$$

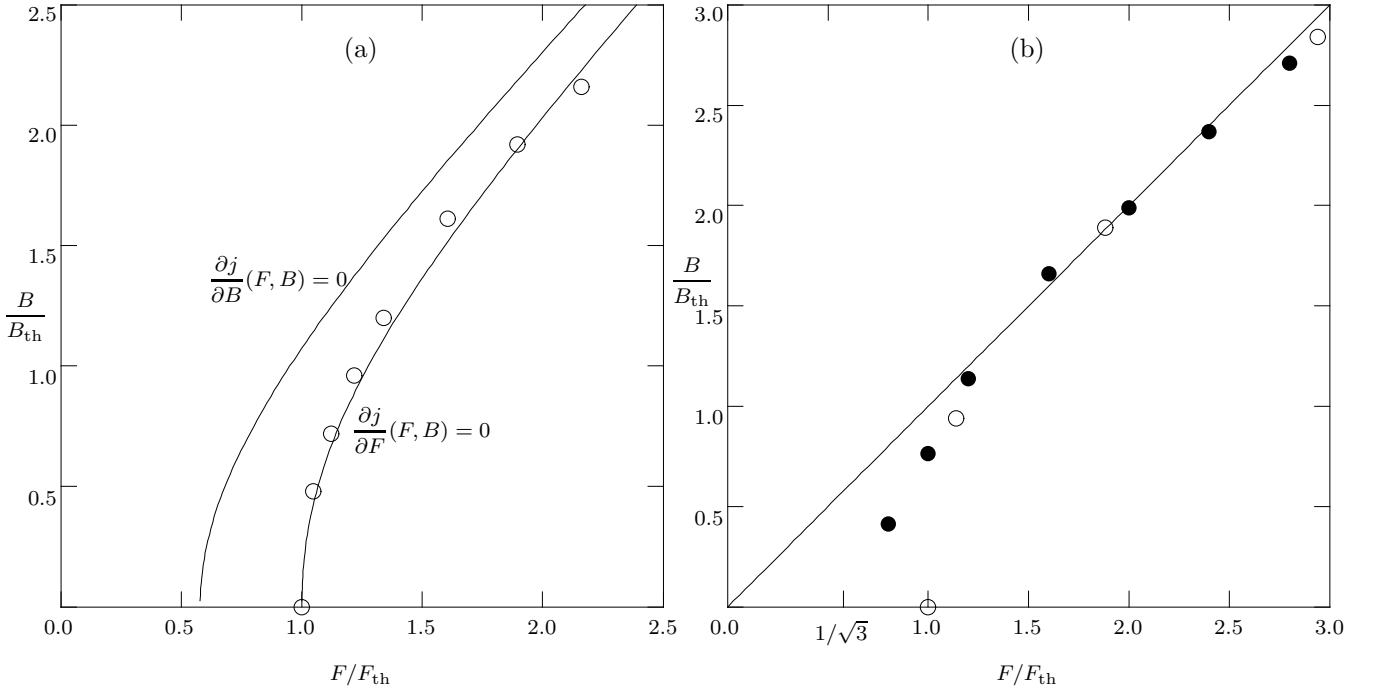


FIG. 2.4. The position of the maximum in I - V characteristics of the superlattice, empty circles, and on I - B characteristics, filled circles. The solid lines are theoretical predictions.

With the increase of the magnetic field $F - F_{\text{th}}$ becomes comparable with F_{th} . This happens when $B \gtrsim B_{\text{th}}$ and in this limit current is given by Eq. (2.26). In this interval of the magnetic field the peak position changes linearly

$$F = \max(v_F, v_T/\sqrt{2}) B = \frac{F_{\text{th}}}{B_{\text{th}}} B. \quad (2.56)$$

The peak in the $I - B$ characteristic is given by the equation $\partial j/\partial B = 0$. In the limit B goes to zero, Eqs. (2.23,2.25) give the solution

$$\left(\frac{F}{F_{\text{th}}}\right)^2 = (\Omega_F \tau)^2 = \frac{1}{3} \quad (2.57)$$

When $B \gtrsim B_{\text{th}}$, the solution to equation $\partial j/\partial B = 0$ coincides with the solution to the equation $\partial j/\partial F = 0$, Eq. (2.56), because the current is a function of F/B , see Eq. (2.26). That is true unless $\Omega_B \tau \gtrsim 1$. In the last case the current acquires the factor $1/B$, Eq. (2.27), and the peak in the $I - B$ curve is shifted to weaker B . In the case of the nondegenerate electron gas and in the limit $\Omega_B \tau \gg 1$ we have the peak position given by $F = v_T B$. Therefore, the peak in the $I - B$ curve lies between $F/(\sqrt{2}v_T)$ and F/v_T depending on $\Omega_B \tau$. In the experiment the peak position in the $I - B$ curve is measured as a function of the applied bias, $V = LF$, where L is the superlattice length, and we have the following useful inequality for the bias corresponding to the peak position

$$\sqrt{\frac{T}{m}} LB \leq V \leq \sqrt{\frac{2T}{m}} LB, \quad B \gtrsim B_{\text{th}}, \quad E_F \ll T. \quad (2.58)$$

In the work of Choi et al⁵¹ the $B - F$ diagram was reported. The superlattice investigated in this experiment has $N = 49$ periods, the length of the period is $l = 166 \text{ \AA}$, the width of the first miniband is $4\Lambda = 0.47 \text{ meV}$, and the concentration of the carriers corresponds to the Fermi energy $E_F = 6 \text{ meV}$. At zero magnetic field the current peak appears near the bias $V_{\text{th}} = NlF_{\text{th}} = 590 \text{ mV}$, and therefore the momentum relaxation time is $\tau = \hbar N/(eV_{\text{th}}) = 0.54 \times 10^{-13} \text{ sec}$. The critical value of the magnetic field is $B_{\text{th}} = 4.2 \text{ T}$. The experimental data from Fig. 7 of this work is plotted in Fig. 2.4(a), empty circles. The solid lines on Fig. 2.4(a) are obtained from Eq. (2.23), since in this experiment $\Omega_B \tau \ll 1$ for the whole range of magnetic fields. The upper curve represents the maximum position on the $I - B$ characteristic and the lower curve represents the maximum position on the $I - F$ characteristic. One can see a good agreement between the lower curve and the experimental points without any fitting parameters.

The both types of measurements (peak position on the $I - B$ curve versus electric field and maximum of the $I - F$ characteristic versus magnetic field) have been reported in the work of Aristone et al⁵⁷. This experiment has been done on low doped samples with E_F much smaller than the temperature $T = 23 \text{ meV}$. The narrowest miniband sample $4\Lambda = 4 \text{ meV}$ has a period $l = 74 \text{ \AA}$ and a length $Nl = 1 \mu\text{m}$. The critical value of the applied bias is $V_{\text{th}} = 500 \text{ mV}$, and therefore the momentum relaxation time is $\tau = \hbar N/(eV_{\text{th}}) = 1.7 \times 10^{-13} \text{ sec}$. Thus, the critical value of the magnetic field is $B_{\text{th}} = 2.1 \text{ T}$. The experimental data from this work is plotted on Fig. 2.4(b). The empty circles represent the peak position on the $I -$

V characteristic taken from Fig. 4 of Ref. 57, and the filled circles represent the peak position on the I - B characteristic taken from Fig. 6 of Ref. 57. On the same graph, Fig. 2.4(b), we draw the line Eq. (2.56) that is asymptotic to the peak positions for intermediate magnetic field. The theoretical prediction for the weak magnetic field regime is not shown on the graph, but one can see that the filled circles (the peak positions on the I - B characteristic measured experimentally) converge to the point $B = 0$, $F = F_{\text{th}}/\sqrt{3}$ in agreement with Eq. (2.57). The good agreement between theory and experiment is obtained without any fitting parameters.

In the experiment of Aristone the samples with the wider minibands were investigated too. The position of the peak on the I - B characteristics of these samples exhibits a weak dependence on the miniband width, that is in agreement with the present theory, since for these samples the limit $\Omega_{B\tau} \sim 1$ is reached. One can check that the inequality Eq. (2.58) is fulfilled for this data.

2.8. CONCLUSIONS

In conclusion, we solved analytically the kinetic equation for the superlattice in crossed electric and magnetic fields, under the assumption that the miniband width is small compared to the Fermi energy or the temperature. Our calculations of the position of the maximum on the I - V and I - B characteristics are in quantitative agreement with experiment. We also found that in a certain range of the magnetic field the current is independent of the electron relaxation time.

2.9. APPENDIX A

The Fourier series expansion of the velocity is

$$v_y(t) = 4v_{\perp} \left(\frac{\pi}{\Omega_B T_{\mathbf{p}}} \right)^2 \sum_{n=1}^{\infty} l_n \operatorname{sech} \left(\frac{\pi l_n K'}{K} \right) \sin \left(\frac{\pi l_n t}{T_{\mathbf{p}}} \right) \quad (2.59)$$

The application of the identity

$$\frac{1}{1 + \tau \partial / \partial t} \sin(\omega t) = \frac{\sin(\omega t) - \omega \tau \cos(\omega t)}{1 + (\omega \tau)^2} \quad (2.60)$$

to each term in the series Eq. (2.59) results in the following series representation for the factor $Q_{\mathbf{p}}$:

$$Q_{\mathbf{p}} = 4v_{\perp} \left(\frac{\pi}{\Omega_B T_{\mathbf{p}}} \right)^2 \sum_{n=1}^{\infty} l_n \operatorname{sech} \left(\frac{\pi l_n K'(k)}{K(k)} \right) \times \left[\frac{\sin(\pi l_n t_{\mathbf{p}} / T_{\mathbf{p}})}{1 + (\pi l_n \tau / T_{\mathbf{p}})^2} - \frac{\pi l_n \tau}{T_{\mathbf{p}}} \frac{\cos(\pi l_n t_{\mathbf{p}} / T_{\mathbf{p}})}{1 + (\pi l_n \tau / T_{\mathbf{p}})^2} \right], \quad (2.61)$$

$$l_n = \begin{cases} n & \Omega > \Omega_B \\ n - 1/2 & \Omega < \Omega_B \end{cases}, \quad (2.62)$$

$$T_{\mathbf{p}} = \frac{K(k)}{\max(\Omega, \Omega_B)}, \quad k = \min \left(\frac{\Omega}{\Omega_B}, \frac{\Omega_B}{\Omega} \right). \quad (2.63)$$

Here $K(k)$ is a Complete Elliptic Integral of the first kind, and $K'(k) = K(\sqrt{1-k^2})$. The division of the factor $Q_{\mathbf{p}}$ into parts odd and even with respect to v_y corresponds to the two terms in the square brackets in Eq. (2.61). If one keeps only the left term then the sum will result in $Q_{\mathbf{p}}^y$, and if one keeps only the right term then the sum will result in $Q_{\mathbf{p}}^x$.

2.10. APPENDIX B

The substitution of Eq. (2.20) into Eq. (2.28) gives

$$R = (16\pi \Lambda p_{\Lambda})^{-1} \times \int \left[\frac{p_y l}{\hbar} - \frac{\pi t_{\mathbf{p}}}{T_{\mathbf{p}}} \theta(\Omega^2 - \Omega_B^2) \right] v_y dp_x dp_y, \quad (2.64)$$

where $\theta(x)$ is the step function. The integral with respect to p_y of the first term in the integrand is trivial but the next integration of this term with respect to p_x diverges. In the second term it is convenient to carry out the integration in variables Ω and t . The integral with respect to Ω also diverges. The sum of the integrals has to converge. So it is convenient to put the limits of the integration in the first term $p_x = -p_M$ and $p_x = p_M$. In the second term the limits are $\Omega = \Omega_F/2 + \Omega_M$ and $\Omega = \Omega_F/2 - \Omega_M$ respectively, where $\Omega_M = \Omega_B p_M / 2p_{\Lambda}$. The result is obtained in the limit $p_M \rightarrow \infty$. Then keeping in mind that the Jacobian of the transformation from variables p_x, p_y to Ω, t is $2(\Omega/\Omega_B)(p_{\Lambda}\hbar/l)$ and calculating the integrals of the elliptic functions with the help of Eqs. (5.136.1) and (5.133.3) of Ref. 70 we have

$$R = \frac{p_M}{2p_{\Lambda}} - \int_{\Omega_B}^{\Omega_M - \Omega_F/2} \frac{\Omega^2 d\Omega}{\Omega_B^3 K(\Omega_B/\Omega)} \times \left[\pi - 2K(\Omega_B/\Omega) \sqrt{1 - \frac{\Omega_B^2}{\Omega^2}} \right] - \int_{\Omega_B}^{\Omega_M + \Omega_F/2} \frac{\Omega^2 d\Omega}{\Omega_B^3 K(\Omega_B/\Omega)} \times \left[\pi - 2K(\Omega_B/\Omega) \sqrt{1 - \frac{\Omega_B^2}{\Omega^2}} \right]. \quad (2.65)$$

When Ω/Ω_B goes to ∞ the integrand here goes to $1/2$. This limit value can be integrated separately and then

$$R = 1 + \int_1^{\infty} \left[1 + 4k\sqrt{k^2 - 1} - \frac{2\pi k^2}{K(1/k)} \right] dk \approx 0.747 \quad (2.66)$$

Chapter 3

Transverse magnetoresistance. II

In this chapter we derive the quantum kinetic equation, which is a valid approach for any relation between four energies Λ , \hbar/τ_p , eFl , $\hbar\Omega_B$. Such a general case can be described quantitatively with the help of the density matrix if an effective electron temperature is large enough. The qualitative results are similar to the results of Chap. 2; there exists a resonant group of electrons with v_x near F/B which gives the main contribution to the current.

We showed in Chap. 2 that the current has a maximum when F/B is close to the characteristic electron in-plane velocity. Therefore, the ratio F/B near the current peak allows one to measure such properties of the in-plane electron distribution function as electron temperature or Fermi energy. If the width of the miniband is smaller than the energy of optical phonons, the cooling of electron gas becomes slow^{35,26}. The effective electron temperature in the region of applied fields near the current peak can be significantly larger than the crystal temperature²⁶. Therefore, we need to have theoretical predictions for this temperature; it can be compared with experimentally measured $m(F/B)^2$ near the current peak.

Therefore, the purpose of this chapter is two-fold. We want to repeat part of the calculations of Chap. 2 starting from the quantum kinetic equation, and we want to see the effect of heating of the electron gas.

Levinson and Yasevichute³⁴ considered for the first time the heating of an electron gas in an anisotropic semiconductor or superlattice. They wrote down the quantum kinetic equation and considered simultaneously two effects: Stark localization and the heating of electron gas. Their results were obtained in the limit $eFl \gg \hbar/\tau$, far away from the current peak; this region of fields **cannot** be observed experimentally in superlattices due to the **instability** of the potential distribution, see Fig. 1.2 and Chap. 5. The same shortage is in the work of Suris and Shchamkhalova³⁵, who concentrated on the interplay between the energy of optical phonons and miniband width.

The calculations in this Chapter follow the work of Laikhtman and Miller²⁶. The presence of the magnetic field is taken into account in the appropriate places. Estimations for electron temperature and heating conditions near the current peak remained the same.

We use the Keldysh technique in order to derive the kinetic equation for the density matrix. We need the Fermi energy or the temperature to be much larger than the energy uncertainty Γ , that covers the upper part of the diagram in Fig. 1.6. In order to obtain analytical results we need to expand the kinetic equation with respect to Λ/T_e , and therefore the region of the miniband transport in Fig. 1.6 is covered only partially. Scattering is considered in the Born approximation. We do not use a translationaly and gauge invariant Green function⁷¹, however we use a translationally and gauge invariant counterpart of the density matrix.

3.1. QUANTUM KINETIC EQUATION.

3.1.1. Quantization of the effective Hamiltonian.

In this subsection we discuss the wave function of an electron moving in a one dimensional periodic superlattice potential $U(y)$ in presence of the crossed electric and magnetic fields. For the purpose of this work we want to know how the external fields modify the wave functions of the lowest miniband produced by the superlattice potential. This problem can be solved by the method of effective Hamiltonian already discussed in Sec. 1.4.

The method of effective Hamiltonian does not contain limitations on the shape of the potential $U(y)$, and in this chapter we consider tight-binding case, since it is most relevant to experiment. In order to quantize the effective Hamiltonian in this case, it is convenient to start calculations in the Wannier representation, which is diagonal with respect to electron states in different potential wells of $U(y)$. The explicit form of the effective Hamiltonian obtained in this way will be equivalent to that which was derived in Sec. 1.4. This can be proved by transformation to Bloch waves.

Electron wave function in the Wannier representation is $S^{-1/2} e^{ip_z z/\hbar + iP_x x/\hbar} w(y - \alpha l)$; this is the wave function of the first level in the α -th well of $U(y)$, l is the period of the superlattice potential $U(y)$, (x, z) are in-plane coordinates, S is normalization area. The electron Hamiltonian of a perfect superlattice in a uniform elec-

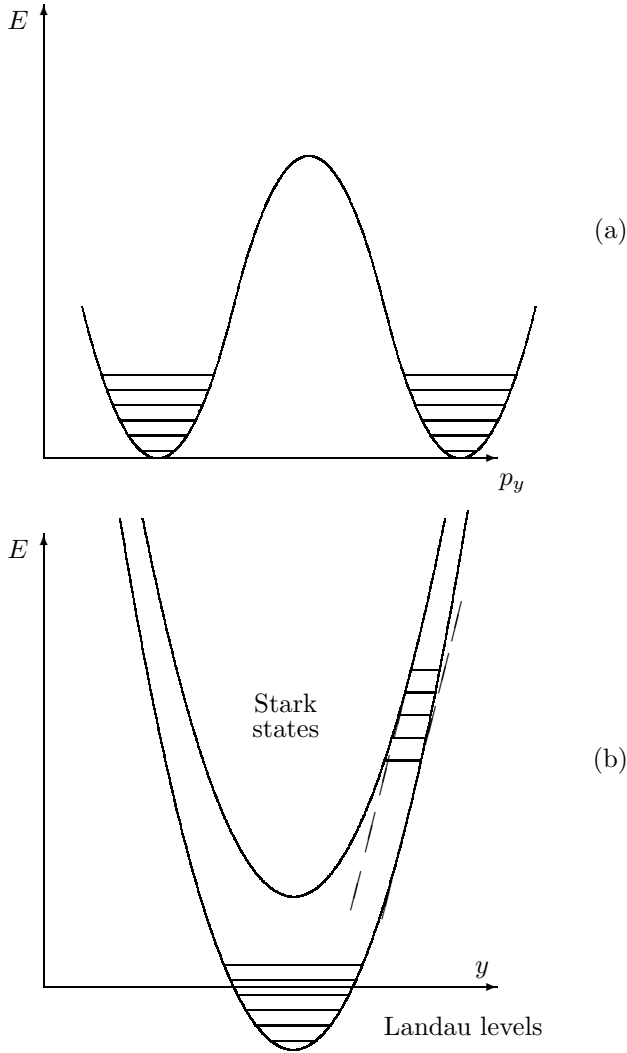


FIG. 3.1. Two ways to quantize the effective Hamiltonian. See explanation in text.

tric field F and z -directed magnetic field B , see Fig. 1.1, is

$$\mathcal{H}_0 = \left(\frac{p_z^2}{2m} + \frac{(P_x + eB\alpha l)^2}{2m} - eFl\alpha \right) \delta_{\alpha\alpha'} - \Lambda(\delta_{\alpha\alpha'+1} + \delta_{\alpha\alpha'-1}). \quad (3.1)$$

Here e and m are the electron charge and mass respectively, and Λ is the tunneling matrix element between first levels in nearest wells; we neglect tunneling on the distance more than one period. We neglect interminiband matrix elements of coordinate y , and presence of other bands; we also neglect field induced corrections to the tunneling. That is possible if the fields F and B are so small that eFl and $eBv_F l$ (v_F —Fermi velocity) are much smaller than the distance between energy levels in a well.

The traditional way to quantize this Hamiltonian is⁴⁷ replacing the operator y or αl by $-i\hbar\partial/\partial p_y$. The field part of Hamiltonian Eq. (3.1) becomes a parabolic “ki-

netic” term proportional to $-\partial^2/\partial p_y^2$ and the tunneling term of Eq. (3.1) becomes a periodic “potential”, $\Lambda \sin(p_y l/\hbar)$. It is shown in Fig. 3.1(a), that quantization of such Hamiltonian leads to formation of Landau levels at the parabolic bottom of each Brillouin zone. However, the tunneling between neighbor Brillouin zones results in the broadening of Landau levels into so-called Harper bands. These Landau levels type states are important for transport if the Fermi energy or temperature of the electron gas are much smaller than the miniband width Λ . Conductivity of the lowest Harper band was computed by Suris and Shchamkhalova⁶¹ by making use of the Kubo formula.

In the opposite case of the large mean kinetic energy of electrons, the greatest contribution to transport is given by the states far above the periodic “potential” shown in Fig. 3.1(a). These states are not similar to Landau levels at all. Berezhkovskii and Suris compute them from a weak binding model for “potential” $\Lambda \sin(p_y l/\hbar)$. We will use another approach in order to give new physical interpretation to these states.

In the framework of the semi-classical approach, one can draw in the same picture miniband boundaries and the potential of an external field bending this miniband, see Fig. 3.1(b). We immediately resolve in this picture two types of states: Landau-like states and Stark-like states. Near the bottom of the low parabola, the Landau-like states are formed (states of the harmonic oscillator). They are slightly broadened by the presence of the top of the miniband, nevertheless they are shown by parallel horizontal lines with an energy spacing $\hbar\Omega_B$. Far away from the center of the parabolas, the two parabolas are almost parallel near some particular energy, see dashed lines in Fig. 3.1(b). Electron wavefunctions are Stark-like near such an energy. Energy separation between Stark-like states is the slope of these parabolas multiplied by the superlattice period.

A Stark-like state is localized around a certain well. The position or number of such a well is a good quantum number, and let’s call it the guiding center of the electron orbit ν . After adding and extracting a few terms containing ν , the Hamiltonian Eq. (3.1) can be rewritten in the form

$$\mathcal{H}_0 = \left(\frac{p_z^2}{2m} + m \frac{v_x^2}{2} - eFl\nu \right) \delta_{\alpha\alpha'} + \mathcal{H}'_0 \quad (3.2)$$

$$\mathcal{H}'_0 = \left(\frac{[eBl(\alpha - \nu)]^2}{2m} + [eBv_x l - eFl](\alpha - \nu) \right) \delta_{\alpha\alpha'} - \Lambda(\delta_{\alpha\alpha'+1} + \delta_{\alpha\alpha'-1}). \quad (3.3)$$

Here $v_x \equiv p_x/m \equiv P_x/m + eBvl/m$. The Hamiltonian \mathcal{H}'_0 contains three terms; a quadratic term, a linear term and a hopping term. If the quadratic term can be neglected, we can use ν as a quantum number, the eigenvalues of \mathcal{H}'_0 are zero and the eigenfunctions are expressed in terms of Bessel functions

$$\psi_{\nu, \mathbf{p}}^S = S^{-1/2} e^{ip_z z/\hbar + i(p_x - eBvl)x/\hbar}$$

$$\times \sum_{\alpha} w(y - \alpha l) J_{\nu - \alpha} \left(\frac{2\Lambda}{eFl - eBv_x l} \right). \quad (3.4)$$

The superscript S here means that this is a Stark-like solution, and the in-plane momentum $\mathbf{p} = (p_z, p_x)$. The size of this state is $|\nu - \alpha| \sim \Lambda/|eBv_x l - eFl|$.

We can neglect the quadratic term in Eq. (3.3) if the obtained state is not too extended. Comparison of the quadratic term with the linear term leads to the condition $|\nu - \alpha| \ll |eFl - eBv_x l|/[(eBl)^2/m]$. Therefore, the Stark-like wave function, Eq. (3.4) is justified when

$$|eBv_x l - eFl| \gg \hbar\Omega_B, \quad (3.5)$$

where the cyclotron frequency Ω_B in our anisotropic case is given by Eq. (1.14). In the Stark-like representation, the Hamiltonian \mathcal{H}_0 becomes diagonal and looks like a Stark ladder

$$\mathcal{H}^S = (E_{\mathbf{p}} - eFl\nu)\delta_{\nu\nu'}, \quad (3.6)$$

where $E_{\mathbf{p}} = (p_x^2 + p_z^2)/(2m)$. This new interpretation of the states far above the ‘‘periodic potential’’ is shown in Fig. 3.1(a).

The wave functions of the system are of Landau type if the linear term in Eq. (3.3) is much smaller than the quadratic term. This happens in the narrow strip of the phase space p_x, p_z , where condition Eq. (3.5) is violated. Inside this strip p_x is not a good quantum number, and it is convenient to define the continuous quantum number $Y \equiv mF/(eB^2) - P_x/(eB)$, which is a position of electron orbit (guiding center). Therefore we don't need the index ν , and it will be used for labeling Landau type states in the rest of this section. Diagonalization of \mathcal{H}_0 leads to

$$\mathcal{H}^L = \left\{ E_{(p_z, mF/B)} - eFY + \hbar\Omega_B \left(\nu + \frac{1}{2} \right) + \tilde{\Lambda}_{\nu}(Y) \right\} \delta_{\nu\nu'}, \quad (3.7)$$

where $\tilde{\Lambda}_{\nu}(Y)$ is a periodic function of Y , $\tilde{\Lambda}_{\nu}(Y + l) = \tilde{\Lambda}_{\nu}(Y)$; this function describes the spreading of Landau levels into Harper bands.^{72,47} The cyclotron frequency in Eq. (3.7) is defined as in Eq. (1.14). The widths of Harper bands can be estimated from the quasiclassical expression for the tunneling amplitude between neighboring Brillouin zones:

$$\text{Var } \tilde{\Lambda}_{\nu} \sim \hbar\Omega_B \exp \left\{ -\frac{4\Lambda}{\hbar\Omega_B} \times \int \sqrt{\frac{1 + \cos(t)}{2} - \frac{\hbar\Omega_B(\nu + 1/2)}{4\Lambda}} dt \right\}, \quad (3.8)$$

where integration has to be performed over positive values of the expression inside the square root. The number of such states is limited by the condition

$$\hbar\Omega_B(\nu + 1/2) \lesssim 4\Lambda, \quad (3.9)$$

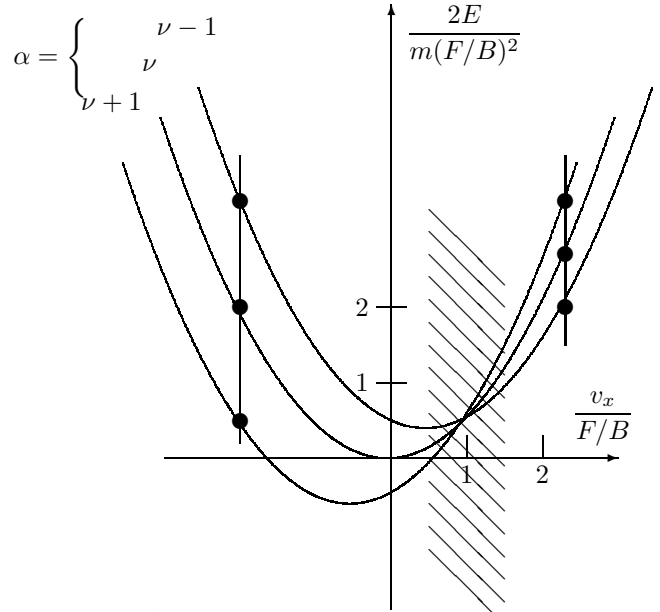


FIG. 3.2. Approximation by Stark type states is not valid in hatched area only. See explanation in the text.

and for the strong enough magnetic field there are no Landau type states at all.

The width of Landau type states can be estimated from the usual Gaussian shape of the linear oscillator wave function as $|\alpha - Y/l| \sim \Lambda\nu/(\hbar\Omega_B)$. These states are more extended in the y direction than the Stark-type states and can give important contribution to the vertical current under very special conditions.

3.1.2. Orthogonality conditions for Stark type wave functions.

Stark like states constructed above are very important for further calculations and we explain now more details about the approximation which has been made. For fixed ν , the Stark like state is a mixture of Wannier states from different wells α . The energies of these Wannier states are in the diagonal part of the Hamiltonian \mathcal{H}_0 minus $p_z^2/(2m)$

$$E_{\alpha\nu} = \frac{m(F/B)^2}{2} \left\{ \frac{1}{2} \left(\frac{v_x}{F/B} \right)^2 + \left(\frac{v_x}{F/B} - 1 \right) \frac{\alpha - \nu}{C} + \frac{1}{2} \left(\frac{\alpha - \nu}{C} \right)^2 \right\}, \quad (3.10)$$

where $C = mF/(eB^2l)$. We wrote this expression in dimensionless form, and plotted it in Fig. 3.2 for $C = 2$ and $\alpha = \nu, \nu \pm 1$. So, in this figure one can see the electron energy in three subsequent wells. The vertical shift of the parabolas is due to the electric field and the horizontal shift is due to the magnetic field. In dimensionless units both shifts are $1/C$.

Tunneling between subsequent wells mixes Wannier states. Two examples of such mixing are shown in Fig. 3.2. Three states marked by filled circles in the vertical line $v_x = \text{const}$ form a new Stark-like state with energy close to the energy of central Wannier state. In order to get wave functions Eq. (3.4) we have to neglect the last term on the right hand side of Eq. (3.10). One may think that this approximation is valid under the condition $C \gtrsim 1$, but that is not true. This approximation is not valid for states in the hatched area in Fig. 3.2, which is given by the inequality opposite to Eq. (3.5).

Let us show that Eq. (3.5) provides a condition for orthogonality of the wave functions Eq. (3.4). We have

$$\begin{aligned} & \int d\mathbf{r} \sum_{\alpha} \psi_{\nu, \mathbf{p}}^{S*}(\alpha, \mathbf{r}) \psi_{\nu', \mathbf{p}'}^S(\alpha, \mathbf{r}) \\ &= \frac{(2\pi\hbar)^2}{S} \delta(p'_z - p_z) \delta(p_x - eB\nu l - p'_x + eB\nu' l) \\ & \times J_{\nu - \nu'} \left(\frac{2\Lambda eBl(v'_x - v_x)}{[eFl - eBv_x l][eFl - eBv'_x l]} \right) \\ & \approx \frac{(2\pi\hbar)^2}{S} \delta(p'_z - p_z) \delta(p'_x - p_x) \delta_{\nu' \nu} \end{aligned} \quad (3.11)$$

We would like also to check the orthogonality condition by integration over momenta and summation over index ν . That is impossible to do, however, because of the pole near $v_x = F/B$.

3.1.3. Matrix elements in the Stark representation.

The operator of the electron velocity in the y direction in the Wannier representation has the form

$$\hat{v}_y = (i\Lambda l/\hbar)(\delta_{\alpha, \alpha'+1} - \delta_{\alpha, \alpha'-1})\delta(x - x')\delta(z - z').$$

It becomes in our Stark-like representation

$$\begin{aligned} \hat{v} &= \frac{(2\pi\hbar)^2}{S} \delta(p_z - p'_z) \delta(p_x - eB\nu l - p'_x + eB\nu' l) \\ & \times \frac{i\Lambda d}{\hbar} \sum_{\alpha} \left(J_{\nu - \alpha}^{p_x} J_{\nu' - \alpha + 1}^{p'_x} - J_{\nu - \alpha}^{p_x} J_{\nu' - \alpha - 1}^{p'_x} \right) \end{aligned} \quad (3.12)$$

$$J_{\nu - \alpha}^{p_x} \equiv J_{\nu - \alpha} \left(\frac{2\Lambda}{eFl - eBv_x l} \right) \quad (3.13)$$

The total Hamiltonian contains \mathcal{H}_0 , and a scattering potential, \hat{U} . We consider that the main scattering mechanism is impurity scattering or scattering on the other type of static potential. The overlap of electron wave functions in different wells is small and only diagonal elements with respect to the wells, $U_{\mathbf{p}\mathbf{p}'}^{\alpha\alpha}$, will be taken into account. Matrix elements of the operators \hat{U} in the Stark representation have the form

$$U_{\mathbf{p}\mathbf{p}'}^{\nu\nu'} = \sum_{\alpha} J_{\nu - \alpha}^{p_x} J_{\nu' - \alpha}^{p'_x} U_{p_z, p_x - eB\nu l; p'_z, p'_x - eB\nu' l}^{\alpha\alpha}, \quad (3.14)$$

and $J_{\nu - \alpha}^{p_x}$ are defined above. The product of two matrix elements averaged over the impurity configuration is

$$\begin{aligned} \overline{U_{\mathbf{p}\mathbf{q}}^{\nu\nu'} U_{\mathbf{p}'\mathbf{q}'}^{\nu'\nu'}} &= N_I (2\pi\hbar)^2 \delta(p_z - q_z + p'_z - q'_z) \\ & \times \delta(p_x - eB\nu l - q_x + eB\mu l + p'_x - eB\nu' l - q'_x + eB\mu' l) \\ & \times \tilde{U}_{p_z, p_x - eB\nu l; q_z, q_x - eB\mu l} \tilde{U}_{p'_z, p'_x - eB\nu' l; q'_z, q'_x - eB\mu' l} \\ & \times \sum_{\alpha} J_{\nu - \alpha}^{p_x} J_{\mu - \alpha}^{q_x} J_{\nu' - \alpha}^{p'_x} J_{\mu' - \alpha}^{q'_x}, \end{aligned} \quad (3.15)$$

where N_I is the sheet density of the impurities and \tilde{U} is the matrix element of the single impurity potential.

3.1.4. Equation for density matrix

We will assume that the Fermi energy and temperature are much larger than the level spacing of \mathcal{H}_0 . This assumption allows us to derive a kinetic equation for the electron density matrix. We will make use of the Keldysh technique and derive this equation in the same way as the Boltzmann equation is usually derived.⁷³ In the Keldysh technique the kinetic equation results from the Dyson equation, which can be written in two equivalent forms

$$\hat{G}_{01}^{-1} G_{12} = \sigma_z + \sigma_z \Sigma_{13} G_{32}, \quad (3.16a)$$

$$\hat{G}_{02}^{-1*} G_{12} = \sigma_z + \Sigma_{13} G_{32} \sigma_z. \quad (3.16b)$$

The matrix Keldysh Green function, G_{12} , depends on two sets of variables, $\{\nu, \mathbf{p}, t\}$ and a sum and integral with respect to the variables with the subscript 3 is implied in Eqs. (3.16a) and (3.16b). The operators on the left hand sides, \hat{G}_{01}^{-1} and \hat{G}_{02}^{-1} are obtained from

$$\hat{G}_0^{-1} = \left(i\hbar \frac{\partial}{\partial t} - \mathcal{H}^S \right) \sigma_z \quad (3.16c)$$

by substitution sets $\{\nu_1, \mathbf{p}_1, t_1\}$ or $\{\nu_2, \mathbf{p}_2, t_2\}$ correspondingly. Definitions of the Green functions Eqs. (3.16) contain also the Pauli matrix σ_z .

Green functions depend on two times, t_1 and t_2 . Instead of them the difference, $t_1 - t_2$, and the sum, $t = (t_1 + t_2)/2$, times can be introduced. The characteristic values of the difference time is of the order of \hbar divided by the characteristic energy, i.e. the maximum of the Fermi energy and temperature. The time t characterizes much more slow variation of occupation numbers. So that in the right-hand sides of Eqs. (3.16a) and (3.16b) all functions can be considered dependent on the same time t and the integration with respect to t_3 is reduced to the integration with respect to difference times. Then the Fourier transform with respect to the difference time leads to the Green functions depending on t and a frequency ω , which is a spectral variable.

The explicit form of the matrix Green function as it is defined in Ref. 74 is

$$G \equiv \begin{pmatrix} G^{--} & G^{-+} \\ G^{+-} & G^{++} \end{pmatrix} = \begin{pmatrix} G^{-+} + G^r & G^{-+} \\ G^{-+} + G^r - G^a & G^{-+} - G^a \end{pmatrix} \quad (3.17)$$

The same pattern holds for self-energies. The difference and half of the sum of $(-+)$ matrix elements of Eqs. (3.16a) and (3.16b) has the form

$$i\hbar \frac{\partial}{\partial t} G_{12}^{-+} - [\mathcal{H}^S, G^{-+}]_{12} = \Sigma_{13}^r G_{32}^{-+} - \Sigma_{13}^{-+} G_{32}^a + G_{13}^r \Sigma_{32}^{-+} - G_{13}^{-+} \Sigma_{32}^a, \quad (3.18)$$

$$\hbar\omega G_{12}^{-+} - \frac{1}{2} \{\mathcal{H}^S, G^{-+}\}_{12} = \frac{1}{2} (\Sigma_{13}^r G_{32}^{-+} - \Sigma_{13}^{-+} G_{32}^a - G_{13}^r \Sigma_{32}^{-+} + G_{13}^{-+} \Sigma_{32}^a). \quad (3.19)$$

For the calculation of self-energies we need also advanced and retarded Green functions. Equations for them are obtained from Eqs. (3.16a) and (3.16b)

$$\hbar\omega G_{12}^r - \frac{1}{2} \{\mathcal{H}^S, G^r\}_{12} = 1 + \frac{1}{2} \{\Sigma^r, G^r\}_{12}, \quad (3.20)$$

$$G_{12}^a = G_{21}^{r*}. \quad (3.21)$$

Here $[a, b] = ab - ba$ and $\{a, b\} = ab + ba$.

The retarded Green function can be found from Eqs. (3.20) and (3.24) (see below). Equations (3.19) and (3.26) (see below) are linear and uniform with respect to $G_{\nu\nu'}^{-+}(\mathbf{p})$ and this function cannot be found from them. Actually, Eqs. (3.19) and (3.26) can be used to find only the dependence of G^{-+} on ω . The integral of G^{-+} with respect to ω , the density matrix

$$\rho_{\mathbf{p}\mathbf{p}'}^{\nu\nu'}(t) = \hbar \int \frac{d\omega}{2\pi i} G_{\nu\mathbf{p};\nu'\mathbf{p}'}^{-+}(\omega, t), \quad (3.22)$$

has to be determined with the help of Eq. (3.18). The equation for the density matrix can be obtained by the integration of Eq. (3.18) with respect to ω ,

$$\frac{\partial \rho}{\partial t} - \frac{1}{i\hbar} [\mathcal{H}^S, \rho] = - \int \frac{d\omega}{2\pi} \left(\Sigma^r G^{-+} - \Sigma^{-+} G^a + G^r \Sigma^{-+} - G^{-+} \Sigma^a \right). \quad (3.23)$$

The superlattice is uniform in the x, z plane and one may expect Green functions as well as self-energies to be diagonal with respect to \mathbf{p} . However, this is not true because we are looking for a solution, which describes electric current, and therefore the density matrix has to contain terms proportional to the matrix element of the velocity y -component. This matrix element Eq. (3.12) is not diagonal with respect to \mathbf{p} , and therefore all elements of the Green function are non-diagonal too.

We consider the case of weak scattering when the energy uncertainty due to the scattering is much smaller than the width of the in-plane electron energy distribution. Then self-energies can be calculated in the first approximation. For simplicity we assume that electrons

in different wells are scattered by different impurities. This implies that the screening radius is smaller than the period of the superlattice. Then

$$\Sigma_{\nu\mathbf{p};\nu'\mathbf{p}'}^r(\omega) = \sum_{\mu\mu'} \int \frac{d\mathbf{q}d\mathbf{q}'}{(2\pi\hbar)^4} \overline{U_{\mathbf{p}\mathbf{q}}^{\nu\mu} U_{\mathbf{q}'\mathbf{p}'}^{\mu'\nu'}} G_{\mu\mathbf{q};\mu'\mathbf{q}'}^r(\omega), \quad (3.24)$$

$$\Sigma_{\nu\mathbf{p};\nu'\mathbf{p}'}^a(\omega) = \Sigma_{\nu\mathbf{p};\nu'\mathbf{p}'}^{r*}(\omega) \quad (3.25)$$

$$\Sigma_{\nu\mathbf{p};\nu'\mathbf{p}'}^{-+}(\omega) = - \sum_{\mu\mu'} \int \frac{d\mathbf{q}d\mathbf{q}'}{(2\pi\hbar)^4} \overline{U_{\mathbf{p}\mathbf{q}}^{\nu\mu} U_{\mathbf{q}'\mathbf{p}'}^{\mu'\nu'}} G_{\mu\mathbf{q};\mu'\mathbf{q}'}^{-+}(\omega). \quad (3.26)$$

These self-energies have to be substituted into the right hand side of Eq. (3.23) which can be solved together with Eqs. (3.18) and (3.19).

The next important approximation is the weak scattering limit, which allows one to neglect terms containing self-energies in Eqs. (3.19) and (3.20). Therefore we are going to take into account scattering in the so-called Born approximation. Computation of the right hand side of Eq. (3.23) is cumbersome and we put it into Appendix 3.3.

3.2. CALCULATION OF THE CURRENT

In order to compute the current we have to find a stationary, translational, and gauge invariant solution to the kinetic equation Eq. (3.23) with the right hand side given by Eqs. (3.47). Equation (3.23) is not gauge invariant, and the density matrix $\rho_{\mathbf{p}\mathbf{p}'}^{\nu\nu'}$ also is not gauge invariant, because wave functions were chosen in the specific gauge. However, in Wannier representation we can introduce translational and gauge invariant⁷¹ counterpart of the density matrix $\wp_{\alpha-\alpha'}(\mathbf{q})$

$$\rho_{\mathbf{r}\mathbf{r}'}^{\alpha\alpha'} = e^{-ieBl \frac{\alpha+\alpha'}{2\hbar}(x-x')} \int \frac{d\mathbf{q}}{(2\pi\hbar)^2} e^{i\mathbf{q}(\mathbf{r}-\mathbf{r}')} \wp_{\alpha-\alpha'}(\mathbf{q}). \quad (3.27)$$

Here $\rho_{\mathbf{r}\mathbf{r}'}^{\alpha\alpha'}$ is not an invariant density matrix defined in the Wannier representation. The first task is to convert both sides of Eq. (3.27) from Wannier to our Stark-like representation. We have to make another approximation in order to perform this transformation.

We will solve Eq. (3.23) only in the case when

$$\Lambda, |eBv_x - eFl| \ll T_e, \quad (3.28)$$

where T_e is the effective electron temperature, which characterizes the width of the electron energy distribution. (We do not assume that a real distribution is the equilibrium one with the temperature T_e . This quantity is used only for estimates.) In the case of an effective energy relaxation $T_e \sim T$. In the case of low temperature and an appreciable heating of the electron gas

$T_e > T$. The estimate of T_e under different conditions can be found from the balance of the heating $\sim jF$ and cooling $\frac{n(T_e - T)}{\tau_e}$, see Eqs. (3.39) and (3.40) below. In the case of zero magnetic field the answer can be found in Ref. 26.

Under the condition Eq. (3.28) we can convert $\rho_{\mathbf{r}\mathbf{r}'}^{\alpha\alpha'}$ and $\wp_{\alpha-\alpha'}(\mathbf{q})$ to $\rho_{\mathbf{p}\mathbf{p}'}^{\nu\nu'}$ and $\wp_{\nu-\nu'}(\mathbf{q})$. Equation (3.27) is converted into Eq. (3.48), see Appendix 3.4 for more details. Substitution of Eq. (3.48) into the quantum kinetic equation Eq. (3.23) and averaging of the scattering probability over energy surface leads to the following resulting equations

$$\hbar \hat{I}_E \wp_0(E) + \Lambda \frac{d}{dE} \Gamma(E) [R(E) + 2\Lambda \frac{d\wp_0}{dE}] = 0, \quad (3.29)$$

$$\begin{aligned} & \pm i(eBv_x l - eFl) \wp_{\pm 1}(\mathbf{p}) \pm i\Lambda eBv_x l \frac{d\wp_0}{dE_{\mathbf{p}}} \\ & = -\Gamma(E_{\mathbf{p}}) \wp_{\pm 1}(\mathbf{p}) - \Lambda \Gamma(E_{\mathbf{p}}) \frac{d\wp_0}{dE_{\mathbf{p}}}, \end{aligned} \quad (3.30)$$

$$R(E) = \int \frac{d\mathbf{p}}{2\pi m} \delta(E - E_{\mathbf{p}}) [\wp_1(\mathbf{p}) + \wp_{-1}(\mathbf{p})] \quad (3.31)$$

where \hat{I}_E is the operator of energy relaxation. Calculations are actually performed in Appendix 3.4. Condition Eq. (3.28) allows us to keep the Stark-like levels difference $\nu - \nu' = 0, \pm 1$. Quantum uncertainty of the energy levels due to scattering $\Gamma(E_p)$ is defined in Eq. (3.53). Equations (3.29) and (3.30) are very reminiscent of the Boltzmann equations for the parts of the electron distribution function even and odd with respect to the electron momentum in the theory of hot electrons in wide band semiconductors^{75,76}.

The main energy relaxation mechanism in the narrow band superlattices is acoustic phonon scattering.^{26,43} We have

$$\hbar \hat{I}_E \wp_0(E) = \frac{d}{dE} Q(E) \left[\wp_0(1 - \wp_0) + T \frac{d\wp_0}{dE} \right], \quad (3.32)$$

where

$$Q(E) = \frac{\pi^2 m \Xi^2}{2\rho_0 d_w^3} \left(1 + \frac{3Em d_w^2}{\pi^2 \hbar^2} \right), \quad (3.33)$$

ρ_0 is the crystal density, m is the in-plane effective mass, d_w is the width of a well, and Ξ is the deformation potential.

Equation (3.30) can be written as

$$\wp_{\pm 1}(\mathbf{p}) = -\Lambda \frac{\Gamma(E_{\mathbf{p}}) \pm ieBv_x l}{\Gamma(E_{\mathbf{p}}) \pm i(eBv_x l - eFl)} \frac{d\wp_0}{dE_{\mathbf{p}}}. \quad (3.34)$$

This solution has a pole at $v_x = F/B$, which is smeared by scattering. The width of this smearing is $\Gamma/(eBl)$ and it has to cover the hatched area in the diagram Fig. 3.2. The condition justifying our whole theory is, therefore,

$$\Omega_B \tau_p \ll 1, \quad (3.35)$$

where $\tau_p \sim \hbar/\Gamma(E_p)$. Equation (3.29) with the help of Eq. (3.32) is reduced to

$$Q(E) \left[\wp_0(1 - \wp_0) + T \frac{d\wp_0}{dE} \right] + 2\Lambda^2 \Gamma(E) \tilde{R}(E) \frac{d\wp_0}{dE} = 0, \quad (3.36)$$

where

$$\tilde{R}(E_{\mathbf{p}}) = \int \frac{d\phi}{2\pi} \frac{(eFl)^2}{\Gamma^2(E_{\mathbf{p}}) + (eBlp \cos(\phi)/m - eFl)^2}. \quad (3.37)$$

Integration can be performed, the same integral was calculated in Chap. 2, see Eq. (2.23).

The solution to Eq. (3.36) is

$$\wp_0 = \left\{ \exp \left[\int_0^E \frac{dE}{T + 2\Lambda^2 \Gamma(E) \tilde{R}(E)/Q(E)} - \zeta \right] + 1 \right\}^{-1}, \quad (3.38)$$

where ζ is a normalization constant. For zero magnetic field this solution was obtained by Laikhtman and Miller.²⁶ Even without an exact calculation Eq. (3.38) allows us to estimate the importance of the heating of the electron gas near the current maximum. We can estimate the momentum and energy relaxation times as $\tau_p \sim \hbar/\Gamma$ and $\tau_e \sim \hbar T_e/Q$ respectively. Near the current maximum, when $eFl \sim \Gamma$, $eBlv_F$, $eBlv_T$, we have $\tilde{R} \sim 1$, and the width of the electron energy distribution T_e in the case of weak heating and the condition for weak heating are

$$T_e \sim T, \quad \frac{\Lambda^2 \tau_e}{T^2 \tau_p} \ll 1. \quad (3.39)$$

Because $\tau_e \gg \tau_p$, the condition Eq. (3.39) is satisfied only for $\Lambda \ll T$. For the band width $4\Lambda \sim 0.5$ meV the last condition is satisfied for temperatures about 30 K and higher. This estimate shows that for lower temperature or for a wider band one can expect an appreciable heating of the electron gas. In such a case

$$T_e \sim \frac{\Lambda^2 \tau_e}{T \tau_p}, \quad \frac{\Lambda^2 \tau_e}{T^2 \tau_p} \gg 1. \quad (3.40)$$

Now it is possible to justify Eq. (3.50). In the estimate we assume that $eFl, |eFl - eBv_F| \sim \Gamma$ because this region of the electric field is close to the current maximum, and $\Gamma^2/\Lambda^2 \ll \tau_e/\tau_p$ because in the opposite case the resonance tunneling is smeared so much that the width of the resonance can be of the order of the separation between the levels in a well. Then for weak heating, Eq. (3.39), $T_e \sim T \geq \Lambda(\tau_e/\tau_p)^{1/2} \gg \Lambda, \Gamma$. In the case of strong heating, Eq. (3.40), $\Gamma/T_e \ll (T/\Lambda)(\tau_p/\tau_e)^{1/2} \ll 1$ and $\Lambda/T_e \sim (T/\Lambda)(\tau_p/\tau_e) \ll (T/\Lambda)(\tau_p/\tau_e)^{1/2} \ll 1$; that is, in both cases Eq. (3.28) is satisfied.

For the uniform electron distribution, the expression for current density is proportional to the trace of the density matrix times the velocity operator, Eq. (3.12)

$$j = \frac{2ie\Lambda}{\hbar} \int \frac{d\mathbf{p}}{(2\pi\hbar)^2} (\wp_{-1} - \wp_1) = -\frac{4e\Lambda^2}{\hbar} \int \frac{d\mathbf{p}}{(2\pi\hbar)^2} \frac{\Gamma(E_{\mathbf{p}})eFl}{\Gamma^2(E_{\mathbf{p}}) + (eBv_x l - eFl)^2} \frac{d\wp_0}{dE_{\mathbf{p}}}. \quad (3.41)$$

This expression shows that Ohm's law is satisfied for $eFl, eBv_x l \ll \Gamma$. The collisionless current is recovered in the opposite case, and

$$j = -\frac{4\pi eF\Lambda^2}{\hbar} \int \frac{d\mathbf{p}}{(2\pi\hbar)^2} \delta(Bv_x - F) \frac{d\wp_0}{dE_{\mathbf{p}}}. \quad (3.42)$$

This result is similar to Eq. (2.26). The important difference is the form of \wp_0 ; in Eq. (3.42) it has to be substituted from Eq. (3.38), whereas in Eq. (2.26) we use the equilibrium distribution function f_0 .

3.3. APPENDIX: COLLISION INTEGRAL OF THE QUANTUM KINETIC EQUATION.

For weak scattering, terms containing self-energies in Eqs. (3.19) and (3.20) can be neglected compared to $\hbar\omega$ and solutions to them are

$$G_{\nu\mathbf{p};\nu'\mathbf{p}'}^r(\omega) = (2\pi\hbar)^2 \frac{\delta_{\nu\nu'}\delta(\mathbf{p} - \mathbf{p}')}{\hbar\omega - E_{\mathbf{p}} + eFl\nu + i0}, \quad (3.43)$$

$$\begin{aligned} \Sigma_{\nu\mathbf{p};\nu'\mathbf{p}'}^r(\omega) &= (2\pi\hbar)^2 \delta(p_z - p'_z) \delta(p_x - eB\nu l - p'_x + eB\nu' l) \\ &\times N_I \sum_{\mu} \int \frac{d\mathbf{q}}{(2\pi\hbar)^2} |\tilde{U}_{p_z, p_x - eB\nu l; q_z, q_x - eB\mu l}|^2 \frac{\sum_{\alpha} J_{\nu-\alpha}^{p_x} J_{\mu-\alpha}^{q_x} J_{\mu-\alpha}^{q_x} J_{\nu'-\alpha}^{p'_x}}{\hbar\omega - E_{\mathbf{q}} + eFl\mu + i0} \end{aligned} \quad (3.44)$$

$$G_{\nu\mathbf{p};\nu'\mathbf{p}'}^{-+}(\omega) = 2\pi i \rho_{\mathbf{p}\mathbf{p}'}^{\nu\nu'} \delta\left(\hbar\omega - \frac{E_p + E_{p'}}{2} + eFl \frac{\nu + \nu'}{2}\right). \quad (3.45)$$

$$\Sigma_{\nu\mathbf{p};\nu'\mathbf{p}'}^{-+}(\omega) = -2\pi i \sum_{\mu\mu'} \int \frac{d\mathbf{q}d\mathbf{q}'}{(2\pi\hbar)^4} \overline{U_{\mathbf{p}\mathbf{q}}^{\nu\mu} U_{\mathbf{q}'\mathbf{p}'}^{\mu'\nu'}} \rho_{\mathbf{q}\mathbf{q}'}^{\mu\mu'} \delta\left(\hbar\omega - \frac{E_q + E_{q'}}{2} + eFl \frac{\mu + \mu'}{2}\right). \quad (3.46)$$

All four terms on the right hand side of Eq. (3.23) can be expressed explicitly in terms of the density matrix:

$$\begin{aligned} -\int \frac{d\omega}{2\pi} (\Sigma^r G^{-+})_{\mathbf{p}\mathbf{p}'}^{\nu\nu'} &= -\frac{iN_I}{\hbar} \sum_{\mu\mu'} \int \frac{d\mathbf{q}}{(2\pi\hbar)^2} |\tilde{U}_{p_z, p_x - eB\nu l; q_z, q_x - eB\mu l}|^2 \rho_{(p_z, p_x - eB(\nu - \mu')l); \mathbf{p}'}^{\mu'\nu'} \\ &\times \frac{\sum_{\alpha} J_{\nu-\alpha}^{p_x} J_{\mu-\alpha}^{q_x} J_{\mu-\alpha}^{q_x} J_{\mu'-\alpha}^{p'_x}}{\left(E_{(p_z, p_x - eB(\nu - \mu')l)} + E_{p'}\right)/2 - eFl \frac{\mu' + \nu'}{2} - E_{\mathbf{q}} + eFl\mu + i0} \end{aligned} \quad (3.47a)$$

$$\begin{aligned} \int \frac{d\omega}{2\pi} (G^{-+} \Sigma^a)_{\mathbf{p}\mathbf{p}'}^{\nu\nu'} &= \frac{iN_I}{\hbar} \sum_{\mu\mu'} \int \frac{d\mathbf{q}}{(2\pi\hbar)^2} |\tilde{U}_{p'_z, p'_x - eB\nu' l; q_z, q_x - eB\mu l}|^2 \rho_{\mathbf{p}; (p'_z, p'_x - eB(\nu' - \mu')l)}^{\nu\mu'} \\ &\times \frac{\sum_{\alpha} J_{\mu'-\alpha}^{p'_x - eB(\nu' - \mu')l} J_{\mu-\alpha}^{q_x} J_{\mu-\alpha}^{q_x} J_{\nu'-\alpha}^{p'_x}}{\left(E_p + E_{(p'_z, p'_x - eB(\nu' - \mu')l)}\right)/2 - eFl \frac{\nu + \mu'}{2} - E_{\mathbf{q}} + eFl\mu - i0} \end{aligned} \quad (3.47b)$$

$$\begin{aligned} \int \frac{d\omega}{2\pi} (\Sigma^{-+} G^a)_{\mathbf{p}\mathbf{p}'}^{\nu\nu'} &= -\frac{iN_I}{\hbar} \sum_{\mu\mu'} \int \frac{d\mathbf{q}}{(2\pi\hbar)^2} |\tilde{U}_{\mathbf{q}}|^2 \rho_{(q_z + p_z, q_x + p_x - eB(\nu - \mu)l); (q_z + p'_z, q_x + p'_x - eB(\nu' - \mu')l)}^{\mu\mu'} \\ &\times \left\{ \frac{E_{(q_z + p_z, q_x + p_x - eB(\nu - \mu)l)} + E_{(q_z + p'_z, q_x + p'_x - eB(\nu' - \mu')l)}}{2} - E_{\mathbf{p}'} - eFl \frac{\mu + \mu'}{2} + eFl\nu' - i0 \right\}^{-1} \end{aligned}$$

$$\times \sum_{\alpha} J_{\nu-\alpha}^{p_x} J_{\mu-\alpha}^{q_x+p_x-eB(\nu-\mu)l} J_{\mu'-\alpha}^{q_x+p'_x-eB(\nu'-\mu')l} J_{\nu'-\alpha}^{p'_x}, \quad (3.47c)$$

$$\begin{aligned} - \int \frac{d\omega}{2\pi} (G^r \Sigma^{-+})_{\mathbf{p}\mathbf{p}'}^{\nu\nu'} &= \frac{iN_I}{\hbar} \sum_{\mu\mu'} \int \frac{d\mathbf{q}}{(2\pi\hbar)^2} |\tilde{U}_q|^2 \rho_{(q_z+p_z, q_x+p_x-eB(\nu-\mu)l); (q_z+p'_z, q_x+p'_x-eB(\nu'-\mu')l)}^{\mu\mu'} \\ &\times \left\{ \frac{E_{(q_z+p_z, q_x+p_x-eB(\nu-\mu)l)} + E_{(q_z+p'_z, q_x+p'_x-eB(\nu'-\mu')l)}}{2} - E_{\mathbf{p}} - eFl \frac{\mu + \mu'}{2} + eFl\nu + i0 \right\}^{-1} \\ &\times \sum_{\alpha} J_{\nu-\alpha}^{p_x} J_{\mu-\alpha}^{q_x+p_x-eB(\nu-\mu)l} J_{\mu'-\alpha}^{q_x+p'_x-eB(\nu'-\mu')l} J_{\nu'-\alpha}^{p'_x}, \end{aligned} \quad (3.47d)$$

and the expression for the commutator on the left hand side of Eq. (3.23) does not change.

3.4. APPENDIX: GAUGE AND TRANSLATIONALLY INVARIANT EQUATIONS.

The derivative of the density matrix with respect to p_x is proportional to $1/\sqrt{mT_e}$ in the high temperature limit. The expansion with respect to this parameter allow us to obtain the expression for the density matrix in the Stark representation. We have from Eqs. (3.28) and (3.4)

$$\begin{aligned} \rho_{\mathbf{p}\mathbf{p}'}^{\nu\nu'} &= \sum_{\alpha\alpha'} J_{\nu-\alpha}^{p_x} J_{\nu'-\alpha'}^{p'_x} (2\pi\hbar)^2 \int d\mathbf{q} \wp_{\alpha-\alpha'}(\mathbf{q}) \delta(p_z - q_z) \delta(p'_z - q_z) \\ &\times \delta\left(p_x - eB \left[\nu - \frac{\alpha + \alpha'}{2} \right] l - q_x\right) \delta\left(p'_x - eB \left[\nu' - \frac{\alpha + \alpha'}{2} \right] l - q_x\right) \end{aligned}$$

and after shift of p_x and p'_x , the above expression becomes

$$\begin{aligned} &\rho_{(p_z, p_x + eB(\nu-\nu')l/2); (p'_z, p'_x + eB(\nu'-\nu)l/2)}^{\nu\nu'} = (2\pi\hbar)^2 \delta(\mathbf{p} - \mathbf{p}') \\ &\times \sum_{\alpha\alpha'} J_{\nu-\alpha}^{p_x + eB(\nu-\nu')l/2} J_{\nu'-\alpha'}^{p'_x + eB(\nu'-\nu)l/2} \wp_{\alpha-\alpha'} \left(p_z, p_x + eBl \frac{\alpha + \alpha'}{2} - eBl \frac{\nu + \nu'}{2} \right) \\ &= (2\pi\hbar)^2 \delta(\mathbf{p} - \mathbf{p}') \sum_{\alpha\alpha'} J_{\nu-\alpha}^{p_x + eB(\nu-\nu')l/2} J_{\nu'-\alpha'}^{p'_x + eB(\nu'-\nu)l/2} \left\{ 1 - eBl \frac{\nu - \alpha + \nu' - \alpha'}{2} \frac{\partial}{\partial p_x} \right\} \wp_{\alpha-\alpha'}(\mathbf{p}) \\ &\approx (2\pi\hbar)^2 \delta(\mathbf{p} - \mathbf{p}') \left[\wp_{\nu-\nu'}(\mathbf{p}) + \frac{\Lambda eBl}{eBp_x l/m - eFl} \frac{\partial}{\partial p_x} \left\{ \wp_{\nu-\nu'+1}(\mathbf{p}) + \wp_{\nu-\nu'-1}(\mathbf{p}) \right\} \right] \end{aligned} \quad (3.48)$$

where high order derivatives with respect to p_x are neglected. The commutator on the left hand side of Eq. (3.23) becomes

$$\begin{aligned} &([H^S, \rho])_{(p_z, p_x + eB(\nu-\nu')l/2); (p'_z, p'_x + eB(\nu'-\nu)l/2)}^{\nu\nu'} \\ &= (2\pi\hbar)^2 \delta(\mathbf{p} - \mathbf{p}') \left[(eBv_x l - eFl)(\nu - \nu') \wp_{\nu-\nu'}(\mathbf{p}) + \Lambda eBl(\nu - \nu') \frac{\partial}{\partial p_x} \left\{ \wp_{\nu-\nu'+1}(\mathbf{p}) + \wp_{\nu-\nu'-1}(\mathbf{p}) \right\} \right] \end{aligned} \quad (3.49)$$

The energy differences $E_p - E_q$ in the collision operator Eq. (3.47) are of the order of T_e . Therefore, we can neglect the terms containing $\frac{\partial}{\partial p_x}$ in Eq. (3.48) for the density matrix when we substitute it in Eq. (3.47). We have to expand first collision integrals in terms of $(eBv_x l - eFl)/T_e$ too. After the expansion, sums with respect to numbers of the Stark levels can be calculated explicitly. Keeping only terms of the first and the second order in Eq. (3.23) we get

$$\begin{aligned} i(eBv_x l - eFl)\nu \wp_{\nu}(\mathbf{p}) + i\Lambda eBl\nu \frac{\partial}{\partial p_x} \left\{ \wp_{\nu+1}(\mathbf{p}) + \wp_{\nu-1}(\mathbf{p}) \right\} &= 2\pi N_I \int \frac{d\mathbf{q}}{(2\pi\hbar)^2} |V_{\mathbf{p}\mathbf{q}}|^2 \left\{ \left[\delta_{\nu,0} \wp_0(\mathbf{q}) - \wp_{\nu}(\mathbf{p}) \right] \delta(E_p - E_q) \right. \\ &+ \Lambda \left[(\wp_1(\mathbf{q}) + \wp_{-1}(\mathbf{q})) \delta_{\nu,0} - \wp_0(\mathbf{q}) (\delta_{\nu,1} + \delta_{\nu,-1}) + \wp_{\nu+1}(\mathbf{p}) + \wp_{\nu-1}(\mathbf{p}) \right] \delta'(E_p - E_q) \\ &\left. + 2\Lambda^2 \delta_{\nu,0} \left[\wp_0(\mathbf{q}) - \wp_0(\mathbf{p}) \right] \delta''(E_p - E_q) \right\} \end{aligned} \quad (3.50)$$

We neglected the term on the collision integral, which is different from the first one on the left hand side of Eq. (3.50) only by a factor. It can be considered as a renormalization of electron charge and can be neglected. Then one can see that if the terms of the order of Λ/T_e are neglected at all, the equation for φ_0 is separated from equations for φ_ν with $\nu \neq 0$ and does not contain fields. This is natural because φ_0 is the distribution function in a layer and without tunneling it does not 'know' about the electric field. Along with the tunneling in this equation it is necessary to take into account inelastic scattering, which was not considered so far. The operator of the inelastic collisions, $I_{\text{in}}\varphi_0$, can be added into Eq.(3.50) without making use of the Keldysh technique.

Equations (3.50) with $\nu \neq 0$ show that $\varphi_\nu \sim (\Lambda/T_e)^{|\nu|}\varphi_0$, i.e., $\varphi_{|\nu|}$ with $|\nu| \geq 2$ can be neglected and we come up with the following equations:

$$\begin{aligned} & \frac{2\pi N_I}{\hbar} \int \frac{d\mathbf{q}}{(2\pi\hbar)^2} |V_{\mathbf{p}\mathbf{q}}|^2 [\varphi_0(\mathbf{q}) - \varphi_0(\mathbf{p})] [\delta(E_p - E_q) + 2\Lambda^2 \delta''(E_p - E_q)] \\ & + \frac{2\pi N_I \Lambda}{\hbar} \int \frac{d\mathbf{q}}{(2\pi\hbar)^2} |V_{\mathbf{p}\mathbf{q}}|^2 [\varphi_1(\mathbf{q}) + \varphi_{-1}(\mathbf{q}) + \varphi_1(\mathbf{p}) + \varphi_{-1}(\mathbf{p})] \delta'(E_p - E_q) + \hat{I}_{\text{in}}\varphi_0(\mathbf{p}) = 0 \end{aligned} \quad (3.51)$$

$$\begin{aligned} & \pm i \frac{eBv_x l - eFl}{\hbar} \varphi_{\pm 1}(\mathbf{p}) \pm \Lambda eBl \frac{\partial}{\partial p_x} \varphi_0(\mathbf{p}) = -\frac{1}{\hbar} \Gamma(E_p) \varphi_{\pm 1}(\mathbf{p}) \\ & + \frac{2\pi N_I \Lambda}{\hbar} \int \frac{d\mathbf{q}}{(2\pi\hbar)^2} |V_{\mathbf{p}\mathbf{q}}|^2 (\varphi_0(\mathbf{p}) - \varphi_0(\mathbf{q})) \delta'(E_p - E_q), \end{aligned} \quad (3.52)$$

where for an isotropic energy spectrum and scattering (i.e. for $|V_{\mathbf{p}\mathbf{q}}|^2$ depending on $|\mathbf{p} - \mathbf{q}|$)

$$\Gamma(E_p) = 2\pi N_I \int \frac{d\mathbf{q}}{(2\pi\hbar)^2} |V_{\mathbf{p}\mathbf{q}}|^2 \delta(E_p - E_q) \quad (3.53)$$

depends only on the energy. For zero electric field Eqs. (3.51) and (3.52) have isotropic solution.

The first term in Eq. (3.51) describes an elastic relaxation in separate wells and is the largest one. If all other terms are neglected it leads to a distribution function depending only on the energy, i.e. $\varphi_0(\mathbf{p}) = \varphi_0(E_p)$. An equation for this function can be obtained by the averaging of Eq. (3.51) with respect to the energy.^{75,76} For example

$$\begin{aligned} & \int \frac{d\mathbf{p}}{2\pi m} \delta(\varepsilon - E_p) \frac{2\pi N_I}{\hbar} \int \frac{d\mathbf{q}}{(2\pi\hbar)^2} |V_{\mathbf{p}\mathbf{q}}|^2 [\varphi_1(\mathbf{q}) + \varphi_{-1}(\mathbf{q}) + \varphi_1(\mathbf{p}) + \varphi_{-1}(\mathbf{p})] \delta'(E_p - E_q) \\ & = \int \frac{d\mathbf{p}}{2\pi m} \delta(\varepsilon - E_p) [\varphi_1(\mathbf{p}) + \varphi_{-1}(\mathbf{p})] \frac{d}{d\varepsilon} \frac{2\pi N_I}{\hbar} \int \frac{d\mathbf{q}}{(2\pi\hbar)^2} |V_{\mathbf{p}\mathbf{q}}|^2 \delta(\varepsilon - E_q) \\ & + \int \frac{d\mathbf{q}}{2\pi m} \delta'(\varepsilon - E_q) [\varphi_1(\mathbf{q}) + \varphi_{-1}(\mathbf{q})] \frac{2\pi N_I}{\hbar} \int \frac{d\mathbf{p}}{(2\pi\hbar)^2} |V_{\mathbf{p}\mathbf{q}}|^2 \delta(\varepsilon - E_p) \\ & = \frac{d}{d\varepsilon} \int \frac{d\mathbf{p}}{2\pi m} \delta(\varepsilon - E_p) [\varphi_1(\mathbf{p}) + \varphi_{-1}(\mathbf{p})] \frac{2\pi N_I}{\hbar} \int \frac{d\mathbf{q}}{(2\pi\hbar)^2} |V_{\mathbf{p}\mathbf{q}}|^2 \delta(\varepsilon - E_q) \\ & = \frac{d}{d\varepsilon} \int \frac{d\mathbf{p}}{2\pi m} \delta(\varepsilon - E_p) [\varphi_1(\mathbf{p}) + \varphi_{-1}(\mathbf{p})] \frac{\Gamma(E_p)}{\hbar} = \frac{d}{d\varepsilon} \Gamma(\varepsilon) R(\varepsilon), \end{aligned}$$

where $R(E)$ was defined in Eq. (3.31). The elastic relaxation is averaged out. On the right hand side of Eq. (3.52) we have

$$\begin{aligned} & \frac{2\pi N_I}{\hbar} \int \frac{d\mathbf{q}}{(2\pi\hbar)^2} |V_{\mathbf{p}\mathbf{q}}|^2 (\varphi_0(\mathbf{p}) - \varphi_0(\mathbf{q})) \delta'(E_p - E_q) \\ & = \frac{2\pi N_I}{\hbar} \int d\varepsilon \int \frac{d\mathbf{q}}{(2\pi\hbar)^2} |V_{\mathbf{p}\mathbf{q}}|^2 (\varphi_0(E_p) - \varphi_0(\varepsilon)) \delta'(E_p - \varepsilon) \delta(E_q - \varepsilon) \\ & = \frac{2\pi N_I}{\hbar} \int d\varepsilon \delta(E_p - \varepsilon) \frac{d}{d\varepsilon} \int \frac{d\mathbf{q}}{(2\pi\hbar)^2} |V_{\mathbf{p}\mathbf{q}}|^2 (\varphi_0(E_p) - \varphi_0(\varepsilon)) \delta(E_q - \varepsilon) = -\frac{\Gamma(E_p)}{\hbar} \frac{d\varphi_0}{dE_p}. \end{aligned}$$

Chapter 4

Longitudinal magnetoresistance

Classical longitudinal magnetoresistance of superlattices is calculated in the framework of a model which includes fluctuations of barrier conductivity. We found that the result depends very significantly on the fluctuations correlation length. We also found that fluctuations of the electron potential are not uniform along the superlattice, and depend on the superlattice length. A good agreement between theory and experiment is obtained.

4.1. INTRODUCTION

In this work we consider the vertical longitudinal magnetoresistance (LMR) of a superlattice; that is the magnetoresistance in the geometry when both electric and magnetic fields are along the growth direction. Purely classical (i.e., without any quantum effects) LMR was observed many times in experiments, but only recently has a qualitative explanation been suggested. It is obvious that in an ideal superlattice, classical LMR has to be zero, because the magnetic field does not affect electron motion parallel to it. For this reason experimentally observed LMR (Refs. 51, 52, 53, 77, 78, 58, 57) has not been explained for a rather long time. The qualitative explanation suggested by Lee *et al.*³⁶ attributes this to nonuniform fluctuations of the superlattice barriers width.

We present resistance calculations for a superlattice with nonuniform barriers. We consider the case of a narrow-miniband superlattice when the vertical transport can be considered as sequential tunneling. Each barrier in this case can be characterized by a conductivity fluctuating around some average value. The opposite case of wide-band superlattices where an electron tunnels across a few barriers between two successive scattering events seems to be less interesting. The effect of the barrier width fluctuations is averaged out as a result of tunneling across a few barriers.

The qualitative picture of the longitudinal magnetoresistance of superlattices with nonuniform barriers suggested by Lee *et al.*³⁶ is as follows. A current across each barrier is larger in places where the conductivity is larger. If high-conductivity regions of adjacent barriers are not positioned against each other, then nonuniform currents

across barriers induce in-plane currents between barriers. The magnetic field perpendicular to the layers brings about a transverse magnetoresistance, reducing these in-plane currents. As a result the current across barriers cannot pass through places with maximal conductivity. In this way the magnetic field in the growth direction increases the superlattice resistance in this direction.

The effective conductivity of a spatially inhomogeneous medium has been considered many times in the literature; see, e.g., the review paper by Landauer.⁷⁹ A superlattice is just another example of such a medium with a specific geometrical structure of the inhomogeneities. We consider this problem for weak fluctuations of the barrier conductivity (the exact parameter will be shown below). We also assume that the conductivity fluctuations of different barriers are not correlated. These assumptions allow us to obtain an analytic expression for the superlattice resistance.

4.2. PERTURBATION THEORY FOR POTENTIAL FLUCTUATIONS

The superlattice consists of $N + 1$ wells separated by N barriers, and the electric potential in the ν th well is $\phi_\nu(\mathbf{r})$, where $\mathbf{r} = (x, z)$ is the in-plane coordinate, see Fig. 4.1. The electric current $j_{\nu, \nu+1}(\mathbf{r})$ from well ν to the well $\nu + 1$ is given by Ohm's law,

$$j_{\nu, \nu+1} = \sigma_{\nu, \nu+1}^\perp (\phi_\nu - \phi_{\nu+1}), \quad (4.1)$$

where $\sigma_{\nu, \nu+1}^\perp(\mathbf{r})$ is the conductance per unit area of the barrier following the ν th well. The formulation of the problem will be completed with the charge conservation law

$$j_{\nu, \nu+1} - j_{\nu-1, \nu} = \nabla \hat{\sigma} \nabla \phi_\nu, \quad (4.2)$$

where $\hat{\sigma} \nabla \phi_\nu$ is an in-plane electric current in the ν th well, and $\hat{\sigma}$ is a two-dimensional conductivity tensor of the well. We will assume that this tensor depends on the magnetic field but does not depend on coordinates. We will also assume that the conductivity in the wells is isotropic, so that $\sigma_{xx} = \sigma_{zz} = \sigma^\parallel$, and $\sigma_{xz} = -\sigma_{zx}$. This assumption gives

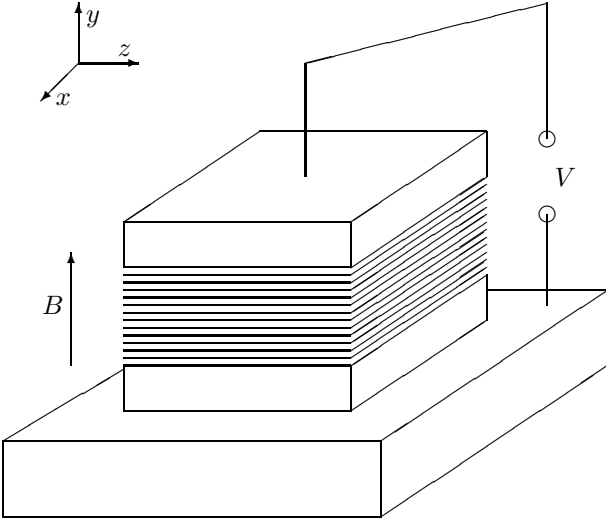


FIG. 4.1. Measurements of LMR in superlattice.

$$\nabla \delta \nabla = \sigma^{\parallel} \nabla^2, \quad (4.3)$$

that is, the Hall conductivity does not enter into the problem. Equations (4.1)-(4.3) have to be solved with some boundary conditions. We will assume that potentials in the first and last wells are independent of \mathbf{r} due to the presence of the highly doped uniform plane contacts, $\phi_0 = NU = \text{const}$ and $\phi_N = 0$.

Equations (4.1) and (4.2) can be solved by means of perturbation theory with respect to the fluctuations of $\sigma_{\nu, \nu+1}^{\perp}$. In the Fourier representation,

$$\sigma_{\nu, \nu+1}^{\perp}(\mathbf{r}) = \sigma^{\perp} + \sum_{\mathbf{q}} \delta \sigma_{\nu, \mathbf{q}} e^{-i\mathbf{q} \cdot \mathbf{r}}, \quad (4.4)$$

where $\delta \sigma_{\nu, \mathbf{q}}$ is considered a small quantity and $\delta \sigma_{\nu, \mathbf{0}} \equiv 0$. The conductivity fluctuations are assumed to be uniform, with a correlation length much shorter than the superlattice plane size, so that

$$\frac{\langle \delta \sigma_{\nu, \mathbf{q}} \delta \sigma_{\nu', \mathbf{q}'}^* \rangle}{(\sigma^{\perp})^2} = \xi_q \delta_{\nu, \nu'} \delta_{\mathbf{q}, \mathbf{q}'}, \quad (4.5)$$

where $\langle \rangle$ means an ensemble average over all possible fluctuation configurations. The function ξ_q is inversely proportional to the barrier area. These conductivity fluctuations induce fluctuations of the potential

$$\phi_{\nu}(\mathbf{r}) = (N - \nu)U + \sum_{\mathbf{q}} \delta \phi_{\nu, \mathbf{q}} e^{-i\mathbf{q} \cdot \mathbf{r}}. \quad (4.6)$$

The Fourier transform of Eqs. (4.1)-(4.3) can be linearized with respect to fluctuations if $\mathbf{q} \neq \mathbf{0}$,

$$\begin{aligned} & \left[(\sigma^{\parallel} / \sigma^{\perp}) q^2 + 2 \right] \delta \phi_{\nu, \mathbf{q}} - \delta \phi_{\nu-1, \mathbf{q}} - \delta \phi_{\nu+1, \mathbf{q}} \\ & = (U / \sigma^{\perp}) (\delta \sigma_{\nu-1, \mathbf{q}} - \delta \sigma_{\nu, \mathbf{q}}). \end{aligned} \quad (4.7a)$$

The second-order terms have to be kept in the same equations for $\mathbf{q} = \mathbf{0}$

$$\begin{aligned} & \left[2\delta \phi_{\nu, \mathbf{0}} - \delta \phi_{\nu-1, \mathbf{0}} - \delta \phi_{\nu+1, \mathbf{0}} \right] \sigma^{\perp} \\ & = \sum_{\mathbf{q}} \left[(\delta \phi_{\nu+1, -\mathbf{q}} - \delta \phi_{\nu, -\mathbf{q}}) \delta \sigma_{\nu, \mathbf{q}} \right. \\ & \quad \left. - (\delta \phi_{\nu, -\mathbf{q}} - \delta \phi_{\nu-1, -\mathbf{q}}) \delta \sigma_{\nu-1, \mathbf{q}} \right]. \end{aligned} \quad (4.7b)$$

The solution to Eq. (4.7a) with the boundary conditions $\delta \phi_{0, \mathbf{q}} = \delta \phi_{N, \mathbf{q}} = 0$ can be expressed in terms of the Green function,

$$\begin{aligned} G_{\nu, \nu'}(q) & = \frac{1}{N} \sum_{j=1}^{N-1} \frac{\sin(\pi j \nu / N) \sin(\pi j \nu' / N)}{\cosh(a_q) - \cos(\pi j / N)} \quad (4.8) \\ & = \frac{1}{\sinh(a_q) \sinh(a_q N)} \\ & \times \begin{cases} \sinh(a_q \nu) \sinh[a_q(N - \nu')], & \nu \leq \nu', \\ \sinh(a_q \nu') \sinh[a_q(N - \nu)], & \nu \geq \nu', \end{cases} \quad (4.9) \end{aligned}$$

where

$$\cosh(a_q) = \left(1 + \frac{\sigma^{\parallel} q^2}{2\sigma^{\perp}} \right). \quad (4.10)$$

One has

$$\delta \phi_{\nu, \mathbf{q}} = U \sum_{\nu'=1}^{N-1} G_{\nu, \nu'}(q) \frac{\delta \sigma_{\nu'-1, \mathbf{q}} - \delta \sigma_{\nu', \mathbf{q}}}{\sigma^{\perp}}, \quad (4.11)$$

with $\mathbf{q} \neq \mathbf{0}$. The derivation of the above expression for the Green function is given in Appendix 4.5.

Physical properties of the result Eq. (4.11) can be seen from the average value of the potential fluctuations squared,

$$\begin{aligned} \langle |\delta \phi_{\nu, \mathbf{q}}|^2 \rangle & = U^2 \xi_q \sum_{\nu'=1}^{N-1} G_{\nu, \nu'}(q) \\ & \times \left[2G_{\nu, \nu'}(q) - G_{\nu, \nu'-1}(q) - G_{\nu, \nu'+1}(q) \right] \\ & = U^2 \xi_q \left[G_{\nu, \nu}(q) + \frac{q}{2} \frac{\partial}{\partial q} G_{\nu, \nu}(q) \right], \end{aligned} \quad (4.12)$$

where $G_{\nu, \nu}(q)$ is given by Eq. (4.9).

Equation (4.12) describes the increase of the potential fluctuations from the contacts toward the middle of the superlattice. For a limited region of q , three situations are conceivable. The first is the case of strong in-plane conductivity, when the potential fluctuations are limited by in-plane currents, and $\langle |\delta \phi_{\nu, \mathbf{q}}|^2 \rangle$, $\nu \neq 0, N$ nearly does not depend on ν . The second is the opposite case, when in-plane currents are not important, and the fluctuations of the potential are similar to the fluctuations in a series of random resistors. In the third intermediate case

the fluctuations increase with the distance from the contacts, but in the internal part of the superlattice they are limited by in-plane currents.

The first case is realized under the condition $\sinh(a_q) \gg 1$; then Eqs. (4.9) and (4.12) give

$$\langle |\delta\phi_{\nu,\mathbf{q}}|^2 \rangle = 2\xi_q \left(\frac{U\sigma^\perp}{\sigma^\parallel q^2} \right)^2, \quad \nu \neq 0, N \quad (4.13a)$$

This result is independent of ν and inverse proportional to the in-plane conductivity. In the second case, $a_q \ll 1/N$, and we have

$$\langle |\delta\phi_{\nu,\mathbf{q}}|^2 \rangle = U^2 \xi_q \frac{\nu(N-\nu)}{N}. \quad (4.13b)$$

In the third intermediate case, $1/N \lesssim a_q \ll 1$, and we have to consider separately the internal region of superlattice and regions near the contacts,

$$\langle |\delta\phi_{\nu,\mathbf{q}}|^2 \rangle = U^2 \xi_q \times \begin{cases} \nu, & a_q \nu \ll 1, \\ N - \nu, & a_q(N - \nu) \ll 1, \\ 1/a_q, & \text{otherwise.} \end{cases} \quad (4.13c)$$

In order to calculate the correction to the average potential, we have to substitute Eq. (4.11) into Eq. (4.7b). This leads to an equation for $\delta\phi_{\nu,\mathbf{0}}$, which should be averaged with the help of Eq. (4.5). The solution to the obtained equation is

$$\langle \delta\phi_{\nu,\mathbf{0}} \rangle = -U \sum_{\mathbf{q}} \frac{\xi_q}{\sigma^\parallel q^2 / \sigma^\perp + 4} \times \left[\frac{\sinh[a_q(N-2\nu)]}{\sinh(a_q N)} + \frac{2\nu - N}{N} \right]. \quad (4.14)$$

The ν dependence of the averaged potential, $(N-\nu)U + \langle \delta\phi_{\nu,\mathbf{0}} \rangle$, becomes more smooth near the contacts; that is near the contacts the electric field is weaker.

One can prove that the perturbation theory developed here is justified if the fluctuations of the potential are small,

$$\sum_{\mathbf{q}} \langle |\delta\phi_{\nu,\mathbf{q}}|^2 \rangle \ll U^2 \quad (4.15)$$

The substitution of the results obtained above, Eqs. (4.13) and (4.14), to this condition leads to

$$\Xi \equiv \sum_{\mathbf{q}} \xi_q \ll \max \left\{ \frac{1}{N}, q_0 \left(\frac{\sigma^\parallel}{\sigma^\perp} \right)^{1/2}, \frac{\sigma q_0^2}{\sigma^\perp} \right\}. \quad (4.16)$$

Here q_0 is the characteristic wave number of the function ξ_q , and the quantity $1/q_0$ can be considered as a conductivity fluctuations characteristic correlation length.

4.3. AVERAGED CURRENT AND LONGITUDINAL MAGNETORESISTANCE

The total current across a barrier,

$$j = \sigma^\perp U - \delta j, \quad (4.17)$$

is the same for all barriers, and can be calculated for the first barrier. Substitution of Eqs. (4.4), (4.7), and (4.11) in Eq. (4.1) with $\nu = 0$, averaging over all possible fluctuations of the barrier conductivity and summation over all q , give

$$\begin{aligned} \delta j &= \sigma^\perp \left\{ U \sum_{\mathbf{q}} \xi_q G_{1,1}(q) + \langle \delta\phi_{1,\mathbf{0}} \rangle \right\} \\ &= \sigma^\perp U \sum_{\mathbf{q}} \frac{2\xi_q}{\sigma^\parallel q^2 / \sigma^\perp + 4} \\ &\times \left[\frac{N-1}{N} + \frac{\sinh[a_q(N-1)]}{\sinh(a_q N)} \right]. \end{aligned} \quad (4.18)$$

This equation is the main result of our paper. It describes the change of the current due to barrier resistance fluctuations. The sign of δj is equal to the sign of the current without fluctuations; that is, fluctuations lead to an increase of the superlattice resistance.

We are particularly interested in the application of this result to a calculation of the magnetoresistance of the superlattices. Here we consider only a weak magnetic field when $\Omega_c \tau \ll 1$, where

$$\Omega_c = \frac{eB}{m}$$

is the cyclotron frequency and τ is the relaxation time. In this case the magnetic-field-induced change of the in-plane conductivity is $\sigma^\parallel(0) - \sigma^\parallel(B) \approx \Omega_c^2 \tau^2 \sigma^\parallel(0)$, and the superlattice magnetoresistance becomes

$$\frac{R(B) - R(0)}{R(0)} = -\frac{\Omega_c^2 \tau^2 \sigma^\parallel}{U \sigma^\perp} \frac{\partial}{\partial \sigma^\parallel} \delta j. \quad (4.20)$$

In transport theory, surface roughness is often approximated by a Gaussian function. Such an approximation immediately gives the Gaussian form for the barrier conductivity fluctuations correlation function, i.e.,

$$\xi_q = \frac{4\pi\Xi}{q_0^2 S} e^{-q^2/q_0^2}, \quad (4.21)$$

where S is the area of the barrier, and Ξ is the standard deviation of the normalized barrier conductivity, which is defined generally in Eq. (4.16). Substitution of Eq. (4.21) into Eq. (4.20) allows us to evaluate the superlattice magnetoresistance

$$\frac{R(B) - R(0)}{R(0)} = \Omega_c^2 \tau^2 \sum_{\mathbf{q}} \xi_q$$

$$\times \begin{cases} \sigma^{\parallel} q^2 N / (6\sigma^{\perp}), & \gamma N^2 \ll 1, \\ \frac{2 [\sigma^{\parallel} q^2 / \sigma^{\perp}]^{1/2}}{[\sigma^{\parallel} q^2 / \sigma^{\perp} + 4]^{3/2}}, & \gamma N^2 \gg 1, \end{cases} \quad (4.22)$$

$$\sim \Xi \Omega_c^2 \tau^2 \begin{cases} \gamma N, & \gamma N^2 \ll 1, \\ \sqrt{\gamma}, & \gamma \ll 1, \\ \ln \gamma / \gamma, & \gamma \gg 1, \end{cases} \quad (4.23)$$

where $\gamma = \sigma^{\parallel} q_0^2 / \sigma^{\perp}$. One can see from Eq. (4.23) that the magnetoresistance disappears for both very small and very large q_0 . The reasons for this, however, are different. The former is a case of effectively “metallic” superlattice wells. They are almost equipotential planes, in-plane currents are small, and magnetoresistance is also small. In addition, in this case barrier conductivity fluctuations are averaged out and δj itself goes to zero. The latter case is a case of effectively “dielectric” planes. The high-conductivity regions of adjacent barriers are located far from each other. In this case the conductances of the in-plane path are small and the in-plane currents are also small.

4.4. DISCUSSION AND SUMMARY

Beside the correction to the current, the surface roughness of superlattice barriers leads to a quite unexpected result: distribution of an electric field along the superlattice appears to be nonuniform. Indeed, for the correction to the average potential drop across one barrier, Eq. (4.14) gives

$$\delta\phi_{\nu-1,0} - \delta\phi_{\nu,0} = U \sum_{\mathbf{q}} \frac{\xi_{\mathbf{q}}}{\sigma^{\parallel} q^2 / \sigma^{\perp} + 4} \times \left[\frac{2}{N} - \frac{\sinh(a_{\mathbf{q}}) \cosh[a_{\mathbf{q}}(2\nu - 1 - N)]}{\sinh(a_{\mathbf{q}} N)} \right]. \quad (4.24)$$

In the middle of the superlattice the sign of this quantity is the same as that of the potential drop without surface roughness, U , and near the contacts it is the opposite, see Fig 4.2. Because of surface roughness the field becomes stronger at the middle and weaker near the contacts. The size of the contact regions is about $1/a_{\mathbf{q}}$ periods. The redistribution of the field along the superlattice is not a large effect, but it can be stronger for more pronounced surface roughness. The physical reason for the field redistribution is that the current is trying to go across the least resistive regions of the barriers. Because of the lack of correlation of the surface roughness in different barriers, this produces an in-plane current which makes the overall resistance larger. Near the contacts where the in-plane potential redistribution is not fully developed, this effect is suppressed.

The correction to the current due to surface roughness strongly depends on $\sigma^{\parallel} q_0^2 / \sigma^{\perp}$. This parameter may significantly vary in experiments. Its value can be estimated

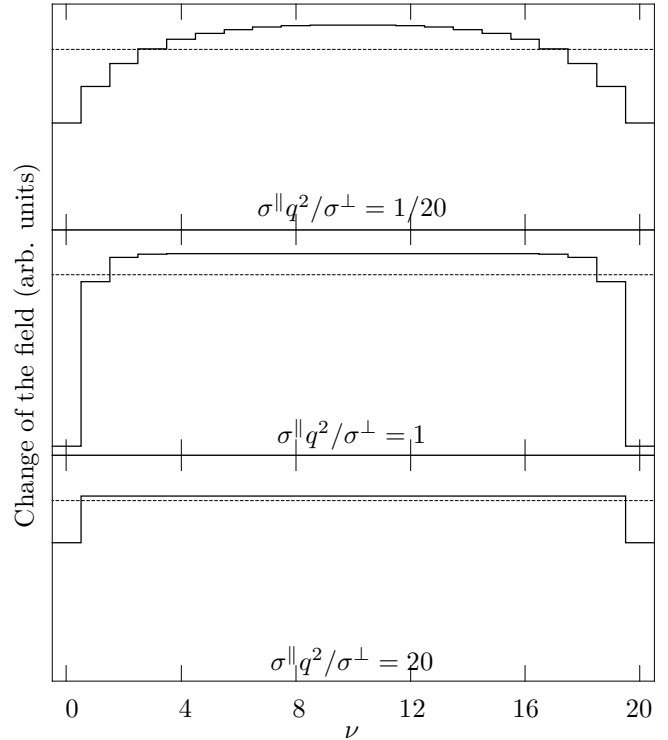


FIG. 4.2. Contribution of the terms with different wave vectors to the change of the averaged field. One can see that the field becomes higher at the middle of superlattice and lower near the contacts. The scales on all the graphs are the same, and the dashed lines show zeros of the field change.

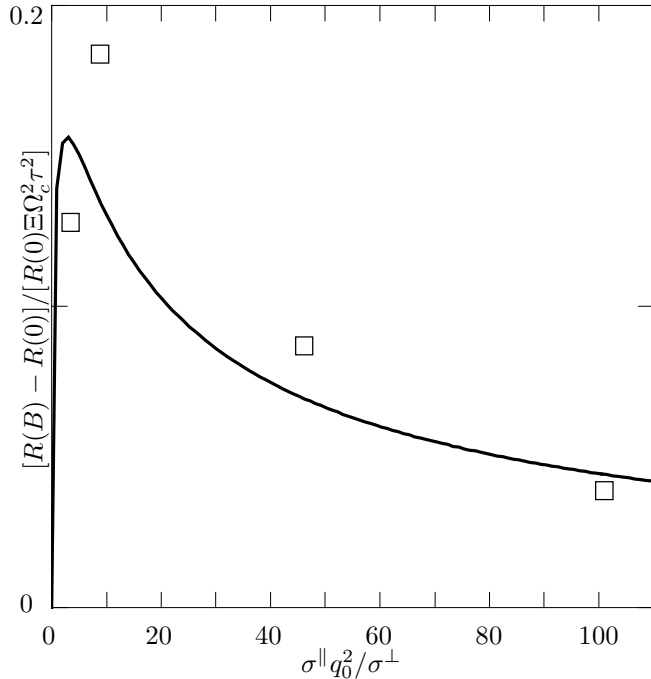


FIG. 4.3. Comparison of the experimental data of Ref. 36, (open squares), with the theoretical prediction of Eq. (4.27), solid line. Combinations $[R(B) - R(0)]/[\Xi R(0)\Omega_c^2 \tau^2]$ and $\sigma^{\parallel} q_0^2 / \sigma^{\perp}$ are calculated from the experimental data summarized in Table 4.4, with two fitting parameters $\tau = 5.3 \times 10^{-13}$ s and $q_0 = 3.3 \mu\text{m}^{-1}$.

in terms of microscopic parameters of the superlattice. We can estimate $\sigma^{\perp} \sim (me^2 \Lambda^2 \tau \hbar^{-4}) [1 - \exp(E_F/T)]$ (Ref. 26), where e and m are the electron charge and mass, respectively, Λ is the transition amplitude between adjacent wells, τ is the relaxation time, E_F is the Fermi energy, T is the temperature, and $\Lambda, \hbar/\tau$ are assumed to be much less than the maximum of E_F, T . In this case we have

$$\sigma^{\parallel} q_0^2 / \sigma^{\perp} \approx \frac{\hbar^2 q^2}{m \Lambda^2} \max(E_F, T) \approx \frac{(lq)^2 \hbar^2}{(\Lambda \tau)^2}, \quad (4.25)$$

where l is the in-plane mean free path. For the conductivity in this expression we used the classical expression $\sigma^{\parallel} \sim ne^2 \tau / m$, where n is the two-dimensional electron concentration. This expression, as well as the phenomenological Eq. (4.2), is correct under the condition $ql \ll 1$. The other basic equation, Eq. (4.1), is justified only under the condition of sequential tunneling, i.e., $\hbar/(\Lambda \tau) \gg 1$. That is, the right-hand side in Eq. (4.25) is the product of a large factor and a small factor, so that all cases in Eq. (4.23) are possible. In these three cases the temperature dependences of the magnetoresistance are $T, T^{1/2}$, and $\ln(T)/T$, respectively.

The condition $ql \ll 1$ means that the characteristic scale of the surface roughness is much larger than the mean free path. The theory can be easily generalized for the case when this condition is not satisfied. The in-plane conductivity in Eq. (4.2) is a response to a uniform electric field. If the electric field is nonuniform at the scale of the mean free path, then the current conservation law, Eq. (4.2), holds but the in-plane conductivity cannot be taken from the phenomenological theory and should be calculated with the help of the Boltzmann equation. The calculation is carried out in Appendix 4.6, and the resulting conductivity depends on q . The only modification in the previous theory is that the expression $\sigma^{\parallel} q^2$ is determined now by Eq. (4.42). The estimate of the magnetoresistance, Eq. (4.23), which was done before for the phenomenological case, is replaced in the limit $q_0 l \gtrsim 1$ by

$$\frac{R(B) - R(0)}{R(0)} = \Xi \Omega_c^2 \tau^2 \frac{\Lambda^2 \tau^2}{\hbar^2 q_0^2 l^2} \ln \left(\frac{\hbar^2}{\Lambda^2 \tau^2} \right). \quad (4.26)$$

In the calculation of the conductivity we neglect quantum corrections. That is justified when the magnetic quantization is smeared by scattering, $\Omega_c \tau \ll 1$, or at high enough temperature, when $\hbar \Omega_c \lesssim T$.

The comparison of the our result with available experimental data is difficult because not all parameters necessary for theoretical calculations are known. Here we compare our results with the measurements of Ref. 36, taking the relaxation time and the characteristic length of interface roughness as adjustable parameters. The widths of wells (d_w) and barriers (d_B) and measured magnetoresistance and barrier conductances in four measured samples are summarized in Table 4.4. We assume that

TABLE 4.1. Summary of experimental data, which was used in Fig. 4.3.

(d_w/d_B) (Å/Å)	Ξ	$\Delta R/(RB^2)$ T^{-2}	$\sigma^\perp = N/(RS)$ S/cm^2
(50/50)	0.36	0.027	1200
(20/80)	0.09	0.032	5500
(80/20)	0.25	0.042	4200
(20/40)	0.19	0.047	14000

fluctuations of the transition amplitude between adjacent wells, $\Delta\Lambda$, result from the fluctuations of the width of the barrier by ± 1 monolayer. The known geometry of the structures allowed us to calculate Λ , and the fluctuations of the barrier conductance were evaluated according to $\Xi \approx (2\Delta\Lambda/\Lambda)^2$. The conductivities in wells were calculated according to $\sigma^\parallel = ne^2\tau/m$, where the two-dimensional electron concentration $n = d_w \times 10^{17} \text{ cm}^{-3}$. The dependence of the magnetoresistance on parameters of the samples can be written in the form

$$\frac{R(B) - R(0)}{R(0)B^2} \frac{m^2}{e^2\tau^2\Xi} = f\left(\frac{\sigma^\parallel q_0^2}{\sigma^\perp}\right). \quad (4.27)$$

For the function in the right-hand side Eq. (4.22) gives

$$f(\gamma) = \int_0^\infty dx e^{-x} \left(\frac{4\gamma x}{(\gamma x + 4)^3}\right)^{1/2}. \quad (4.28)$$

In Fig. 4.3 we show the theoretical curve for this function and the experimental results for four samples. The best fit is obtained for $\tau = 5.3 \times 10^{-13} \text{ s}$ and $q_0 = 3.3 \mu\text{m}^{-1}$. We have to note an obvious qualitative and good quantitative agreement between the theory and experiment. The discrepancy (no more than 10%) can be attributed to slightly different relaxation times τ and surface roughness characteristics in different samples.

The results of the fitting give $q_0 l \approx 0.2$, which justifies the phenomenological expression for σ^\parallel used in the calculations. The estimate of the surface roughness relaxation time for a quantum well with $d_w = 50 \text{ Å}$ and $q_0 = 3.3 \mu\text{m}^{-1}$ gives a value of $2 \times 10^{-10} \text{ s}$. That is, the dominant scattering mechanism is probably impurity scattering, which explains approximately equal relaxation times in samples with different values of d_w . The surface roughness correlation length of 3000 Å seems large, but even values larger by an order of magnitude have been reported.

In summary, we calculated the correction to the superlattice resistance due to nonuniform fluctuations of the conductivity of each of the barriers. Our results explain the classical longitudinal magnetoresistance of superlattices. We found that the magnetoresistance has a non-trivial dependence on the characteristic length scale of fluctuations; it goes to zero for both very large-scale and

very-small scale fluctuations. The fluctuations of the barrier conductivity lead also to a nonuniform distribution of the electric field along the superlattice. The results of the theory give a good quantitative agreement with experimental data.

4.5. DERIVATION OF THE GREEN FUNCTION

Trigonometric sums can be calculated with the help of the equation

$$2 \cosh(\lambda)u(\nu) - u(\nu + 1) - u(\nu - 1) = 0, \quad 0 < \nu < N. \quad (4.29)$$

The general solution to Eq. (4.29) has the form

$$u(n) = C_1 e^{\lambda n} + C_2 e^{-\lambda n}, \quad (4.30)$$

and the eigenvalues and the eigenfunctions of Eq. (4.29) with the boundary conditions $u_0 = u_N = 0$ are

$$\begin{aligned} \cosh(\lambda_j) &= \cos(\pi j/N), \quad 1 \leq j \leq N-1, \\ u_j(\nu) &= \left(\frac{2}{N}\right)^{1/2} \sin(\pi j\nu/N). \end{aligned} \quad (4.31)$$

Let us consider the function $G_{\nu,\nu'}$ satisfying the equation

$$2 \cosh(\lambda)G(\nu, \nu') - G_{\nu+1,\nu'} - G_{\nu-1,\nu'} = \delta_{\nu,\nu'} \quad (4.32)$$

with the boundary conditions $G_{0,\nu'} = G_{N,\nu'} = 0$. This can be expressed in terms of the eigenfunctions Eq. (4.31),

$$G_{\nu,\nu'} = \frac{1}{N} \sum_{j=1}^{N-1} \frac{\sin(\pi j\nu/N) \sin(\pi j\nu'/N)}{\cosh(\lambda) - \cosh(\lambda_j)} \quad (4.33)$$

and this is the first line in Eq. (4.8), with $\lambda \equiv a_q$.

The same function can be calculated in another way with the help of the general solution Eq. (4.30). Apparently, Eq. (4.32) with the boundary conditions is satisfied by the function

$$\begin{aligned} G_{\nu,\nu'} &= A_1 \sinh(\lambda\nu), \quad \nu < \nu', \\ G_{\nu,\nu'} &= A_2 \sinh[\lambda(N - \nu)], \quad \nu > \nu'. \end{aligned} \quad (4.34)$$

The only problem is with the values $\nu = \nu'$. The values of A , B , and $G_{\nu',\nu'}$ can be obtained by substitution of the solutions Eq. (4.34) into Eq. (4.32) for $\nu = \nu', \nu' \pm 1$, that leads to the system of equations

$$\begin{aligned} A_1 \sinh(\lambda\nu') - G_{\nu',\nu'} &= 0, \\ A_1 \sinh[\lambda(\nu' - 1)] - 2 \cosh(\lambda)G_{\nu',\nu'} \\ &+ A_2 \sinh[\lambda(N - \nu' - 1)] = -1, \\ G_{\nu',\nu'} - A_2 \sinh[\lambda(N - \nu')] &= 0, \end{aligned} \quad (4.35)$$

which has a solution

$$\begin{aligned} A_1 &= \frac{\sinh[\lambda(N - \nu')]}{\sinh(\lambda) \sinh(\lambda N)}, \\ G_{\nu', \nu'} &= \frac{\sinh(\lambda \nu') \sinh[\lambda(N - \nu')]}{\sinh(\lambda) \sinh(\lambda N)}, \\ A_2 &= \frac{\sinh(\lambda \nu')}{\sinh(\lambda) \sinh(\lambda N)}, \end{aligned} \quad (4.36)$$

and the final expression for the Green function is

$$G_{\nu, \nu'} = \begin{cases} \frac{\sinh \lambda \nu \sinh \lambda(N - \nu')}{\sinh \lambda \sinh \lambda N}, & \nu \leq \nu', \\ \frac{\sinh \lambda \nu' \sinh \lambda(N - \nu)}{\sinh \lambda \sinh \lambda N}, & \nu \geq \nu', \end{cases} \quad (4.37)$$

This result is also an explicit expression for the sum in Eq. (4.33) and this is the second expression in Eq. (4.9).

4.6. WAVE-VECTOR-DEPENDENT IN-PLANE MAGNETOCONDUCTIVITY

The Fourier transformation of the Boltzmann kinetic equation for the two-dimensional electron gas in the conducting layer is

$$i\mathbf{q} \cdot \mathbf{v} f_{\mathbf{q}} + e[\mathbf{v} \times \mathbf{B}] \frac{\partial f_{\mathbf{q}}}{\partial \mathbf{p}} - ie\mathbf{q} \cdot \mathbf{v} \phi_{\mathbf{q}} \frac{\partial f}{\partial E} = -\frac{f_{\mathbf{q}}}{\tau}, \quad (4.38)$$

where $f(E)$ is the equilibrium distribution function, $f_{\mathbf{q}}$ is the Fourier transform of the distribution function perturbation, $\phi_{\mathbf{q}}$ is the fluctuation of the electron potential, and \mathbf{B} is the magnetic field, which is considered to be perpendicular to the layers, see Fig. 4.1 i.e., $\mathbf{q} \perp \mathbf{B}$. By introducing $\mathbf{q} = (q, 0, 0)$, $\mathbf{v} = (v \cos(\theta), 0, v \sin(\theta))$, and $\mathbf{B} = (0, m\Omega_c/e, 0)$ we reduce the kinetic equation to

$$\Omega_c \frac{\partial f_{\mathbf{q}}}{\partial \theta} - \left[\frac{1}{\tau} + iqv \cos(\theta) \right] f_{\mathbf{q}} = -iqve\phi_{\mathbf{q}} \cos(\theta) \frac{\partial f}{\partial E}. \quad (4.39)$$

It is easy to solve this first-order differential equation, and the answer is a function of v and θ :

$$\begin{aligned} f_{\mathbf{q}} &= e\phi_{\mathbf{q}} \frac{\partial f}{\partial E} \left\{ 1 - \int_0^\infty \frac{d\theta'}{\Omega_c \tau} \right. \\ &\quad \left. \times \exp\left(\frac{-\theta'}{\Omega_c \tau} + i\frac{qv}{\Omega_c} [\sin(\theta) - \sin(\theta' + \theta)]\right) \right\} \end{aligned} \quad (4.40)$$

For Eq. (4.2) only the current divergence is necessary,

$$i\mathbf{q} \cdot \mathbf{j}_{\mathbf{q}} = \int \frac{2d\mathbf{p}}{(2\pi\hbar)^2} ie\mathbf{q} \cdot \mathbf{v} f_{\mathbf{q}} = \sigma^\parallel q^2 \phi_{\mathbf{q}}. \quad (4.41)$$

The last equality is the definition of σ^\parallel . An integration with respect to angles in Eq. (4.41) can be performed, but the integration from Eq. (4.40) still remains

$$\begin{aligned} \sigma^\parallel q^2 &= -\frac{e^2}{\tau} \frac{m}{\pi\hbar^2} \int_0^\infty dE \frac{\partial f}{\partial E} \int_0^\infty d\theta' e^{-\theta'} \\ &\quad \times \left[1 - J_0 \left(2\frac{qv}{\Omega_c} \sin \frac{\Omega_c \tau \theta'}{2} \right) \right]. \end{aligned} \quad (4.42)$$

For the case $ql \ll \max(\Omega_c \tau, 1)$, this equation gives the usual classical result,

$$\sigma^\parallel(B) = \frac{\sigma^\parallel(0)}{1 + \Omega_c^2 \tau^2}. \quad (4.43)$$

Chapter 5

Theory of high-field-domain structures in superlattices.

A number of experimental works provide evidence for the existence of the high-field domains in superlattices when the applied voltage exceeds some critical value. A theoretical description of the structure of such a domain is developed. We confine ourselves to the case of narrow-band superlattices, where electrons are strongly localized in the wells. We find that the minimum length of the high-field domain can be larger than one superlattice period. The maximum current in the oscillating part of the I - V characteristic can be significantly smaller than the value of the current at the voltage where the first instability comes about. The oscillation period can be considerably smaller than the value corresponding to the energy separation between the first and the second level in a well. For the case of the domain formation at some distance from the anode, we study the field distribution in the low-field region downstream of the domain.

5.1. INTRODUCTION

During the past 20 years a number of interesting experimental works have been performed in order to investigate transport properties of superlattices in the growth direction.^{6,24,81,82,83,84,51,52,9,85,18,28} Under a weak applied bias the superlattice looks like a homogeneous medium and exhibits Ohm's law. Near some critical field F_{th} an instability appears and destroys the homogeneous state. As a result of the instability the superlattice breaks down into three regions: the low-field region with transport in the first mini-band, the high-field domain and the low-field region where electrons are injected into the second miniband from the high-field domain and then relax down to the first miniband; see Fig. 5.1. An electron can move 1000\AA in the second mini-band before it drops down,^{86,87,88} because the inter-subband relaxation rate is relatively small. A further increase of the applied bias leads to an expansion of the high-field region and the current exhibits an oscillatory behavior. The period of this oscillation can be associated with the intersubband space but generally it is smaller^{82,24}. Under higher bi-

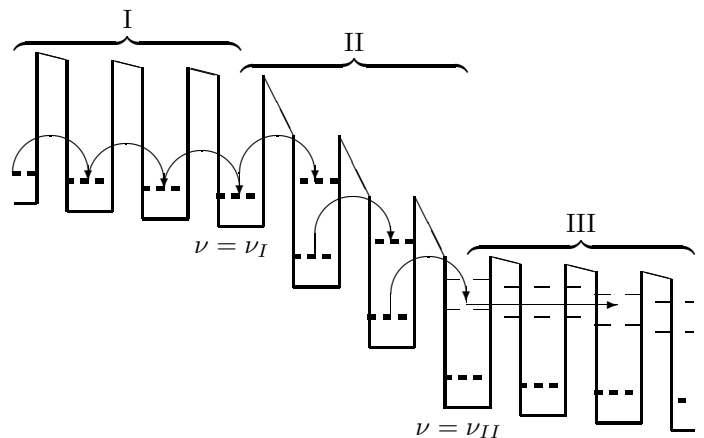


FIG. 5.1. Regions of different conductivity in the superlattice. I and III are low-field domains, II is a high-field one. Dashed lines show the level positions. Levels are broadened due to scattering. The second levels in region III form a mini-band and the long dashed lines show its edges. Arrows show the hopping of electrons between the levels. In region III most of the electrons move in the second mini-band.

ases upper minibands become involved in the transport process.

There is no general physical law forbidding domain formation at any place in the superlattice. However, in the undoped superlattices a domain appears naturally at the anode⁸⁵, see Figs. 1.3 and 5.2(a). In the doped superlattices domain can be formed in the middle of the superlattice, Fig. 5.1, or near the cathode, Fig. 5.2(b). In the last case one has to observe a significant increase of the current after the instability point.

A phenomenological model that described a superlattice by an equivalent electric circuit was suggested by Laikhtman.²³ In this model each barrier was replaced by a nonlinear resistor parallel to the capacitor. The model explained current oscillations and the hysteresis usually observed in the experiment. Prengel, Wacker and

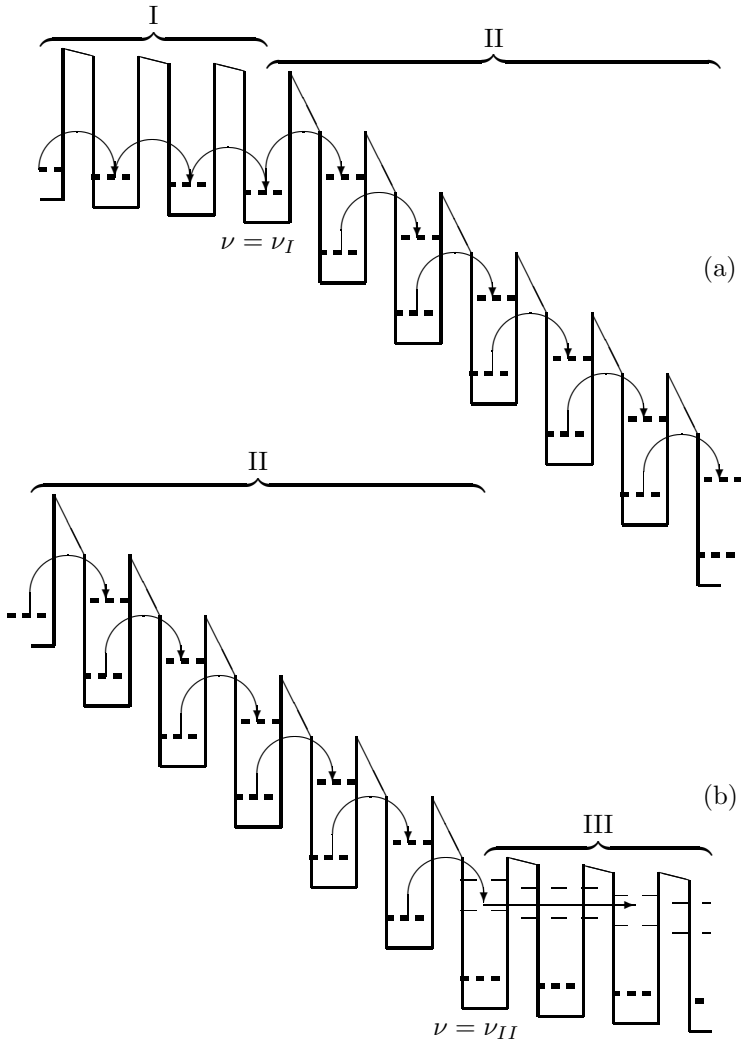


FIG. 5.2. Particular cases of the potential distribution from Fig. 5.1. Domain growth from anode, (a), this is the most often observed experimentally case. Domain growth from cathode, (b), this situation has never been reported in the literature, however, it has very specific fingerprint on the I - V curve and it can be observed.

Schöll⁸⁹ considered a model for a realistic superlattice which included electron tunneling between different levels in the adjacent wells and the relaxation processes inside one well. They obtained multistability of the current-voltage characteristic and various hysteretic transitions which arose upon sweeping the applied voltage and which they associated with changes in the domain size.

The purpose of the present work is not to simulate the I - V characteristics in a specific superlattice but to understand the general structure of the high-field domain. A diffusion current induced by a charge accumulation at the domain boundary appears to be very important. We calculate the field and the carrier distribution in the steady state and get the main features of the current-voltage characteristic of the superlattice in some interval of the applied bias. The size and the position of the domain is

also discussed.

The physical processes characterizing transport in the superlattice are described briefly in the next section. In Sec. 5.3 we derive the equation for the hopping current between two levels in the different wells. In Secs. 5.4, 5.5, and 5.6 we calculate the field distribution in regions I, II, and III respectively. We discuss the results and make some comparisons with available experimental data in Sec. 5.7.

5.2. PHYSICAL PICTURE

Let us see what happens when the bias applied to the superlattice increases and goes beyond the instability threshold. If as a result of the instability development a short high-field domain is spontaneously generated⁶ then the field in the low-field regions is reduced by F_H/N , where F_H is the field in the high-field region and N is the number of the superlattice periods. The current in the low-field region is $j \approx 2j_0 F F_{th} / (F^2 + F_{th}^2)$, where F_{th} is the threshold field and j_0 is the current just before the instability point²⁶. So the generation of the short domain causes the reduction of the current by $\delta j \approx j_0 (F_H / F_{th} N)^2$. Usually F_H is only 10 or 15 times larger than F_{th} , but the number of periods can range from 50 to 100, and therefore the reduction of the current is small, $\delta j \ll j$.

The formation of the high-field domain is accompanied by the accumulation of electrons in the well just upstream of the domain and with the depletion of electrons in the well just downstream of the domain. The accumulation of electrons in one well gives rise to a diffusion current upstream of this well in the direction opposite to the total current. Since the total current is the same across all of the barriers the diffusion current across one barrier has to be compensated for with the conduction part of the current. This compensation may be impossible, because the electric current is too close to its maximum value j_0 . That is, for a such a value of the total current a steady state does not exist. A steady state can come about only for a domain extended enough when the total current isn't too close to its maximum value j_0 . Therefore there exist a minimal length of the high-field domain and an upper limit of the total current in a steady state j^* .

Generally, after the formation of the high-field domain with an increase of the applied bias, the total current drops below j^* . A further increase of the bias leads the growth of the current and when it reaches the j^* the high-field domain expands by one period and the current drops again; see Fig. 1.2.

The change of the potential drop across the high-field domain when it expands by one period is usually associated with the energy spacing E_g between the first and the second levels in a well.^{6,81,82,83,52,9,85} It is assumed that in the high-field domain the first level in one well is in resonance with the second level in the neighboring well.

The number of electrons in the first $n^{(1)}$ and second $n^{(2)}$ levels can be found from the simple balance equation,

$$\frac{n^{(1)} - n^{(2)}}{\tau_t} = \frac{n^{(2)} - n^{(1)}e^{-E_g/T}}{\tau_{21}}, \quad (5.1)$$

where $n^{(1)} + n^{(2)} = \bar{n}$ is the total concentration. Here $\tau_t = \hbar\Gamma/\Lambda_{12}^2$ is the transition time between adjacent wells⁵, Γ is the width of the level, Λ_{12} is the overlap between the wave functions of the first level in one well and the second level in the adjacent well, and τ_{21} is the relaxation time from the second level to the first one in the same well. If $\tau_t \ll \tau_{21}$, then the current is $e\bar{n}[1 - \exp(-E_g/T)]/2\tau_{21}$. This current must be smaller than j^* , which is not always the case. If $\tau_t \gg \tau_{21}$ the current is $e\bar{n} \tanh(E_g/T)/\tau_t$. However this quantity is even larger than $j_0 = e\bar{n}\Lambda_{11}^2/\max(E_F, T)$, where Λ_{11} is the overlap between the wave functions of the first levels in adjacent wells.²⁶

We see that under resonance conditions the current in the high-field domain sometimes appears to be larger than the maximum possible current in region I and such a regime cannot exist. Due to the limitation of the current in region I, resonance in region II is not reached. The current in this region is smaller than its resonance value for two reasons. The tunneling probability is reduced because of a lack of resonance and not all electrons in the second level in one well have enough energy to move to the first level in the neighboring well.

If the resonance between the first and the second level in adjacent wells does not exist, the expansion of the high-field domain by one period requires a voltage increase smaller than that corresponding to E_g . This is the explanation of a small period of the current oscillations sometimes observed in experiments^{24,81,82,52}.

The well at the boundary between regions II and III is depleted. The reduction of the electron concentration in this well corresponds to a field discontinuity between the high-field domain and region III. If the necessary reduction is larger than the average electron concentration in a well, then the domain is located near the anode, where a depletion layer is formed⁸⁵.

In doped superlattices electrons come from the high-field domain to the second miniband in region III and relax there down to the first miniband. The relaxation length depends on the relation between the mobilities in the first and the second minibands and an intersubband relaxation time. The redistributing of electrons between two minibands can result in a field inhomogeneity in region III.

5.3. ELECTRIC CURRENT BETWEEN ADJACENT WELLS.

In this work we consider the case of elastic scattering so strong that an electron is scattered in a well before tunneling to the next well, at least in the first miniband. So

for the calculation of the current we need the transition probabilities between adjacent wells. Since the widths of levels are typically much smaller than the energy separations between them, only the tunneling between those levels that are close to resonance is important.

The general form of the transition probability between such levels is

$$w \propto \frac{\Lambda^2}{\hbar} \frac{\Gamma}{\Gamma^2 + \Delta^2}, \quad (5.2)$$

where Δ is the energy separation between levels. In the low-field region this equation describes the transition between lowest levels and it is justified for $\Lambda_{11} \ll \Gamma$; see Ref. 26. For the transition from the first level to the second level in the adjacent well such an equation was derived by Kazarinov and Suris.⁵ In this case Eq. (5.2) is justified for an arbitrary relation between Λ and Γ .

The overlap integral Λ and the level width due to an elastic scattering Γ are different for different pairs of levels. The overlap integral increases with the level number because the penetration length of the wave function under the barrier increases with the energy. The parameter Γ in Eq. (5.2) is different for the transition from the first level to the first level and for the transition from the first level to the second level, because in the latter case the presence of the first level gives more possibilities for momentum relaxation.

In a part of region III electrons can travel in the second subband, which can be wide. Therefore in this region instead of Eq. (5.2) we use Ohm's law.

The transition probability Eq. (5.2) gives the following expression for the electric current from the i -th level in the ν -th well to the i' -th level in the $\nu + 1$ -th well:

$$j_{ii'} = \frac{e}{\hbar} \int \frac{2d\mathbf{p}}{(2\pi\hbar)^2} \frac{2\Gamma\Lambda_{ii'}^2}{\Gamma^2 + \Delta_{\nu,ii'}^2} (\rho(E_p) - \rho'(E_p + \Delta_{\nu,ii'})), \quad (5.3a)$$

$\Delta_{\nu,ii'} > 0,$

when the level in the ν -th well is higher and

$$j_{ii'} = \frac{e}{\hbar} \int \frac{2d\mathbf{p}}{(2\pi\hbar)^2} \frac{2\Gamma\Lambda_{ii'}^2}{\Gamma^2 + \Delta_{\nu,ii'}^2} (\rho(E_p - \Delta_{\nu,ii'}) - \rho'(E_p)), \quad (5.3b)$$

$\Delta_{\nu,ii'} < 0,$

when the level in the ν -th well is lower. In these equations $\Lambda_{ii'}$ is the overlap integral between electron wave functions of the levels i and i' in the ν -th and $\nu + 1$ -th wells correspondingly. The energy space between these two levels is denoted by $\Delta_{\nu,ii'}$. The diagonal elements of the electron density matrix related to these two levels ρ and ρ' can be considered as a function of the energy $E_p = \mathbf{p}^2/2m$, where m is the effective mass of the electron, since the in-plane motion of electrons is isotropic and this density matrix element is independent of the direction of \mathbf{p} . Usually Γ is a smooth function of the energy and we assume it to be a constant.

We see from Eq. (5.3) that the value of the current depends on the shape of the electron distribution function.

Equation (5.3) is simplified in three cases. The first is the case of weak electron heating when the electron distribution function is close to the equilibrium one.

In the second case the electron gas is degenerate and Δ smaller than the Fermi energy. Then the difference of the distribution function in the integrands of Eq. (5.3) is proportional to Δ and the tail of the distribution function above the Fermi energy does not play any role.

In the third case the electron gas is heated significantly so that the electron-electron scattering is very effective and leads to a fast relaxation of the electron distribution function to the Fermi function with an effective temperature, T , and a chemical potential $\zeta_\nu^{(i)}$, where ν is the index of the well and i is the index of the level. We should note, however, that even a strong deviation of the electron distribution from the Fermi function does not change qualitative results of the present work.

Under these two assumptions the integration in Eq. (5.3) results in

$$j_{ii'} = \frac{2e\Lambda_{ii'}^2}{\hbar} \frac{\Gamma}{\Gamma^2 + \Delta_{\nu,ii'}^2} [n_\nu^{(i)} - n(\zeta_{\nu+1}^{(i')} - \Delta_{\nu,ii'})], \quad (5.4a)$$

when the level in the ν -th well is higher, and

$$j_{ii'} = \frac{2e\Lambda_{ii'}^2}{\hbar} \frac{\Gamma}{\Gamma^2 + \Delta_{\nu,ii'}^2} [n(\zeta_\nu^{(i)} + \Delta_{\nu,ii'}) - n_{\nu+1}^{(i')}], \quad (5.4b)$$

when the level in the ν -th well is lower. In these two equations

$$n_\nu^{(i)} = n(\zeta_\nu^{(i)}) \equiv g_0 T \log(e^{\zeta_\nu^{(i)}/T} + 1) \quad (5.5)$$

is the concentration of electrons in the ν -th well at the i -th level and $g_0 = m/\pi\hbar^2$. We will omit the subscripts of Δ when it does not lead to a confusion. The barrier for the second level is lower than for the first level, so one can expect that $\Lambda_{11} < \Lambda_{12} < \Lambda_{22}$.

The difference in the square brackets in Eq. (5.4) can be simplified,

$$\begin{aligned} & n_\nu^{(i)} - n(\zeta_{\nu+1}^{(i')} - \Delta_{\nu,ii'}) \\ &= n_\nu^{(i)} - n_{\nu+1}^{(i')} + \Delta_{\nu,ii'} \left(\frac{\partial n}{\partial \zeta} \right)_{\zeta_{\nu+1}^{(i')}} \end{aligned}, \quad (5.6)$$

in any of two cases, $\zeta - \Delta \gg T$ or $\zeta \lesssim T$, $\Delta \ll T$.

In the case when the expansion Eq. (5.6) is used one can distinguish between the diffusion current and the conduction current. The former is proportional to the concentration difference and the later is proportional to Δ . Note that

$$\left(\frac{\partial n}{\partial \zeta} \right)_{\zeta_{\nu+1}^{(i')}} \equiv g = g_0 (1 - e^{-n_{\nu+1}^{(i')}/g_0 T}). \quad (5.7)$$

is not a constant, but depends on the electron concentration, which can be different for different levels.

5.4. LOW-FIELD REGION UPSTREAM OF THE DOMAIN.

We assume that in the low-field region upstream of the domain there are electrons in the first miniband only. Motion of electrons in the narrow miniband $\Lambda \ll \Gamma$ can be described in terms of hopping between adjacent wells²⁶. So, a current via each barrier can be found from Eq. (5.4a), where $i = i' = 1$, and these indices will be omitted throughout this section.

The electric field in this low field region is inhomogeneous only near the boundary with the high-field domain. The field distribution near this boundary can be calculated from the Poisson equation together with the condition that the current is the same through all barriers in this region. One can see from Eq. (5.4a) that the current through a barrier is a nonlinear function of the electron concentrations near this barrier and of the field in this barrier, $\Delta/(el)$. For simplicity we consider only the degenerate electron gas. In this case $\partial n/\partial \zeta$ in Eq. (5.6) is a constant; it is equal to g_0 , see Eq. (5.7). This restriction is not very strong since additional electrons come to this region from region III if it exists or from the anode contact. Therefore the electron gas in region I near the boundary of the high-field domain is typically degenerate.

In this case the condition that allows us to use the expansion Eq. (5.6), is $\Delta_\nu < n_{\nu+1}/g_0$. Since the current in the superlattice with the high-field domain is smaller than j_0 , the potential drop per period far from the domain boundary in region I is small, i.e. $\Delta < \Gamma$. On the other hand, the theory is limited by the condition $\Gamma \lesssim E_F$, and we see that far from the domain $\Delta < E_F$. The field in the barriers increases with the approaching the high-field domain boundary, however, the electron concentration also increases and the necessary condition is usually fulfilled. It makes sense to note that the necessary condition (for Δ_ν) contains the concentration downstream of the ν -th barrier where it is larger than that which is upstream ($n_\nu < n_{\nu+1}$).

We introduce here two quantities which can be measured in practice. The first of them is the linear conductivity in the low subband σ . One can find from Eqs. (5.4)-(5.7) that $\sigma = 2e^2 g l \Lambda_{11}^2 / \hbar \Gamma$, see also Ref. 26. The second one is the critical field F_{th} . This field corresponds to the instability of the homogeneous steady state. In Ref. 26 it was shown that $F_{th} \approx \Gamma/el$. The substitutions of these quantities into Eq. (5.4a) gives

$$j = \frac{\sigma}{l} \frac{\phi_\nu - \phi_{\nu+1} + (n_\nu - n_{\nu+1})/eg}{1 + [(\phi_\nu - \phi_{\nu+1})/F_{th}l]^2}, \quad (5.8a)$$

where $\nu < \nu_I$, and ν_I is the number of the well between the regions I and II, see Fig. 5.1.

Here ϕ_ν is the diagonal matrix element of the electric potential in the ν -th well. The term proportional to the concentration difference on the right hand side of Eq. (5.8a) is a diffusion current. In region I the electron

concentration grows in the vicinity of the high-field domain and therefore the direction of the diffusion current is opposite to the direction of the total current. In terms of these potentials $\Delta_{\nu,ii'} = e\phi_{\nu} - e\phi_{\nu+1}$.

The given definition of the potentials allows us to avoid taking into consideration the well polarization. This effect is taken into account in Ref. 26, where the integrated Poisson equation was derived. It provides necessary connection between potentials ϕ_{ν} and concentrations n_{ν}

$$\Delta_{\nu}[\phi] + \frac{e}{C_{\text{eff}}}\Delta_{\nu}[n] = -\frac{4\pi el}{\bar{\epsilon}}(n_{\nu} - \bar{n}). \quad (5.8b)$$

Here C_{eff} and $\bar{\epsilon}$ are constants, which can be calculated for a given superlattice, $\Delta_{\nu}[f] \equiv f(\nu+1) + f(\nu-1) - 2f(\nu)$, and \bar{n} is the average electron concentration. The second term on the left hand side of Eq. (5.8b) describes the capacitance of one well²⁶.

The system of Eqs. (5.8) has two boundary conditions. First, when ν goes to $-\infty$ the difference $\phi_{\nu} - \phi_{\nu+1}$ goes to $F_{\infty}l$. Second, Eq. (5.8b) for $\nu = \nu_I$ contains the difference $\phi_{\nu_I} - \phi_{\nu_I+1}$ which is defined by the field in the high-field region, F_H , and therefore it is about F_Hl . Far from the boundary with region II Eq. (5.8a) becomes

$$j = \frac{\sigma F_{\infty}}{1 + (F_{\infty}/F_{\text{th}})^2}. \quad (5.9a)$$

This equation shows that the current in region I is limited from above and reaches a maximum at $F_{\infty} = F_{\text{th}}$

$$j < j_0 = \frac{1}{2}\sigma F_{\text{th}}. \quad (5.9b)$$

It is convenient to introduce a dimensionless field f_{ν} and displacement h_{ν} as following,

$$f_{\nu} = \frac{2[(\phi_{\nu} - \phi_{\nu+1})/l - F_{\infty}]F_{\infty}}{3(F_{\text{th}}^2 - F_{\infty}^2)}, \quad (5.10a)$$

$$h_{\nu} - h_{\nu-1} = \frac{8\pi e F_{\infty}/\bar{\epsilon}}{3(F_{\text{th}}^2 - F_{\infty}^2)}(n_{\nu} - \bar{n}), \quad (5.10b)$$

where $\nu \leq \nu_I$. Equations (5.8) take the form:

$$f_{\nu} - \lambda_1^{-2}\Delta_{\nu}[h] - (3/2)(f_{\nu})^2 = 0, \quad (5.11a)$$

$$h_{\nu} + \lambda_2^{-2}\Delta_{\nu}[h] - f_{\nu} = 0, \quad (5.11b)$$

where

$$\lambda_1^2 = \frac{4\pi e^2 gl}{\bar{\epsilon}} \frac{F_{\text{th}}^2 - F_{\infty}^2}{F_{\text{th}}^2 + F_{\infty}^2}, \quad (5.12a)$$

$$\lambda_2^2 = \frac{4\pi l C_{\text{eff}}}{\bar{\epsilon}}. \quad (5.12b)$$

The boundary conditions for Eqs. (5.11) are

$$\lim_{\nu \rightarrow -\infty} f_{\nu} = 0, \quad (5.13a)$$

$$f_{\nu_I} = \frac{2(F_H - F_{\infty})F_{\infty}}{3(F_{\text{th}}^2 - F_{\infty}^2)}. \quad (5.13b)$$

The coefficient λ_2 depends only on the superlattice parameters. From the definitions of the $\bar{\epsilon}$ and C_{eff} in Ref. 26 one can easily get that $\lambda_2 > 2$. The parameter λ_1 depends on F_{∞} and therefore on the current through the superlattice $\lambda_1^2 \propto \sqrt{1 - j^2/j_0^2}$, see Eqs. (5.9, 5.12a). Therefore λ_1 goes to zero when the current approaches its maximum value.

The analytic solution to nonlinear difference equations Eqs. (5.11) can be obtained in some limiting cases, but we consider here only one important example. Later we give a numeric solution in the general case.

For $\lambda_1 \ll 1, \lambda_2$ the variation of f_{ν} and h_{ν} from well to well is small. Hence, the second difference $\Delta_{\nu}[\]$ can be replaced with the second derivative $d^2/d\nu^2$ and it can be neglected in Eq. (5.11b). The resulting differential equation has the solution

$$h_{\nu} = f_{\nu} = \frac{1}{\cosh^2(\lambda_1 \nu/2 + \text{const})}. \quad (5.14)$$

The constant in Eq. (5.14) can be found from the boundary condition Eq. (5.13b). The important property of this solution is that it is limited from above. Such a limitation is not connected with a small value of λ_1 but is a general property of Eq. (5.11). This limitation ultimately results from the limitation of the current in the first miniband; see e.g., Eq. (5.9a). In general, the upper limit of the solution to Eq. (5.11), which satisfies boundary condition Eq. (5.13a), depends on λ_1 and λ_2 .

$$f_{\nu_I} < \Upsilon(\lambda_1, \lambda_2), \quad (5.15)$$

Equations (5.11) can be reduced to the recurrent relation

$$f_{\nu-1} = \mathcal{G}(f_{\nu}), \quad (5.16)$$

where the function $\mathcal{G}(x)$ depends on the parameters λ_1 and λ_2 and does not depend on ν . This function has to satisfy the boundary condition Eq. (5.13a) i.e. $\mathcal{G}(x)$ vanishes when x goes to zero. For $x \ll 1$ function $\mathcal{G}(x)$ can be calculated explicitly.

Typical plots for $\mathcal{G}(x)$ are shown in Fig. 5.3. One can get the sequences of values of f_{ν} by iterations of the function $\mathcal{G}(x)$. For example, $f_{\nu_I-2} = \mathcal{G}(\mathcal{G}(f_{\nu_I}))$, f_{ν_I} is given by Eq. (5.13b). These iterations are shown in Fig. 5.3 by dashed lines. One can see that

$$\Upsilon = \max(\mathcal{G}^{-1}(x)), \quad (5.17)$$

where $\mathcal{G}^{-1}(x)$ is the function inverse to $\mathcal{G}(x)$, $\mathcal{G}(\mathcal{G}^{-1}(x)) = x$. The position of this maximum is also marked in Fig. 5.3 by a square. In Fig. 5.4 this maximum Υ is plotted as a function of λ_1^2 for different values of λ_2^2 .

A calculation²⁶ shows that $\lambda_2^2 \geq 4(d_B \epsilon_{\text{eff}}/d_W \epsilon + 1)$, where d_B and d_W are the widths of the barrier and the well respectively, ϵ is dielectric constant in the barrier,

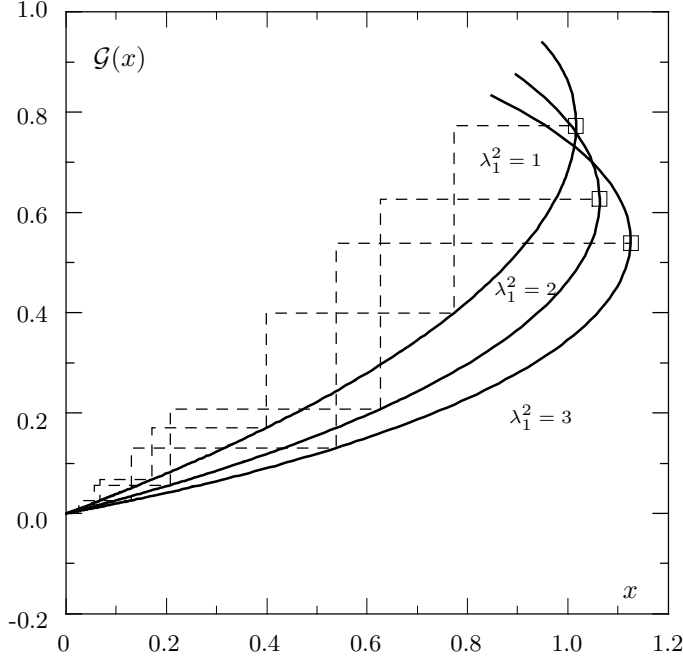


FIG. 5.3. $\mathcal{G}(x)$ for different values of λ_1^2 and $\lambda_2^2 = 20$. The quantities f_ν , which are proportional to the electric field in the barrier ν , can be obtained by iteration of the function $\mathcal{G}(x)$ and the dashed lines show the example of such an iteration. The iteration starts from the value of f that corresponds to the field in the high-field domain. Squares show the maximum value of that f .

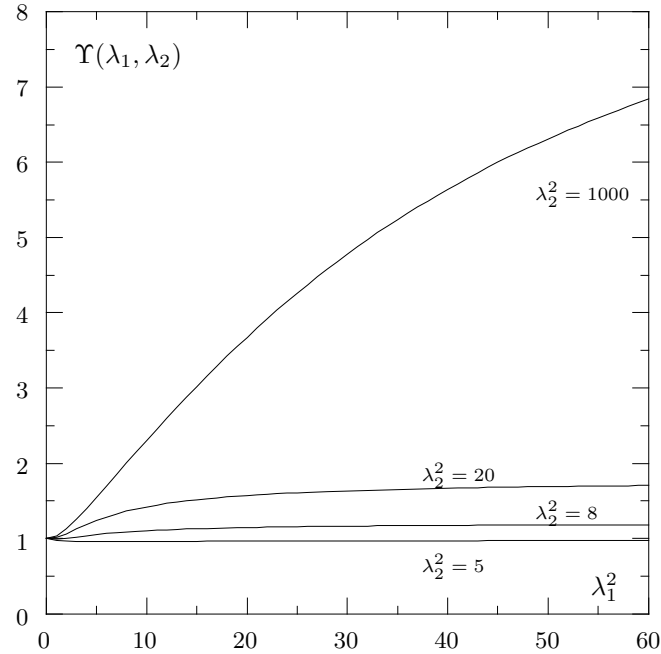


FIG. 5.4. Υ as a function of λ_1^2 is plotted for different values of λ_2^2 .

and ϵ_{eff} is the effective dielectric constant in the well. Although ϵ_{eff} is proportional to the number of electrons in the well, usually $\epsilon_{\text{eff}} \sim \epsilon$ and $d_B \sim d_W$. Thus a typical value of λ_2^2 is 8–10. It becomes large only in the limit of extremely narrow wells or highly doped wells. The other parameter, λ_1^2 can be estimated by means of Eq. (5.12a). It gives $\lambda_1^2 < e^2 g_0 l = l/24\text{\AA}$. Even if the superlattice period is 500\AA $\lambda_1^2 < 20$. We plot Υ for λ_1^2 that ranges from 0 to 60; see Fig. 5.4. The estimate for typical values of λ_1^2 and λ_2^2 shows that usually $\Upsilon \approx 1$.

The condition Eq. (5.15) can be rewritten in terms of the current j by making use of Eq. (5.13b) and Eq. (5.9)

$$j < j^* , \quad (5.18)$$

where j^* can be found from following equation

$$\frac{j^*}{j_0 + (3\Upsilon - 1)\sqrt{j_0^2 - (j^*)^2}} = \frac{F_{\text{th}}}{F_{\text{H}}} . \quad (5.19)$$

The quantity j^* is the upper limit of the current in the superlattice with the high-field domain. The current through the superlattice is also limited by Eq. (5.9b), but $j^* < j_0$, and therefore Eq. (5.18) is a stronger restriction. This restriction comes from the properties of the boundary between regions I and II. Indeed, the excess of electrons in the well at this boundary caused by a large field gradient generates a diffusion current opposite to the current through the superlattice. Usually the diffusion backflow of electrons is compensated by a local increase of the field. This compensation is possible only if the current through the superlattice is smaller than the maximum current in region I.

The condition Eq. (5.18) also implies that there exists an upper limit of the field in the low-field region. When this field exceeds that limit value, the system becomes unstable. The development of this instability leads to the expansion of the high-field region, and the field in the low-field region decreases abruptly.

5.5. DESCRIPTION OF THE HIGH-FIELD REGION.

In the high-field region the main contribution to the current is the electron tunneling from the first level of one well to the second level of the neighboring well followed by the relaxation from the second level to the first one. The main mechanism of the energy relaxation is the emission of optical phonons, if the inter-subband energy space E_g is larger than the phonon energy $\hbar\Omega_{\text{LO}}$. In this case the relaxation time τ_{21} ranges from 0.5×10^{-12} to 10^{-11} sec. depending on the inter-subband energy space^{90,91,86,92,93,94,95}. This is larger than the relaxation time in the bulk material, because the scattering probability is inversely proportional to the transfer momentum squared and the transfer momentum in the inter-subband relaxation, $2m\sqrt{(E_g - \hbar\Omega_{\text{LO}})}$, is larger than

that in the bulk material $2m[\sqrt{(E)} - \sqrt{(E - \hbar\Omega_{LO})}] \approx 2m\hbar\Omega_{LO}/\sqrt{(E)}$, see Ref. 87. In the case of $E_g < \hbar\Omega_{LO}$ the main relaxation mechanism is the electron-electron interaction and τ_{21} is about $10^{-10} - 10^{-9}$ sec.^{96,86,88} The transition time τ_t can vary in a wide range depending on the superlattice parameters. This time has been measured in $40\text{\AA}/40\text{\AA}$ and in $30\text{\AA}/30\text{\AA}$ GaAs–GaAlAs superlattices, see Ref. 97, and appeared about 3.6×10^{-11} sec and 5.3×10^{-12} sec respectively. In a $123\text{\AA}/21\text{\AA}$ superlattice τ_t has been found about 6×10^{-11} sec; see Ref. 95.

In the case when the first and the second levels in adjacent wells are not in resonance one can not use the simple balance equation Eq. (5.1). The current j_{12} in region II is described by Eq. (5.4b) with $i = 1$ and $i' = 2$. The energy space between these levels $\Delta = eF_{\nu}l - E_g < 0$. The current is equal to the number of electrons that relax from the second level to the first level per unit time

$$j_{12} = e \frac{n^{(2)}}{\tau_{21}}. \quad (5.20)$$

For simplicity we neglect in these calculations $\exp(-E_g/T)$ compared to unity, because usually $E_g \gtrsim T$. So, the generalized balance equations become

$$\frac{n(\zeta^{(1)} + \Delta) - n^{(2)}}{\tau_t} = \frac{n^{(2)}}{\tau_{21}} \quad (5.21a)$$

$$n(\zeta^{(1)} + \Delta) + n^{(2)} = \bar{n} \quad (5.21b)$$

In this equation, the inverse transition time $1/\tau_t = 2\Lambda_{12}^2\Gamma/\hbar(\Delta^2 + \Gamma^2)$.

The elimination of $n^{(2)}$ from Eqs. (5.21) leads to

$$j = \frac{e}{\hbar} \frac{2\Lambda_{12}^2\Gamma n(\zeta^{(1)} + \Delta)}{\Delta^2 + \Gamma^2 + 2\Lambda_{12}^2\Gamma\tau_{21}/\hbar}. \quad (5.22)$$

This equation together with Eq. (5.21) describes the current-voltage characteristics of the high-field domain, i.e. the dependence of the current on the potential drop per period, F . In general, this quantity is different from the value corresponding to the resonance between the first level in one well and the second level in the neighboring well, E_g/e . Usually it is assumed that the deviation from the resonance is negligibly small^{6,82,52}. Actually the levels can be considered in resonance only if $|\Delta| \lesssim \Gamma$. However, this is not always the case.

The results of Sec. 5.4 show that the current in the superlattice with the high-field domain is smaller than j^* . If τ_{21} is not very large, then

$$j^* \ll e\bar{n}/2\tau_{21}. \quad (5.23)$$

In the other possible case, $j^* \approx e\bar{n}/2\tau_{21}$, the levels have to be in the resonance and therefore $\Delta \approx 0$. The condition, Eq. (5.23), means that $n^{(2)} \ll \bar{n}$, and the last inequality is satisfied in two cases, $n(\zeta^{(1)} - |\Delta|) \ll \bar{n}$ or $\tau_t \gg \tau_{21}$. In the first case

$$|\Delta| > T, E_F, \quad (5.24a)$$

i. e. the deviation from the resonance is rather large. In the second case $\Delta^2 + \Gamma^2 \gg 2\Lambda_{12}^2\Gamma\tau_{21}/\hbar$. Usually $\Gamma \sim 3-5$ meV, $\tau_{21} > 0.5 \times 10^{-12}$ sec., $\Lambda_{12} \gtrsim 3-5$ meV, and therefore $\Gamma \lesssim \Lambda_{12}^2\tau_{21}/\hbar$. That is, in this case

$$|\Delta| \gg \sqrt{\Lambda_{12}^2\Gamma\tau_{21}/\hbar} \gtrsim \Gamma. \quad (5.24b)$$

These inequalities for Δ show that under the condition Eq. (5.23), the increase of the applied bias necessary for the extension of the high-field domain by one period can be considerably smaller than the resonance value E_g/e .

The limitation of the current by the value of j^* originates from the boundary between regions I and II, see Sec. 5.4. When, with the increase of the bias, the high-field domain extends over the entire superlattice, this boundary disappears. Then the current jumps up sharply and reaches the value defined by conditions of the resonant tunneling,

$$j_{\text{res}} = \frac{\bar{n}}{\tau_t + 2\tau_{21}} = \frac{e}{\hbar} \frac{2\Lambda_{12}^2\bar{n}}{\Gamma + 4\Lambda_{12}^2\tau_{21}/\hbar}. \quad (5.25)$$

5.6. LOW-FIELD REGION DOWNSTREAM OF THE DOMAIN.

In this region, if it exists, electrons are injected into the second miniband from the high-field domain. They can move 1000\AA before they drop down to the first miniband⁸⁷. The injection of electrons into the first miniband can be neglected. Therefore the current in the first mini-band vanishes near the boundary with the high-field domain and increases away from it, owing to the relaxation from the second miniband.

In doped superlattices the screening length is about one period. In other words, the drop of the field at the boundary between regions II and III causes the depletion of only the one well closest to the high-field domain and all other wells in the region III can be considered to be electroneutral. The relaxation of electrons from the second miniband, where their mobility is high, into the first miniband, where the electron mobility is much smaller, leads to the fields inhomogeneity on the scale of the relaxation length. We calculate the field distribution in the most interesting case, when this length is much larger than the superlattice period.

A relaxation length large compared to the superlattice period and to the screening length allows us to use the condition of electroneutrality and to replace difference equations with differential ones. The total current j is the sum of the currents in the first mini-band, j_1 , and in the second mini-band, j_2 :

$$j = j_1 + j_2, \quad (5.26a)$$

$$j_1 = \frac{\mu_1}{l} \left(n^{(1)} eF - T \frac{dn^{(1)}}{dy} \right), \quad (5.26b)$$

$$j_2 = \frac{\mu_2}{l} \left(n^{(2)} eF - T \frac{dn^{(2)}}{dy} \right), \quad (5.26c)$$

where μ_1 and μ_2 are the mobilities in the first and the second miniband respectively. Here we assume the Boltzmann distribution in both mini-bands and neglect the field dependence of the mobilities. The first assumption is reasonable because one can expect a significant heating of electrons injected into region III. The second assumption is natural due to the following circumstance. The field dependence of the mobility is appreciable when the field is close enough to the instability threshold field F_{th} . Usually the field in the high field domain F_{H} is significantly larger than F_{th} . Equation (5.19) shows that in this case j^* is significantly smaller than j_0 and therefore F_{∞} cannot be close to F_{th} . In the part of region III where the current goes mostly in the second miniband, the field is even smaller.

The next two equations are the conditions of the electroneutrality and the continuity equations are

$$n = n^{(1)} + n^{(2)}, \quad (5.26d)$$

$$\frac{dj_2}{dx} = -\frac{en^{(2)}}{\tau_{21}l} \quad (5.26e)$$

In the general case the electric field can be found from Eqs. (5.26b) – (5.26d)

$$\frac{F}{F_{\infty}} = \frac{j_1}{j} + \frac{\mu_1}{\mu_2} \frac{j_2}{j} = 1 - \left[1 - \frac{\mu_1}{\mu_2} \right] \frac{j_2}{j}, \quad (5.27)$$

where F_{∞} is the electric field far from the domain. After eliminating the current j_2 and the concentration $n^{(2)}$ from Eqs. (5.26c), (5.26e), and (5.27) one can get the differential equation for the field in region III

$$L_{\mathcal{D}}^2 \frac{d^2}{dy^2} \frac{F}{F_{\infty}} = L_{\text{Dr}} \frac{F}{F_{\infty}} \frac{d}{dy} \frac{F}{F_{\infty}} + \frac{F}{F_{\infty}} - 1. \quad (5.28)$$

The redistributing of electrons between two minibands and the field profile are characterized by two lengths: a diffusion length $L_{\mathcal{D}}$ and a drift length L_{Dr} , where

$$L_{\mathcal{D}}^2 = \frac{\mu_2 \tau_{21} T}{e}, \quad (5.29)$$

and

$$L_{\text{Dr}} = \mu_2 \tau_{21} F_{\infty}. \quad (5.30)$$

The former length is the distance that electrons diffuse in the second miniband before the relaxation to the first miniband. The latter length is the distance that electrons run in the second miniband under the electric field before the relaxation. Equation (5.28) has to be solved near the boundary for an arbitrary relation between these two lengths. Far from the boundary we calculate the distribution of electric field separately in two limiting cases, when one of these two lengths is much larger than the other.

At $y = 0$ there is no current in the first miniband and Eq. (5.27) gives the boundary condition for Eq. (5.28),

$$\left. \frac{F}{F_{\infty}} \right|_{x=0} = \frac{\mu_1}{\mu_2}. \quad (5.31)$$

One can see that near the boundary F/F_{∞} is small if $\mu_1 \ll \mu_2$. That can be expected because the second miniband is usually wider than the first miniband. Thus we can neglect F/F_{∞} on the right hand side of Eq. (5.28). This simplification allows us to solve this equation in terms of Airy functions. The result is

$$\frac{F}{F_{\infty}} = - \left(4 \frac{L_{\mathcal{D}}^2}{L_{\text{Dr}}^2} \right)^{1/3} \frac{\text{Ai}'((y - y_0)/L_0)}{\text{Ai}((y - y_0)/L_0)}, \quad (5.32)$$

where $\text{Ai}'(\xi)$ denotes the derivative of the Airy function with respect to its argument and $L_0 = (2L_{\mathcal{D}}^4/L_{\text{Dr}})^{1/3}$.

The other parameter y_0 can be found by substitution of Eq. (5.32) into the boundary condition Eq. (5.31). This gives for $\xi = -y_0/L_0$

$$q = -\text{Ai}'(\xi)/\text{Ai}(\xi), \quad (5.33)$$

where $q = (\mu_1/\mu_2)(L_{\text{Dr}}^2/4L_{\mathcal{D}}^2)^{1/3}$

The solution Eq. (5.32) shows that the electric field increases away from the boundary. Far from the boundary where $F \sim F_{\infty}$ the solution Eq. (5.32) is not valid any more. In the case of a short drift length $L_{\text{Dr}} \ll L_{\mathcal{D}}$ one can neglect the first term on the right hand side of Eq. (5.28) because it contains a small parameter $L_{\text{Dr}}/L_{\mathcal{D}}$. We can show this by replacing $y/L_{\mathcal{D}}$ by a dimensionless variable. In this case the solution to Eq. (5.28) is

$$\frac{F}{F_{\infty}} = \frac{j_1}{j} + \frac{\mu_1}{\mu_2} \frac{j_2}{j} = 1 - \left[1 - \frac{\mu_1}{\mu_2} \right] \exp(-y/L_{\mathcal{D}}), \quad (5.34)$$

where the point $x = 0$ corresponds to the boundary between regions II and III. The characteristic length of the electron relaxation from the second miniband to the first one is in this case the diffusion length $L_{\mathcal{D}}$.

In the opposite case when $L_{\text{Dr}} \gg L_{\mathcal{D}}$, Eq. (5.28) can be simplified in the region where $(L_{\mathcal{D}}/L_{\text{Dr}})^{2/3} \ll F/F_{\infty}$, namely, the term on the left hand side of Eq. (5.28) can be neglected. The solution to the resulting equation is

$$F/F_{\infty} - \log(1 - F/F_{\infty}) = (y - y_0)/L_{\text{Dr}}. \quad (5.35)$$

Here y_0 is the same number as in Eq. (5.32). This can be proven by matching the asymptotes of the both solutions, Eq. (5.32) and Eq. (5.35), in the region where $(L_{\mathcal{D}}/L_{\text{Dr}})^{2/3} \ll F/F_{\infty} \ll 1$.

The very important property of Eqs. (5.26) is that the number of electrons in the second miniband explicitly depends on the interminiband relaxation time. One can get from Eq. (5.32) together with Eqs. (5.26e) and (5.27)

$$n^{(2)}|_{x=0} = 2 [q^3 - q\xi(q)] n. \quad (5.36)$$

The parameter q , which defines the number of electrons in the second mini-band near the boundary with region

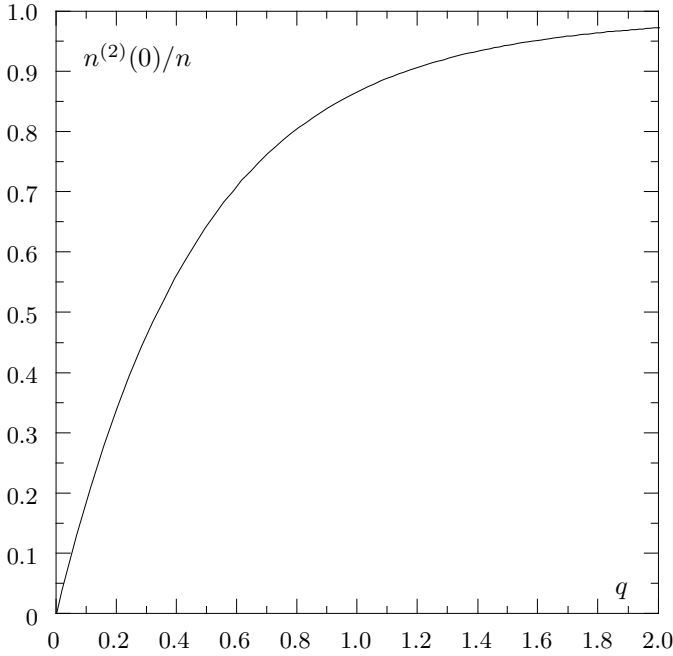


FIG. 5.5. The concentration of the electrons in the second mini-band in region III of the superlattice close to the boundary with region II is plotted versus the parameter $q = (e\mu_1^3\tau_{21}F_\infty^2/\mu_2^2T)^{1/3}$.

II, is proportional to $\tau_{21}^{1/3}$. When q is small $\xi \approx -1$ and $n^{(2)}(0) \approx 2qn$. When q is large the asymptote of the Airy function gives $q \approx \xi^{-1}/4 + \xi^{1/2}$ and $n_2 \approx n$. The concentration $n^{(2)}$ as a function of q is plotted in Fig. 5.5.

The obtained field distribution is not valid at the distance of about one screening length from the high-field domain because the electro-neutrality condition Eq. (5.26d) cannot be used there. Thus in the well at the boundary between regions II and III, see Fig. 5.1, where the field changes significantly, the concentration of electrons has to be found from the Poisson equation. The field change near the next well, $\nu = \nu_{II} + 1$ is much smaller and we can consider it and the rest of region III as electro-neutral. Therefore the solution to Eqs. (5.26) is valid up to well number $\nu = \nu_{II} + 1$, and $n_{\nu_{II}+1}^{(2)} = n^{(2)}|_{x=0}$. The field in the barrier between wells number ν_{II} and $\nu_{II} + 1$ can be easily computed from Eqs. (5.4a) and (5.8b) with $\nu = \nu_{II}$. In the case when the relaxation length of electrons from the second mini-band to the first one is much larger than one superlattice period we can neglect the current between first levels and also put in the Eq. (5.4a) $j_{11} = 0$ and $j_{22} = j$.

5.7. DISCUSSION

In this section we give a qualitative description of the current-voltage characteristic of the entire superlattice. Under a small external bias the superlattice exhibits Ohm's law. At a higher bias the current reaches

a maximum value. The uniform potential distribution in the superlattice is unstable at this point of the I - V characteristic. The theory of instability was developed by the present authors^{23,26}. The instability eventually leads to the formation of the high-field domain and a sharp current drop. In Sec. 5.2 we argued that due to the charge accumulation at the high-field domain boundary, its length can be more than one superlattice period. Now we estimate this length.

The threshold value of the bias just before the instability point is $NF_{th}l$, where N is the number of the superlattice periods. Right after the instability point this bias is a sum of the voltage drop across the high field region $F_H N_{II}l$ and the low field region $\approx (N - N_{II})F_\infty l$. Here we neglect a field inhomogeneity near the domain boundaries. So we have

$$NF_{th}l = F_H N_{II}l + (N - N_{II})F_\infty l, \quad (5.37)$$

and

$$N_{II} = N \frac{F_{th} - F_\infty}{F_H - F_\infty}. \quad (5.38)$$

This equation shows that in very long superlattices the length of the high-field domain is proportional to the length of the superlattice. This fact is a direct consequence of the upstream diffusion current near the boundary of the high-field domain. Without the diffusion the minimal length of the high-field domain is one superlattice period and $F_{th} - F_\infty \propto 1/N$. Due to the diffusion current F_∞ is limited from above by a value independent of the superlattice length. From Eqs. (5.9a), (5.18), and (5.19) we have

$$\sqrt{F_H^2 + 3F_{th}^2} - F_H \geq F_\infty. \quad (5.39)$$

For $F_{th} \geq F_\infty$ one can easily see that N_{II} decreases monotonically with increasing F_∞ . Then Eqs. (5.38) and (5.39) give the following condition for N_{II}

$$N_{II} \geq N \frac{F_H + 3F_{th} - \sqrt{F_H^2 + 3F_{th}^2}}{3(F_H + F_{th})} \quad (5.40)$$

Actually the field in regions I, II, and III is inhomogeneous. As a result there is a correction to the right-hand side of Eq. (5.40). Usually this correction can be neglected because it does not contain the factor N .

With a further increase of the bias the current nearly periodically increases and drops down. After Esaki and Chang,⁶ each oscillation is associated with the extension of the high-field domain by one period and the number of oscillation N_{osc} is expected to be equal to $N - 1$. Equation (5.40) shows that N_{osc} can be less than $N - 1$ and that really is the case in some experiments. For instance, Kawamura et al.²⁴ observed a current-voltage characteristic with $N_{osc} = 35$ in a superlattice that had $N = 39$ barriers, see Fig. 5.6. The difference between N and N_{osc}

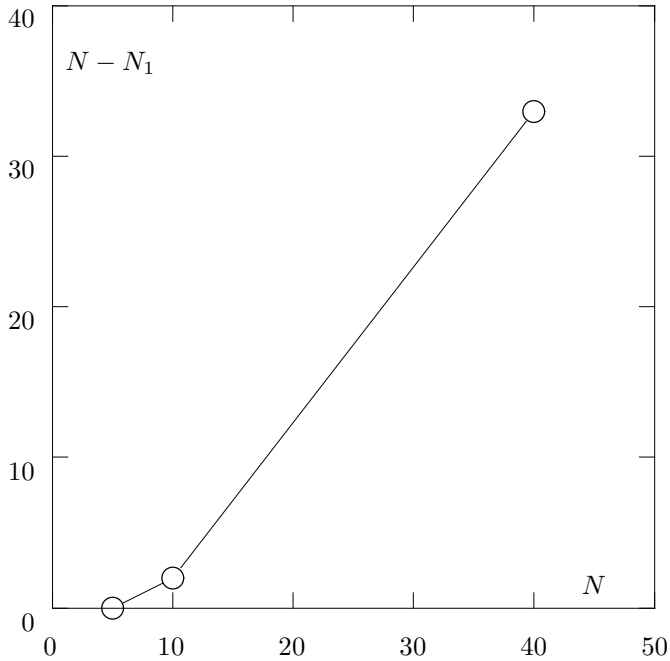


FIG. 5.6. Well number dependence of oscillation repetition number from the experimental work of the Y. Kawamura. *et al*²⁴

can be interpreted as the formation of a high-field domain with the minimal length $N_{\text{II}} = 4$. The value of the threshold field, $F_{\text{th}}l$, in this experiment can be obtained by dividing the threshold voltage, $\approx 0.5\text{V}$, by the number of superlattice barriers. The voltage drop across a barrier in the high-field domain $F_{\text{H}}l$ is equal to the period of the oscillations, 0.14V . The substitution of these values into Eq. (5.40) gives $N_{\text{II}} > 3.1$ which is in agreement with the value obtained from the number of the oscillations.

In order to understand how a large domain comes about, we performed a numeric calculation of the instability development. The simulation was made for 20 period superlattice with the inter-subband energy separation 100meV , and the electron concentration corresponding to the Fermi energy 40meV . We assume some reasonable relations between transition and relaxation times. The parameters characterizing screening in the superlattice were $\lambda_1^2 = 4$, and $\lambda_2^2 = 8$. The results of the simulation are shown in Figs. 5.7 and 5.8. One can see that the domain starts to grow as a large scale instability²⁶ which transforms into a short domain with a length of three periods.

In the case of low doping there are not enough electrons to form the depletion layer downstream of the domain. As the result the domain is formed near the anode⁸⁵ and region III does not exist. The position of the high-field domain in a highly doped superlattice is determined by unintentional nonuniformity of the superlattice or by a fluctuation that initiated the domain.

For fields larger than F_{th} , the oscillating current is limited from above by the value of j^* . It is important to note that this value is usually smaller than j_0 , i. e. the current

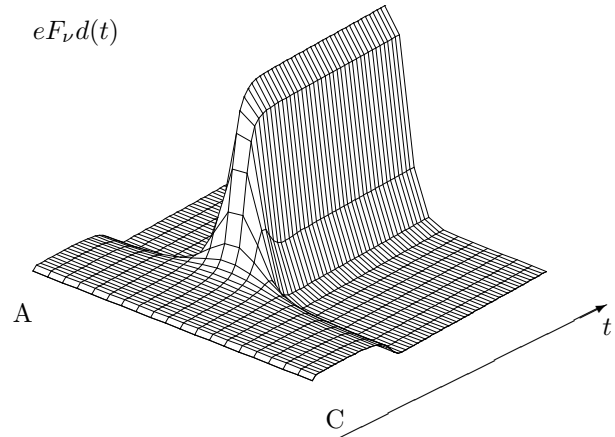


FIG. 5.7. The time evolution of the voltage drops distribution. The superlattice has 20 periods, cathode and anode are marked by C and A respectively. The interlevel spacing in the well is 100meV , whereas the domain height is only 70meV per period.

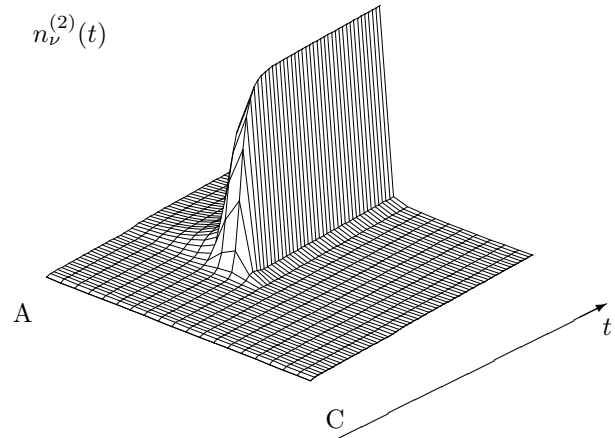


FIG. 5.8. The time evolution of the concentration at the second level in each well. The superlattice has 20 periods, cathode and anode are marked by C and A respectively. One can see the tail of the electron distribution in region III (behind the domain).

value at $F = F_{\text{th}}$, see Sec. 5.4. Such a feature of the I - V characteristic is typically observed in experiment^{24,52}. We will show now that the high-field domain expands by joining another period from region I even in the case when region III does exist. For this purpose we make use of an equation similar to Eq. (5.37), where we take into account the nonuniformity of the field at the accumulation layer near the domain boundary. So instead of Eq. (5.37) we have

$$V = el \sum_{\nu} F_{\nu} = ((N_{\text{I}} - 1)F_{\infty} + F_{\nu_{\text{I}}-1} + N_{\text{II}}F_{\text{H}})l + V_{\text{III}}, \quad (5.41)$$

where V is the applied bias, N_{I} and N_{II} are the numbers of periods in regions I and II respectively, ν_{I} is the number of the first barrier in the high-field domain, V_{III} is the potential drop across region III. Equation (5.41) resembles Eq. (5.37), however, it explicitly takes into account the field inhomogeneity in regions I and III.

As the applied voltage increases, dV/dj goes to infinity which eventually leads to a current discontinuity and extension of the high field domain by one period. One can see from Eq. (5.41) that $dV/dj \rightarrow \infty$ when in one of the barriers $dF/dj \rightarrow \infty$. This cannot take place in region II, where the maximum value of the current is larger than that in region I. The infinite value of dF/dj or zero value of dj/dF is ultimately connected with the maximum in the I - V characteristic of one barrier. This maximum is reached only in the regions where current is confined in the first mini-band, i.e. in region I and in a part of region III. The largest field in these regions is in the last barrier of region I, $F_{\nu_{\text{I}}-1}$, see the end of the Sec. 5.4. The field in this barrier corresponding to $dF/dj \rightarrow \infty$ is larger than F_{th} for the following reason. In this barrier $dj/dF = dj_{\text{cond}}/dF + dj_{\text{diff}}/dF$. Since the field in region I grows faster than in region II, the concentration in the well between these regions decreases. Therefore the diffusion current also decreases which means that $dj_{\text{diff}}/dF > 0$ because the diffusion current is directed against the conduction current. As a result $dj/dF = 0$ not when $dj_{\text{cond}}/dF = 0$ (i.e. $F = F_{\text{th}}$), but when $dj_{\text{cond}}/dF < 0$, (i.e. $F > F_{\text{th}}$).

The field in region II is about E_g/el and the field in region I is smaller or about $F_{\text{th}} = \Gamma/el$. Usually Γ is only a few meV. So, in experiments with a big energy separation^{24,81}, $E_g \approx 200\text{meV}$, the field difference between regions I and II is also large and it causes a large charge accumulation at the boundary between these regions. In these experiments $eF_{\text{H}}l \approx 140\text{meV}$, $eF_{\text{th}}l \approx 12.5\text{meV}$, so $F_{\text{th}}/F_{\text{H}} \approx 0.089$ and Eq. (5.19) gives $j^* \approx 0.30j_0$. That value is in good agreement with the ratio of the maximum of the current in the oscillating region to the peak value of the current at the instability threshold, see Fig. 2(b) in Ref. 24, reproduced in Fig. 1.2 of the present work.

The oscillations of the current in a superlattice with a high-field domain caused by the expansion of this domain

with an increase of the applied bias have a period which can be associated with the potential drop per superlattice period in the high-field region $F_{\text{H}}l$. However, Eq. (5.24) shows that the potential drop per period in the domain is less than the energy separation between levels E_g by a significant quantity, which can reach a few tens of meV.

Such a big difference between the period of the oscillations of the current-voltage characteristic and the energy separation between the levels was detected in the experiment of Kawamura et al.⁸¹, see Fig. 3 in the cited work. One can see that the difference between the inter-subband energy space and the electric current oscillation period increases with E_g . This has a simple physical meaning: in samples with larger E_g the upper limit of the current j^* is lower and therefore the resonance in region II is weaker. Other examples of such a difference can be found in Refs. 82, 84, and 98.

The main assumption which was made in our calculation concerns a small deviation of the electron distribution function from the Fermi function with effective temperature and chemical potential. Necessary conditions justifying this assumption (see Sec.III) may not be satisfied in the high-field domain. However, the features of the current-voltage characteristic discussed in the present work do not depend on the detailed shape of the electron distribution.

In conclusion, we have studied the field distribution and I - V characteristic of the superlattice in the voltage region when a high-field domain exists. The accumulation of electrons at the domain boundary causes a strong limitation of the current. Due to this limitation the minimal length of the high-field domain can be not one but a few superlattice periods. The current limitation also results in the reduction of the period of the current oscillations compared to that corresponding to the energy separation between the first and second levels in a well. These results are in good agreement with available experimental data. The field distribution in the region downstream of the high-field domain (if it exists) is nonuniform due to electron relaxation from the second miniband to the first miniband.

References

- ¹ cited after Michel De Montaigne, *Essays* (Penguin books, Baltimore, 1967).
- ² C. Weisbuch, in *Application of Multiquantum Wells, Selective Doping and Superlattices.*, Vol. 24 of *Semiconductors and Semimetals*, edited by R. Dingle (Academic Press Inc, San Diego, 1987), Chap. I, p. 1.
- ³ L. Esaki and R. Tsu, IBM J. Res. Dev. **14**, 61 (1970).
- ⁴ R. F. Kazarinov and R. A. Suris, Fiz. Tekn. Poluprovodn. **5**, 797 (1971), [Sov. Phys.-Semicond. **5**, 707 (1971)].
- ⁵ R. F. Kazarinov and R. A. Suris, Fiz. Tekn. Poluprovodn. **6**, 120 (1972), [Sov. Phys.-Semicond., **6**, (1972)].
- ⁶ L. Esaki and L. L. Chang, Phys. Rev. Lett. **33**, 495 (1974).
- ⁷ F. Capasso, K. Mohammed, A. Y. Cho, IEEE J. Quantum Electron. **QE-22**, 1853 (1986).
- ⁸ B. F. Levine, K. K. Choi, C. G. Bethea, J. Walker, and R. J. Malik, Appl. Phys. Lett. **51**, 934 (1987).
- ⁹ M. Helm, P. England, E. Colas, F. DeRosa, and S. J. Allen, Jr., Phys. Rev. Lett. **63**, 74 (1989).
- ¹⁰ J. Faist, F. Capasso, C. Sirtori, D. L. Sivco, J. N. Bailargeon, A. L. Hutchinson, S.-N. G. Chu, and A. Y. Cho, Appl. Phys. Lett. **68**, 3680 (1996).
- ¹¹ G. Schwarz, A. Wacker, F. Prengel, E. Schöll, J. Kastrup, H. T. Grahn, and K. Ploog, Semicond. Sci. Technol. **11**, 475 (1996).
- ¹² H. Le Person, C. Minot, L. Boni J. F. Palmier, and F. Mollot, Appl. Phys. Lett. **60**, 2397 (1992).
- ¹³ S. H. Kwok, T. B. Norris, L. L. Bonilla, J. Galán, F. C. Martínez, J. M. Molera, H. T. Grahn, K. Ploog, and R. Merlin, Phys. Rev. B **51**, 10171 (1995).
- ¹⁴ H. Grahn, J. Kastrup, K. Ploog, L. Bonilla, J. Galan, M. Kindelan and M. Moscoso, Jpn. J. Appl. Phys. **34**, 4526 (1995).
- ¹⁵ R. Klahn, S. H. Kwok, H. T. Grahn, and R. Hey, Phys. Rev. B **52**, 8680 (1995).
- ¹⁶ A. Wacker, M. Moscoso, M. Kindelan, and L. L. Bonilla, Phys. Rev. B **55**, 2466 (1997).
- ¹⁷ J. Kastrup, R. Hey, K. H. Ploog, H. T. Grahn, L. L. Bonilla, M. Kindelan, M. Moscoso, A. Wacker and J. Galán, Phys. Rev. B **55**, 2476 (1997).
- ¹⁸ A. Sibille, J. F. Palmier, and F. Mollot, Appl. Phys. Lett. **60**, 457 (1992).
- ¹⁹ K. Fujiwara, K. Kawashima, T. Yamamoto, N. Sano, R. Cingolani, H. T. Grahn, and K. Ploog, Phys. Rev. B **49**, 1809 (1994).
- ²⁰ A. Sibille, in *Semiconductor Superlattices, Growth and Electronic Properties*, edited by H. T. Grahn (World Scientific, London, 1995), Chap. 2. Miniband transport.
- ²¹ G. Bastard, J. A. Brum, and R. Ferreira, in *Semiconductor Heterostructures and Nanostructures*, Vol. 44 of *Solid State Physics*, edited by H. Ehrenreich and D. Turnbull (Academic Press, Inc, San Diego, 1991), Chap. II. The envelop function approximation, p. 232.
- ²² D. L. Smith and C. Mailhot, Rev. Mod. Phys. **62**, 173 (1990).
- ²³ B. Laikhtman, Phys. Rev. B **44**, 11260 (1991).
- ²⁴ Y. Kawamura, K. Wakita, H. Asahi, and K. Kurumada, Jap. J. Appl. Phys. **25**, L928 (1986).
- ²⁵ *Semiconductor Superlattices, Growth and Electronic Properties*, edited by H. T. Grahn (World Scientific, London, 1995).
- ²⁶ B. Laikhtman and D. Miller, Phys. Rev. B **48**, 5395 (1993).
- ²⁷ D. L. Miller and B. Laikhtman, Phys. Rev. B **50**, 18426 (1994).
- ²⁸ S. H. Kwok, R. Merlin, H. T. Grahn and K. Ploog, Phys. Rev. B **50**, 2007 (1994).
- ²⁹ J. Kastrup, H. T. Grahn, K. Ploog, F. Prengel, A. Wacker, and E. Schöll, Appl. Phys. Lett. **65**, 1808 (1994).
- ³⁰ F. Aristone, J. F. Palmier, P. Gassot, J. C. Portal, and F. Mollot, Appl. Phys. Lett. **67**, 2916 (1995).
- ³¹ E. M. Epshtein, Izv. Vuzov, Radiofizika **22**, 373 (1979).
- ³² F. G. Bass, A. A. Bulgakov, and A. P. Tetervov, *High-frequency properties of semiconductors with superlattice* (Novoscience Publisher Inc., New-York, in press 1996), Chap. 7. Conduction and galvanomagnetic effects.
- ³³ D. L. Miller and B. Laikhtman, Phys. Rev. B **52**, 12191 (1995).
- ³⁴ I. B. Levinson and Ya. Yasevichute, Sov. Phys.-JETP **35**, 991 (1972).
- ³⁵ R. A. Suris and B. S. Shchamkhalova, Sov. Phys. Semicond. **18**, 738 (1984).
- ³⁶ M. Lee, N. S. Wingreen, S. A. Solin, and P. A. Wolff, Solid State Comm. **89**, 687 (1994).
- ³⁷ D. L. Miller and B. Laikhtman, Phys. Rev. B **54**, (1996).
- ³⁸ E. E. Mendez, F. Agullo-Rueda, and J. M. Hong, Phys. Rev. Lett. **60**, 2426 (1988).
- ³⁹ K. Kawashima, T. Yamamoto, K. Kobayashi, and K. Fujiwara, Phys. Rev. B **47**, 9921 (1993).
- ⁴⁰ G. Cohen, I. Bar-Joseph, and H. Shtrikman, Phys. Rev. B **50**, 17316 (1994).
- ⁴¹ R. Tsu and G. Döhler, Phys. Rev. B **12**, 680 (1975).
- ⁴² P. Leisching, P. Haring Bolivar, W. Beck, Y. Dhaibi, F. Brüggemann, R. Schwedler, H. Kurz, K. Leo, and K. Köhler, Phys. Rev. B **50**, 14389 (1994).
- ⁴³ G. Von Plessen, T. Meier, J. Feldmann, E. O. Göbel, P. Thomas, K. W. Goosen, J. M. Kuo, and R. F. Kopf, Phys. Rev. B **49**, 14058 (1994).
- ⁴⁴ R. Peierls, Z. Physik **80**, 763 (1933).
- ⁴⁵ J. M. Luttinger, Phys. Rev. **84**, 814 (1951).
- ⁴⁶ E. I. Blount, Phys. Rev. **126**, 1636 (1962).
- ⁴⁷ A. M. Berezhkovskii and R. A. Suris, Zh. Eksp. Teor. Fiz.

- 86**, 193 (1984), [Sov. Phys.– JETP **59**, 109 (1984)].
- ⁴⁸ A. A. Abrikosov, *Fundamentals of the theory of metals* (North-Holland, Oxford, 1988), Chap. 10 p. 198.
- ⁴⁹ E. M. Lifshitz and L. P. Pitaevsky, *Statistical Physics, Part 2*, Vol. 9 of *Landau and Lifshitz: course of theoretical physics* (Pergamon Press, Oxford, 1980), Chap. VI. Electrons in the crystal lattice. §56.
- ⁵⁰ L. Esaki, in *Molecular Beam Epitaxy and Heterostructures*, edited by L. L. Chang and K. Ploog (Martinus Nijhoff Publishers, Dordrecht, 1985), Chap. 1.
- ⁵¹ K. K. Choi, B. F. Levine, N. Jarosik, J. Walker, and R. J. Malik, *Phys. Rev. B* **38**, 12362 (1988).
- ⁵² T. H. H. Vuong, D. C. Tsui, and W. T. Tsang, *J. Appl. Phys.* **66**, 3688 (1989).
- ⁵³ R. A. Davies, D. J. Newson, T. G. Powell, M. J. Kelly, and H. W. Myron, *Semicond. Sci. Technol.* **2**, 61 (1987).
- ⁵⁴ A. Sibille, J. F. Palmier, A. Celeste, J. C. Portal, and F. Mollot, *Europhys. Lett.* **13**, 279 (1990).
- ⁵⁵ M. Lee, S. A. Solin, and D. R. Hines, *Phys. Rev. B* **48**, 11921 (1993).
- ⁵⁶ W. Müller, H. T. Grahn, K. von Klitzing, and K. Ploog, *Phys. Rev. B* **48**, 11176 (1993).
- ⁵⁷ F. Aristone, A. Sibille, J. F. Palmier, D. K. Maude, J. C. Portal, and F. Mollot, *Physica B* **184**, 246 (1993).
- ⁵⁸ H. J. Hutchinson, A. W. Higgs, D. C. Herbert, and G. W. Smith, *J. Appl. Phys.* **75**, 320 (1994).
- ⁵⁹ A. Ya. Shik, *Fiz. Tekh. Poluprovodn.* **7**, 261 (1973), [Sov. Phys.– Semicond. **7**, 187 (1973)].
- ⁶⁰ T. Ando, *J. Phys. Soc. Jpn.* **50**, 2978 (1981).
- ⁶¹ R. A. Suris and B. S. Shchamkhalova, *Fiz. Tekh. Poluprovodn.* **24**, 1638 (1990), [Sov. Phys. Semicond. **24**, 1023 (1990)].
- ⁶² B. Movaghar, *Semicond. Sci. Technol.* **2**, 185 (1987).
- ⁶³ J. F. Palmier, A. Sibille, G. Etemadi, A. Celeste, and J. C. Portal, *Semicond. Sci. Technol.* **7**, 283 (1992).
- ⁶⁴ R. Z. Sagdeev, D. A. Usikov, and G. M. Zaslavsky, *Non-linear Physics* (Harwood Academic Publishers, New York, 1988).
- ⁶⁵ E. M. Lifshitz and L. P. Pitaevsky, *Physical kinetic*, Vol. 10 of *Landau and Lifshitz: course of theoretical physics* (Pergamon Press, Oxford, 1980), Chap. III. Landau damping §30.
- ⁶⁶ T. Ruf, J. Spitzer, V. F. Sapega, V. I. Belitsky, M. Cardona, and K. Ploog, *Phys. Rev. B* **50**, 1792 (1994).
- ⁶⁷ L. L. Chang, H. Sakaki, C. A. Chang, and L. Esaki, *Phys. Rev. Lett.* **38**, 1489 (1977).
- ⁶⁸ E. M. Lifshitz and L. P. Pitaevsky, *Physical Kinetics*, Vol. 10 of *Landau and Lifshitz: course of theoretical physics* (Pergamon Press, Oxford, 1980), Chap. IX. Metals. §84.
- ⁶⁹ Yu. M. Galperin, V. D. Kagan, and V. I. Kozub, *Zh. Eksp. Teor. Fiz.* **62**, 1521 (1972), [Sov. Phys.– JETP **35**, 798 (1972)].
- ⁷⁰ I. S. Gradsteyn and I. M. Ryzhik, *Tables of Integrals, Series and Products* (Academic, New York, 1980).
- ⁷¹ B. Laikhtman and E. L. Altshuler, *Ann. Phys.* **232**, 332 (1994).
- ⁷² P. G. Harper, *Proc. Phys. Soc. London, Sect. A* **68**, 879 (1955).
- ⁷³ L. B. Keldysh, *Zh. Eksp. Teor. Fiz.* **47**, 1525 (1964), [Sov. Phys. JETP **20**, 1018 (1965)].
- ⁷⁴ E. M. Lifshitz and L. P. Pitaevsky, *Physical Kinetics*, Vol. 10 of *Landau and Lifshitz: course of theoretical physics* (Pergamon Press, Oxford, 1980), Chap. X. §93, §94.
- ⁷⁵ S. V. Gantsevich and V. L. Gurevich, *Fiz. Tverd. Tela* **7**, 2400 (1965), [Sov. Phys. Solid State **7**, 1939(1966)].
- ⁷⁶ V. L. Gurevich and R. Katilius, *Zh. Eksp. Teor. Fiz.* **49**, 1145 (1965), [Sov. Phys. JETP **22**, 796(1966)].
- ⁷⁷ B. J. Skromme, R. Bhat, M. A. Koza, S. A. Schwarz, T. S. Ravi, and D. M. Hwang, *Phys. Rev. Lett.* **65**, 2050 (1990).
- ⁷⁸ F. Piazza, L. Pavesi, H. Cruz, M. Micovic, and C. Mendonça, *Phys. Rev. B* **47**, 4644 (1993).
- ⁷⁹ R. Landauer, in *Electrical Transport and Optical Properties of Inhomogeneous Media*, edited by J. C. Garland and D. B. Tanner (AIP, New York, 1978).
- ⁸⁰ D. Bimberg, J. Christen, T. Fukunada, H. Nakashima, D. E. Mars and J. N. Miller, *J. Vac. Sci. Technol. B.* **5**, 1191 (1987).
- ⁸¹ Y. Kawamura, K. Wakita, and K. Oe, *Jap. J. Appl. Phys.* **26**, L1603 (1987).
- ⁸² K. K. Choi, B. F. Levine, R. J. Malik, J. Walker, and C. G. Bethea, *Phys. Rev. B* **35**, 4172 (1987).
- ⁸³ B. F. Levine, K. K. Choi, C. G. Bethea, J. Walker, and R. J. Malik, *Appl. Phys. Lett.* **50**, 1092 (1987).
- ⁸⁴ K. K. Choi, B. F. Levine, C. G. Bethea, J. Walker, and R. J. Malik, *Appl. Phys. Lett.* **50**, 1814 (1987).
- ⁸⁵ H. T. Grahn, H. Schneider, and K. von Klitzing, *Phys. Rev. B* **41**, 2890 (1990).
- ⁸⁶ M. Artaki and K. Hess, *Phys. Rev. B* **37**, 2933 (1988).
- ⁸⁷ D. C. Herbert, *Semicond. Sci. Technol.* **3**, 101 (1988).
- ⁸⁸ V. I. Falko, *Phys. Rev. B* **47**, 13585 (1993).
- ⁸⁹ F. Prengel, A. Wacker, and E. Schöll, *Phys. Rev. B* **50**, 1705 (1994).
- ⁹⁰ C. H. Yang and S. A. Lyon, *Physica* **134B**, 305 (1985).
- ⁹¹ A. Seilmeier, H.-J. Hübner, G. Abstreiter, G. Weimann, and W. Schlapp, *Phys. Rev. Lett.* **59**, 1345 (1987).
- ⁹² J. K. Jain and S. Das Sarma, *Phys. Rev. Lett.* **62**, 2305 (1989).
- ⁹³ R. J. Bäuerle, T. Elaesser, W. Kaiser, H. Lobentanzer, W. Stolz, and K. Ploog, *Phys. Rev. B* **38**, 4307 (1988).
- ⁹⁴ M. C. Tatham, J. F. Ryan, and C. T. Foxon, *Phys. Rev. Lett.* **63**, 1637 (1989).
- ⁹⁵ H. T. Grahn, H. Schneider, W. W. Rühle, K. von Klitzing, and K. Ploog, *Phys. Rev. Lett.* **64**, 2426 (1990).
- ⁹⁶ D. Y. Oberli, D. R. Wake, M. V. Klein, J. Klem, T. Henderson, and H. Morkoç, *Phys. Rev. Lett.* **59**, 696 (1987).
- ⁹⁷ B. Deveaud, A. Chomette, B. Lambert, and A. Regreny, *Solid State Commun.* **57**, 885 (1986).
- ⁹⁸ H. T. Grahn, *Physica Scripta.* **T49**, 507 (1993).